Pressure drop in fixed beds of non-spherical biomass char particle mixtures

HW Honiball

orcid.org/ 0000-0001-5164-2300

Dissertation accepted in fulfilment of the requirements for the degree *Master of Engineering in Chemical Engineering* at the North-West University

Supervisor:	Dr FH Conradie
Co-supervisor:	Mr AF van der Merwe

Graduation: April 2024

ACKNOWLEDGEMENTS

I would like to thank the following people for the role they played throughout the completion of this study

- My study leaders, Dr FH Conradie and Mr AF vd Merwe, for their advice, wisdom and support over the past 2 years.
- My parents and my sister for their undying love and support.
- Mr A Brock and Mr J Kroeze from the workshop for their help with the experimental setup.
- Prof R Coetzer and Dr S Liebenberg for helping with the statistical models.
- Mr R Horn for his friendship and support over the past 2 years

ABSTRACT

Biomass gasification is an important engineering process for the production of fuel gases. The pressure drop of gas flowing through fixed beds is an important parameter for the design and operation of gasifiers. Pressure drop over gasifiers with biomass feedstocks is not as widely researched as fossil fuel feedstocks.

Biomass char particles were used as the packing material to make fixed bed particle mixtures. Five batches of particles ranging from +2.36mm and -13.2mm were used to make binary and ternary mixtures for bed voidage and pressure drop experiments. Experiments were done to gain information on the particles' shape characteristics. These shape characteristics were used in modelling the bed voidage and pressure drop. Pressure drop and bed voidage determination experiments were conducted with mono-sized, binary and ternary particle mixtures.

The voidage models produced satisfactory results with percentage errors of less than 10%. The two linear bed voidage models used, namely the Aim-Golf model and the linear packing density model. The Aim-Golf model modelled bed voidage for binary mixtures with a percentage error of 4.99%. The linear packing density model modelled bed voidage for binary mixtures with a percentage error of 3.82%. The non-linear models used for binary mixtures were the Toufar model and the modified Kwan model. The Toufar model modelled bed voidage for binary mixtures with a percentage error of 3.94%. The modified Kwan model modelled bed voidage for binary mixtures with a percentage error of 4.25%. The three non-linear models for ternary mixtures were the Wong, Chang and De Larrard models. The Wong model had a percentage error of 8.22%. The Chang model had a percentage error of 9.95%. The De Larrard model had a percentage error of 12.0%.

Five fundamental pressure drop models were used for modelling. The Ergun equation and four of its modified versions were tested. The modified versions included the Montillet, Tallmadge, KTA and Foscolo equations. These equations did not yield satisfactory results. The Ergun equation and its modifications could not model pressure drop for mixtures of char particles with percentage errors of less than 17%. Three statistical models were used to model pressure drop through mixtures of char particles with percentage errors of less than 10%. The statistical models include quadratic, Padé and 3rd-order polynomials. Their modelling percentage errors were 9.0%, 8.4% and 8.1% respectively. These models only considered interactions between the particles of which the mixtures were made and the fluid gas flow velocity. This study found that more research is required to study the effects of particle interactions when modelling pressure drop through packed beds of char particles. These interactions may in future be included in the fundamental pressure drop models.

Keywords: Pressure drop, fixed beds, gasifiers, biomass gasification

TABLE OF CONTENTS

1.INTRODUCTION 1
1.1 Background and motivation 1
1.2 Problem statement 2
1.3 Aim and objectives 3
1.4 Scope 3
1.5 Study outline 4
2.LITERATURE REVIEW 5
2.1 Biomass in engineering 5
2.2 Pressure drop modelling 5
2.3 Bed voidage Measurement and modelling 10
2.4 Particle sphericity 23
2.5 Polynomial modelling 26
3.METHODOLOGY 27
3.1 Materials 27
3.2 Sample preparation 27
3.3 Particle shape characterisation 27
3.4 Bed voidage determination 28
3.5 Pressure drop experiments 28
3.6 Binary voidade test models 30
3.6 Ternary voidade test models 30
3.7 Pressure drop per meter test models 30
3.8 Voidage and pressure drop repeatability and uncertainty 30
4.RESULTS & DISCUSSION 32
4.1 Particle characterisation results 32
4.2 Particle diameter and sphericity confidence intervals 33
4.3 Voidage and pressure drop repeatability and uncertainty results 35
4.4 Binary Voidage models prediction performance 38
4.3 Ternary voidage models prediction performance 50
4.5 Parameters influencing pressure drop 66
4.6 Modified Ergun models 70
4.7 Statistical Modelling of Pressure Drop 74
5.CONCLUSION & RECOMMENDATIONS 78
5.1 Conclusion 78
5.2 Recommendations 80
BIBLIOGRAPHY 81
APPENDIX A: RHOVOL RESULTS AND ANALYSIS 84
APPENDIX B: BINARY VOIDAGE MODELLING RESULTS 90

APPENDIX C: MULTIPLE LINEAR REGRESSION RESULTS 102

LIST OF FIGURES

Figure 2-1: Packing parameters of bed voidage modelling..... **Error! Bookmark not defined.**

Figure 2-1: Packing parameters of bed voidage modelling..... 13

Figure 2-2: Binary voidage diagram and model parameters..... 13

Figure 2-3: Different volume types..... **Error! Bookmark not defined.**

Figure 2-3: Different volume types..... 23

Figure 3-1: Pressure drop experimental setup..... 29

Figure 4-1: Rhovol intercept sphericity results on individual particles.... **Error! Bookmark not defined.**

Figure 4-1: Rhovol intercept sphericity results on individual particles..... 34

Figure 4-2: Sphericity results obtained using the KC equation on fixed beds of biochar particles..... **Error! Bookmark not defined.**

Figure 4-2: Sphericity results obtained using the KC equation on fixed beds of biochar particles..... 35

Figure 4-3: Pressure drop repeatability for the unmixed batch of particles where dp = 13.0mm..... 36

Figure 4-4: Pressure drop repeatability for the unmixed batch of particles where dp = 4.50mm..... 37

Figure 4-5: Pressure drop repeatability for a binary mixture of particles where dpsm = 6.69mm..... 37

Figure 4-6: Pressure drop repeatability for a ternary mixture of particles where dpsm = 7.71mm..... 38

Figure 4-7: Parity plot for the Aim-Golf model with new regressed empirical constants. **Error! Bookmark not defined.**

Figure 4-8: Voidage diagrams for ternary mixtures..... **Error! Bookmark not defined.**

Figure 4-9: Continuation of voidage diagrams for ternary mixtures..... **Error! Bookmark not defined.**

Figure 4-10: Voidage parity plot for the De Larrard model and ternary mixtures..... **Error! Bookmark not defined.**

Figure 4-11: ΔP vs. U for the mono-sized batches batches.... **Error! Bookmark not defined.**

Figure 4-12: Parity plot for the Ergun Equation with the Ergun constants regressed for char mixtures..... **Error! Bookmark not defined.**

Figure 4-13: ΔP vs. dp at constant gas flow velocity..... **Error! Bookmark not defined.**

Figure 4-14: ΔP vs. dp at maximum gas flow velocity..... **Error! Bookmark not defined.**

Figure 4-15: Parity plots for the statistical approximations ..... **Error! Bookmark not defined.**

LIST OF TABLES

Table 2-1: Diameter mean for a sample of particles 7
Table 2-2: Ergun constants for coal, charred coal and ash particles 8
Table 2-3: Ergun constants for cylindrical particles (Nemec & Levec, 2005) 9
Table 2-4: Ergun Equation modifications 10
Table 2-5: Bed voidage ranges for biomass and biochars 11
Table 2-6: Linear bed voidage models for binary mixtures 14
Table 2-7: Toufar voidage model 15
Table 2-8: Kwan and modified Kwan voidage models 16
Table 2-9: Linear voidage model RMSE comparison 17
Table 2-10: Wong voidage model 18
Table 2-11: De Larrard voidage model 19
Table 2-12: Chang's voidage model 20
Table 2-13: Parameter values for Koekemoer's voidage equation 21
Table 2-14: Voidage models information 21
Table 2-15: Voidage models performance for other particles 22
Table 2-16: Biomass particles sphericities 25
Table 3-1: Batch particle sieve sizes 27
Table 3-2: Rhovol Equations 28
Table 3-3: Experimental setup instrument list 29
Table 4-1: Particle characterisation results of the Rhovol analysis 32
Table 4-2: Confidence intervals of MCD of biochar particles 33
Table 4-3: Confidence intervals of sphericity of biochar particles 33
Table 4-4: Voidage uncertainty levels 35
Table 4-5: AG regression for char particles 39
Table 4-6: LPD model regression for char particles 41
Table 4-7: Toufar regression for char particles 43
Table 4-8: Modified Kwan model regression for char particles 47
Table 4-9: Regression parameters for the Wong model 54
Table 4-10: Wong model percentage errors where d_1 = 6.72 mm, d_2 = 10.8 mm, d_3 = 13.0 mm 55
Table 4-11: Wong model percentage error where d_1 = 4.50 mm, d_2 = 10.8 mm, d_3 = 13.0 mm 55
Table 4-12: Regression parameters for Chang's model 57
Table 4-13: Chang's model percentage errors for d_1 = 4.50 mm, d_2 = 6.72 mm, d_3 = 13.0 mm 58
Table 4-14: Chang's model percentage errors for d_1 = 4.50 mm, d_2 = 10.8 mm, d_3 = 13.0 mm 58
Table 4-15: Brownell equation regression parameters 60

Table 4-16: Koekemoer voidage model parameter values 62
Table 4-17: Comparison of voidage models' performances 63
Table 4-18: A and B regressed for biochar particles..... 68
Table 4-19: Modifications of the Ergun Equation incorporating sphericity and the modified Reynolds number..... 70
Table 4-20: Modified Ergun Equation models' results 70
Table 4-21: Statistical models' equations 74
Table 4-22: α and β values for the polynomial models 75
Table 4-23: Statistical models' performance..... 77

NOMENCLATURE

Symbol	Meaning	Unit
ΔP	Pressure drop	(Pa)
A	Empirical viscous energy loss constant	(dimensionless)
a	Loosening effect parameter	(dimensionless)
A_p	Particle surface area	(m^2)
B	Empirical kinetic energy loss constant	(dimensionless)
b	Wall effect parameter	(dimensionless)
c	Wedge effect parameter	(dimensionless)
D	Column diameter	(m)
d_p	Particle diameter	(m)
g	Gravitational acceleration constant	(m/s^2)
h_p	Height of cylindrical particle	(m)
L	Length of packed bed	(m)
n	Total number of particles/samples	#
Re	Reynolds number	(dimensionless)
Re_m	Modified Reynolds number for packed beds	(dimensionless)
s	Ratio between the small and large particle size	(-)
U	Gas flow velocity	(m/s)
V_p	Particle volume	(m^3)
X_i	Volume fraction	(dimensionless)
Greek symbols		
α	Coefficient parameter	(dimensionless)
β	Coefficient parameter	(dimensionless)
ε	Bed voidage	(dimensionless)
f	friction fraction of fluid flowing over a particle	(dimensionless)
μ	dynamic viscosity of fluid	(Pa.s)
ρ	fluid density	(kg/m^3)
φ	Particle sphericity	(dimensionless)
Acronyms		
PFD	Process flow diagram	(-)
RMSE	Root mean squared error	(-)
RSD	Relative standard deviation	(dimensionless)

1. INTRODUCTION

1.1 BACKGROUND AND MOTIVATION

The knowledge of pressure drop over packed beds of particles is deemed essential for fixed bed systems because it influences the capital costs of such processs units. Pressure drop per meter is also important for designing and sizing fixed bed gasifiers and filters, of which are common fixed bed applications. Modelling pressure drop per meter also helps engineers to specify compressors and pumps required to overcome the pressure drops for gasifiers and filters (Bock *et al.*, 2021).

Pressure drop over gasifiers is an important parameter for engineers and operators. Pressure drop influences reaction kinetics, heat transfer and mass transfer effects. According to Fogler, a more significant pressure differential will also allow reactants to be consumed more effectively during gas-phase reactions (Fogler, 2016). Larger pressure differentials over fixed bed systems also require more work to be done by the compressor that forces gas through a packed bed (Jacobs, 1976).

Engineers consider pressure drop a crucial parameter during the design of gasifiers and filters. While this phenomenon is relevant to fluidized bed and entrained flow gasifiers, this research will predominantly concentrate on its significance in fixed bed types. It is also necessary to understand packing characteristics, such as bed voidage of the materials in the system, to be able to model pressure drop (Koekemoer & Luckos, 2015). The pressure differential for fluid flow through a packed bed of particles has long been known to be governed by the summation of viscous energy loss, which is proportional to the fluid velocity, and a kinetic energy loss which is proportional to the velocity squared. The two approaches that help describe flow through packed beds are the discrete particle model and the pipe flow analogy. The Ergun equation is an example of a model based on the pipe flow analogy. The Ergun equation is used to predict the pressure drop of gases flowing through fixed beds and determine the system's energy throughput (Macdonald *et al.*, 1979).

An effective particle diameter, effective bed voidage and a particle shape factor, typically sphericity, are three essential parameters that are used in the Ergun equation (Koekemoer & Luckos, 2015). Most researchers make use of the volume-to-surface-area mean diameter as an effective particle diameter. The traditional way of determining sphericity is by using particles' envelope volume and surface area, while the bed voidage is usually determined by liquid submersion experiments. Due to the irregular shapes of particles determining the envelope volume and surface area is generally done by volume displacement of a solid or liquid medium, with the disadvantage of the latter being that a fluid medium might be absorbed into the pores of wood or charcoal particles (Webb, 2001). The same will happen to the

particles during the bed voidage determination experiments. Bed voidage is determined by either submerging a bed of particles in a liquid with known density or by knowing the particle density and bulk density of the bed (Mandal *et al.*, 2013).

The global energy supply and demand rely heavily on fossil fuels. However, energy generation using fossil fuels damages the environment, and these resources are finite. The world's energy demand will only increase, thus, the need for more renewable alternatives for energy generation will also increase (Jahromi *et al.*, 2020).

Biomass feedstocks, such as wood or biochar, can also be used in gasifiers to make producer gas which can be used as a fuel gas. This gas can be burned for cooking purposes, fuel for internal combustion engines and some applications use producer gas in gas turbines for small-scale electricity production. Producer gas is formed by the gasification of biomass, such as charcoal and is a mixture composed of carbon monoxide, hydrogen, nitrogen and carbon dioxide (Sheth & Babu, 2009). This is achieved by exposing the biomass to high temperatures (>700˚C) by limiting the amount of oxidising agent in the gasifier. Common oxidising agents include air, pure oxygen and steam (Jahromi et al., 2020).

Biochar can also used in filter applications to remove microbes from wastewater (Perez-Mercado et al., 2019). Biochar particles have irregular shapes and are porous, making it difficult to determine some parameters needed to operate and design gasifiers (Salam & Bhattacharya, 2006). Two of these parameters include particle sphericity and bed voidage.

Previous studies reported that different types of particles have unique packing arrangements. This results in the packed particles having unique friction factors and consequently, laboratory tests must usually be done to obtain empirical relations that can be used for predicting pressure drop, especially for non-spherical particles (Allen *et al.*, 2013).

It would be advantageous to gain knowledge of pressure drop behaviour in packed beds of wood and charcoal particles if these feedstocks are used more in the future.

1.2 PROBLEM STATEMENT

The study of pressure drop in fixed-bed gasifiers fed with biomass particles is underexplored compared to other feedstock particle types. Determining essential parameters for pressure drop modelling, such as sphericity and bed voidage, is labour-intensive and necessary for every new gasifier design because of the lack of universally applicable models. Additional research is needed to investigate the influence of different-sized particle mixtures on bed voidage and pressure drop in biomass-packed beds to provide insights into design considerations and operational behaviour.

1.3 AIM AND OBJECTIVES

Aim: To model pressure drop over a fixed bed of biomass char particles by studying the effect of the particles' characteristics on fixed bed structure.

Objectives:

- Determine which of a particle's shape characteristics influence the bed voidage for different size biomass char particles when packed in binary and ternary mixtures.
- Evaluate the effects of particle and packing characteristics in fixed beds of biomass char on measured and modelled pressure drop values

1.4 SCOPE

The study required analysis to be done of 5 batches of biochar particles varying in size.

- Binary and ternary mixtures were then made from these 5 batches. The char particles were supplied by Ignite Products.
- The char particles were crushed, washed, and left to air dry. The dried particles were sieved to separate them into 5 batches.
- The particles in the 5 batches were characterised using Rhovol equipment from Debtech to acquire particle diameters and sphericities.

Experiments were conducted to determine bed voidage of 5 pure sized batches (referred to as mono-sized batches), binary and ternary mixtures.

- The voidage experiments were conducted by submerging the particle bed in water
- After the voidage experiments, the particles were left to air dry and sieved back into their respective batches.
- Gas flow pressure drop experiments were conducted through the mono-sized, binary and ternary mixtures.
- The gas used was compressed air. After the pressure drop experiments, the particles were sieved back into their original batches.

Modelling of bed voidage was done by making use of known linear and non-linear models. Regression was done on the empirical variables of these models to fit the modelled voidage values closer to the experimental voidage values. Pressure drop was modelled using known models derived from fundamental principles and statistical approximations. Results from the pressure drop experiments were used to regress empirical variables for the pressure drop models.

Limitations of the study include:

- Only one char particle type was considered.
- Only fixed bed systems were investigated.

1.5 STUDY OUTLINE

The study comprises 5 chapters, including an introduction, literature review, methodology, results discussion and conclusions and recommendations.

- The literature review gives details about the modelling of gas flow pressure drop through packed beds. Commonly used models for different particle types are then introduced. Through these models, the parameters required to model pressure drop through packed beds are discussed. Methods to model and determine these parameters are also discussed.
- The methodology describes how experiments were conducted and how models were chosen to model bed voidage and pressure drop. The methodology also includes the characterisation results for the mono-sized char particle batches.
- The results and discussions chapter show and elaborate on the bed voidage and pressure drop experimental results along with the modelling results.
- The final chapter outline the conclusions and recommendations for this study. The different models used for voidage and pressure drop per meter are compared and commented on.

2. LITERATURE REVIEW

The literature review provides a background of pressure drop modelling. Methods on experimentation and particle characterisation are discussed. This chapter also provide reviews of models used for pressure drop and voidage modelling.

2.1 BIOMASS IN ENGINEERING

Biomass feedstocks can be used to produce biofuels via processes such as gasification. The use of biomass and biofuels have recieved attention as the drive towards cleaner energy increased. The carbon dioxide emissions resulting from the use of biofuels are regarded as zero due to the fact that the released CO_2 was retained from the atmosphere and captured during the process of photosynthesis. Biomass feedstocks also includes low amount of sulphur and nitrogen. This results in lower emissions of harmful gasses such as SO_2 and NO_x compounds. These advantages make biomass and biofuels attractive prospectives for renewable energy sources (Qian *et al.*, 2015). The use of biomass in gasifiers have also developed further than just feedstocks for such processes.

2.2 PRESSURE DROP MODELLING

Pressure drop through packed beds does not only occur due to the frictional resistance at a particle's surface. Pressure drop also occurs due to the expansion and contraction of the fluid flowing between the particles. Two main approaches exist to describe fluid flow through packed beds. This includes the discrete particle model and the more commonly used pipe flow analogy. The discrete particle model approximates flow through packed beds as if the bed consists of multiple distinct particles with their individual boundary layers. The pipe flow analogy assumes that fluid flow through packed beds can be described as fluid flowing through multiple equally sized tubes. The pipe flow analogy has been refined to produce the constricted tube model. The constricted tube model simulates flow through packed beds as a fluid flowing through channels of varying cross-sections and with multiple twists and turns. This refined model works well to simulate the varying dimensions and pores between particles in packed beds (Yang, 2003).

A fluid flowing through packed beds is described generally as a Newtonian fluid that follows Darcy's law at low Reynolds numbers. According to Darcy's law, a fluid's pressure gradient is proportional to the fluid's superficial velocity and viscosity (Li & Park, 1998). The total pressure drop across a fixed bed is given by the sum of frictional interactions between the fluid and particles and the gravitational potential difference of the fluid rising through the bed. This pressure drop is given by Equation 2-1 (Gibilaro, 2001).

$$\Delta P = \Delta P_{fr} + \rho_f g h \quad \textbf{2-1}$$

The frictional pressure drop for flow through packed beds is given by the sum of two energy loss terms. These terms include viscous energy losses (A) and kinetic energy losses (B) in proportion to the fluid velocity (U), as seen in Equation 2-2,

$$\frac{\Delta P_{fr}}{L} = AU + BU^2 \quad \textbf{2-2}$$

where ΔP is the pressure drop over a packed bed and L is the length of the bed. The A term is proportional to the fluid velocity, and the B term is proportional to the fluid velocity squared. The values of a and b are empirical parameters. These empirical parameters can be determined by measuring the ΔP and L values over a packed bed and varying the U values through experiments (Koekemoer & Luckos, 2015).

The Ergun equation is an example of a constricted tube model analogy and is used extensively to model pressure drop over packed beds. Ergun employs Blake's definition of the friction factor and Reynolds number, as seen in Equations 2-3 and 2-4.

$$f_b = \frac{\Delta P}{L}\frac{d_p}{\rho_f U^2 g}\frac{\varepsilon^3}{(1-\varepsilon)} \quad \textbf{2-3}$$

$$Re = \frac{\rho_f U d_p}{\mu(1-\varepsilon)} \quad \textbf{2-4}$$

(Yang, 2003)

Equation 2-5 shows the Ergun equation,

$$\frac{\Delta P_{fr}}{L} = A\frac{(1-\varepsilon)^2}{\varepsilon^3}\frac{\mu U}{(\varphi_s d_p)^2} + B\frac{(1-\varepsilon)}{\varepsilon^3}\frac{\rho_g U^2}{\varphi_s d_p} \quad \textbf{2-5}$$

(Koekemoer & Luckos, 2015)

The Ergun equation defines the pressure drop of fluid flowing through a packed bed as the sum of viscous and inertial energy losses. This definition makes the Ergun equation valid for laminar and turbulent flow regimes. The first term of Equation 2-5 corresponds to laminar flow and the second term corresponds to turbulent flow (Dukhan *et al.*, 2014). The A and B coefficients do not have any physical meaning on their own. The A and B values have been determined to be 150 and 1.75 respectively (Ergun, 1952).

The original Ergun equation had a few limitations. These limitations include:

- The fixed bed's composition is assumed to be homogeneous. It's assumed that the particles have been distributed uniformly throughout the bed.
- The fluid flowing through the bed is at steady state. The fluid flow is assumed to be fully developed.

- Interparticle forces are ignored. It's assumed that van der Waals forces and electrostatic interactions can be neglected.
- Only single-phase flow occurs throughout the fixed bed. It's assumed that no gas-liquid interactions occur as the fluid flows between the particles.
- The particles are assumed to be spherical.

The first 4 points of the limitations of the Ergun equation are widely assumed when modelling pressure drop through fixed beds. However, the last point of the particles being spherical is rarely the case. The original Ergun equation looked like Equation 2-5, except it didn't include the φ_s parameter. Later modifications started incorporating sphericity to get Equation 2-5. Even with the incorporation of sphericity in the Ergun equation, the values of A and B are still widely accepted to be 150 and 1.75 respectively (Koekemoer & Luckos, 2015).

In engineering applications, the particles will have discrete dimensions, and thus the packing particles will have different particle diameter (d_p) values. To compensate for this, the population diameter is described by a single value. This single value is usually described as the diameter mean. Table 2-1 shows a list of common diameter means (Markov *et al.*, 2022) used for sample sizing.

Table 2-1: Diameter mean for a sample of particles

Mean percentile	Equation	Common name
D_{10}	$D_{10} = \frac{\sum n_i d_i}{N}$	Arithmetic mean
D_{20}	$D_{20} = \left[\frac{\sum n_i d_i^2}{N}\right]^{\frac{1}{2}}$	Surface area mean
D_{50}	$D_{50} = \left[\frac{\sum n_i d_i^5}{N}\right]^{\frac{1}{5}}$	Median mean
D_{90}	$D_{90} = \left[\frac{\sum n_i d_i^9}{N}\right]^{\frac{1}{9}}$	-

The Sauter mean is a widely used mean diameter for characterising a sample's diameter. The Sauter mean is the diameter with the same volume-to-surface area ratio of an entire sample (Markov *et al.*, 2022). Equation 2-6 shows another way of how the Sauter mean can be calculated,

$$d_{pSM} = \frac{1}{\Sigma \frac{x_i}{d_{p,i}}} \quad \textbf{2-6}$$

where x_i is the mass or volume fraction of particles in size interval i and $d_{p,i}$ is the mean particle diameter of the i^{th} range (Koekemoer & Luckos, 2015).

Through experimentation, Sabri Ergun determined values for A and B of 150 and 1.75, respectively. The packing material he conducted the experiments with consisted of particles where φ_s equals values close to 1 (Ergun, 1952). Over time, researchers discovered that the values for A and B change when working with particles of different and irregular shape characteristics. A study from 2015 showed how the A and B constants vary for packed beds of coal, charred coal, and ash particles. Table 2-2 shows the results for the A and B constants from that study (Koekemoer & Luckos, 2015).

Table 2-2: Ergun constants for coal, charred coal and ash particles

Particle type	A	B
Coal	77.4	2.8
Charred coal	160.4	2.8
Ash	229.7	2.3

Particles ranged in +1.7 mm – 53 mm were used in the experiments to obtain the results for Table 2-2. The results from Table 2-2 differ significantly from the results of the original constants regressed by Ergun. The Ergun equation with the values from Table 2-2 modelled pressure drop with a percentage error of less than 10%. The percentage error is defined in Equation 2-7 (Koekemoer & Luckos, 2015).

$$Percentage\ error = \frac{100}{n}\sum_{i}\frac{|Experimental\ value - Modelled\ value|}{Experimental\ value} \qquad \textbf{2-7}$$

Table 2-3 shows A and B values gathered by Nemec et. al for cylindrical particles with varying dimensions and packing characteristics. The values for the Ergun constants varied significantly from their original values. The particles used in experiments to compile Table 2-3 were in the range of + 1.66 mm – 7.5 mm. The fluid flow regime experimented on for this study ranged in the laminar regime for 0 < Re < 1000. The values of A and B in Table 2-3 are all larger than the values of the original Ergun equation (Nemec & Levec, 2005).

The Ergun equation has also been modified extensively. Researchers have redefined specific parameters in the Ergun equation to define their modifications. Some of these modified versions of the Ergun equation are shown in Table 2-4. These models were tested using water and air as the fluid media. The modifications were found by redefining a particle's equivalent diameter, correlating the Ergun coefficients with Reynolds numbers, regression of exponential dependencies and investigating new empirical correlations for the friction pressure loss coefficient. The authors of these modified versions did not all provide the same information of

the bed and particle characteristics for their studies. The KTA model had one of the lowest percentage error when tested. The percentage error of the KTA model was 15% when subjected to new packing arrangements. Some of the other models' percentage errors ranged between 20% - 40% (Kang, 2012). Some parameters were not specified, such as the column-to-particle diameter ratios and voidage ranges. The determination of the equivalent diameter for the packed beds were also not specified. All these studies did, however, specify the Re and/or Re_m ranges for which they have done their experiments.

Table 2-3: Ergun constants for cylindrical particles (Nemec & Levec, 2005)

$\frac{h_p}{d_p}$	φ_s	ε	A	B
0.37	0.757	0.418-0.500	280	4.60
0.72	0.862	0.323-0.490	190	2.70
0.91	0.872	0.336-0.588	200	2.50
1.00	0.874	0.363	200	2.00
1.00	0.874	0.350	180	2.00
1.33	0.866	0.368-0.420	210	1.90
1.91	0.835	0.334-0.682	210	2.50
2.94	0.782	0.437	240	2.40
3.81	0.722	0.402-0.492	230	2.50
5.77	0.762	0.484-0.526	250	2.50

Pressure drop due to wall effects of some particles in packing arrangements were found to be prominent when D/d_p = 3.65. The study by (Kang, 2012) found that pressure drop models did not always work for specific ranges of D/d_p and Re_m. Some models only performed well at certain exact values for D/d_p and Re_m. The KTA model performed well when D/d_p had values of 19, 9.5 and 6.33. When D/d_p = 3.65, the KTA model overpredicted pressure drop values from experimental results. This is speculated to be the result of wall effects becoming prominent in that range (Kang, 2012). The D/d_p = 3.65 ratio is somewhat lower than findings by other publications. A publication by (Nemec & Levec, 2005) stated that pressure drop due to wall effects become prominent when D/d_p < 10.

Table 2-4: Ergun Equation modifications

Model	Equation	ε	$\frac{D}{d_p}$	Re/Rem
Handley & Heggs	$\frac{\Delta P}{L} = 368\left(\frac{(1-\varepsilon)^2}{\varepsilon^3}\right)\left(\frac{\mu U}{d_p^2}\right) + 1.24\left(\frac{\rho U^2}{d_p}\right)\left(\frac{1-\varepsilon}{\varepsilon^3}\right)$	0.390	8-24	399 < Re < 3985
Yu et al.	$\frac{\Delta P}{L} = 203\left(\frac{(1-\varepsilon)^2}{\varepsilon^3}\right)\left(\frac{\mu U}{d_p^2}\right) + 1.95\left(\frac{\rho U^2}{d_p}\right)\left(\frac{1-\varepsilon}{\varepsilon^3}\right)$	0.364 – 0.379	30	797 < Re < 2449
Montillet	$\frac{\Delta P}{L} = \left(\frac{1410}{Re} + 16 + \frac{45}{Re^{0.45}}\right)\left(\frac{\rho U^2}{d_p}\right)$	0.367	12.2	30 < Re < 1500
Wentz & Thodos	$\frac{\Delta P}{L} = \left(\frac{(1-\varepsilon)^2}{\varepsilon^3}\right)\left(\frac{0.396 Re_m}{{Re_m}^{0.05}} - 120\right)\left(\frac{\rho U^2}{d_p}\right)$	0.354 – 0.882	11.2	1460 < Re < 7661
Tallmadge	$\frac{\Delta P}{L} = \left(\frac{(1-\varepsilon)^2}{\varepsilon^3}\right)\left(\frac{\mu U}{d_p^2}\right)(150 + 4.2{Re_m}^{0.833})$	-	-	0.1 < Re < 10^5
KTA	$\frac{\Delta P}{L} = \left(\frac{320}{\left(\frac{Re}{1-\varepsilon}\right)} + \frac{6}{\left(\frac{Re}{(1-\varepsilon)}\right)^{0.1}}\right)\left(\frac{1-\varepsilon}{\varepsilon^3}\right)\left(\frac{U^2}{2d_p}\right)$	0.36 – 0.42	-	10 < Re_m < 10^5
Brauer	$\frac{\Delta P}{L} = \left(160 + 3.1{Re_m}^{0.9}\right)\left(\frac{\mu U}{d_p^2}\right)\left(\frac{(1-\varepsilon)^2}{\varepsilon^3}\right)$	-	-	2 < Re_m < 20 000
Foscolo	$\frac{\Delta P}{L} = 1.73\left(\frac{1-\varepsilon}{\varepsilon^{4.8}}\right)\left(\frac{\mu U}{d_p^2}\right) + 0.336\left(\frac{1-\varepsilon}{\varepsilon^{4.8}}\right)\left(\frac{\rho U^2}{d_p}\right)$	-	-	0.2 < Re < 500

From these models in Table 2-4 it can be seen that bed voidage plays a big part in pressure drop modelling through fixed beds. Unlike parameters such as fluid velocity, fluid viscosity, particle diameter and fluid density, bed voidage is a parameter that's not as easy to specify, or gain information of. Bed voidage values can have a significant impact on modelled pressure drop. An decreased voidage value of 20% can increase pressure drop by 300% (Koekemoer & Luckos, 2015). It's therefore advantageous to be able to model such a parameter along with pressure drop.

2.3 BED VOIDAGE MEASUREMENT AND MODELLING

Bed voidage is defined as the fraction of volume occupied by a gas that passes through a bed of particles. Studies have found that bed voidage can be correlated with mixtures of different-sized materials (Liu *et al.*, 2020).

Multiple methods exist to determine the bed voidage of packed beds. A common method that is used for relatively heavy particles such as coal is based on liquid displacement. A column containing packing material is filled with a liquid of known density. If the packing material is porous, the liquid is allowed to saturate the pores over time to let the column be filled completely. When the column is filled, the liquid is drained from the column and weighed. This

allows the volume unoccupied by the packing material to be measured where the gas will flow between particles in a fixed bed (Koekemoer & Luckos, 2015).

X-ray tomography is another method to determine bed voidage. Computed tomography (CT) and numerical simulation have been combined to evaluate pore structures in sinter cakes. Voidage values obtained with CT were compared with values measured by the traditional mercury intrusion method commonly used when working with sinter cakes. The results showed that CT has as many advantages as the traditional mercury method. The biggest advantage of the CT method is that it can distinguish between open and closed pores (Zhou *et al.*, 2017).

Another method is by slicing casts made with packed beds and incorporating image analysis. This method includes filling a bed of particles with an epoxy resin that preferably does not shrink when it hardens. The hardened resin block is then cut into multiple slices. Digital images can be taken of the flat sides of the slices. Image processing software counts pixels with different colours and determine an average bed voidage using images of all the slices (Hamel & Krumm, 2008).

Biomass particles are usually relatively lightweight particles. Charcoal particles usually have specific gravity (SG) values of around 0.3 (Samarawickrama *et al.*, 2020). These low SG values make it difficult to use a liquid such as water to determine the bed voidage since the particles will float on water and additional precautions would have to be made to ensure that the particles do not escape from the column. Table 2-5 show voidage ranges for biomass and biochar particle beds. The voidage for these particle types range between 0.2 – 0.64 and can go up to 0.75 for pelletised particles.

Table 2-5: Bed voidage ranges for biomass and biochars

Particle type	Particle diameter (mm)	D/d_p	Voidage
Almond shells	1	60	0.4 – 0.6
Pine bark	2 - 6	8.3 - 25	0.2 – 0.6
Sugarcane bagasse	0.25 – 1.75	104 - 728	0.5
Wood pellets	4.1 – 47.5	2 - 23.1	0.32 – 0.40
Milled wheat straw pellets	0.50 – 0.85	106 - 180	0.39 – 0.75
Crushed charred spruce	0.18 – 7.10	6 - 225	0.2 – 0.5
Activated carbon	1 - 2	80 - 160	0.55
Granular activated carbon	0.41 – 6.05	9 - 139	0.47 – 0.64

Linear and non-linear models have been derived to model bed voidage in packed beds with multi-sized particles. An early and simple linear voidage model for binary mixtures was the

Fumas model. Equations 2-8 to 2-10 shows the Fumas model. The Fumas model made use of the diameters of the fine (d_1) and coarse (d_2) particles (Liu *et al.*, 2020).

$$\varepsilon_1 * = (1 + \varepsilon_2) \cdot d_2 - 1 \quad \textbf{2-8}$$

$$\varepsilon_2 * = d_2 + (1 + \varepsilon_1) \cdot d_1 - 1 \quad \textbf{2-9}$$

$$\varepsilon_{min} = \max(\varepsilon_i *), i = 1,2 \quad \textbf{2-10}$$

The Fumas model considered that smaller particles fill the voids between larger particles and do not alter the total volume of the packed bed. This model proved to become inaccurate when the ratio between the diameters of the fine particles and coarse particles (s) became larger. As the s value increase, the interaction between the particles increased as well. During the mixing process of particles of different sizes, phenomena such as loosening, wall and wedging effects become more prominent. The wall effect for voidage should not be confused with the wall effect for pressure drop of a fluid flowing through a pipe. Loosening occurs when the finer particles are too large to fit into the void between the coarse particles. This causes the coarse particles to be forced out by the fine particles and the total bed voidage to increase. The wall effect happens when the fine particles wrap around the coarse particles and generate pores on the surface of the coarse particles. Wedging happens when the voids between the coarse particles are formed due to the trapping of fine particles in the narrow gaps of the coarse particles when the coarse particles are dominant. Wedging also happens when the fine particles are dominant, and gaps form in adjacent particles due to the wrapping of fine particles. Figure 2-1 show an illustration of these effects. The loosening, wall and wedging effects increase as the bed's particles have low sphericity values. The Fumas model does not take these effects into consideration. The wedging effect increases bed voidage when the gaps between the coarse particles are not large enough to hold an entire layer of fine particles. These complicated effects have only been related to particle sizes (Liu et al., 2020).

Other linear packing models which have been refined to include these effects are shown in Table 2-6. Figure 2-2 is a graphical representation of the symbols used in the equations in Table 2-6. Voidage models are usually empirical or semi-empirical in nature. Fundamental models are not commonly incorporated for this type of modelling. These empirical and semi-empirical models have been proven to be useful in modelling discrete and continuous particulate mixtures. The parameter that has the highest impact on most voidage models is the ratio between the size of the fine particles to the coarse particles (s). Loosening, wall and wedging effects become more prominent for higher s ratios. Most voidage models usually perform well for smaller s values, but their accuracy decreases as s increase (Liu et al., 2020).

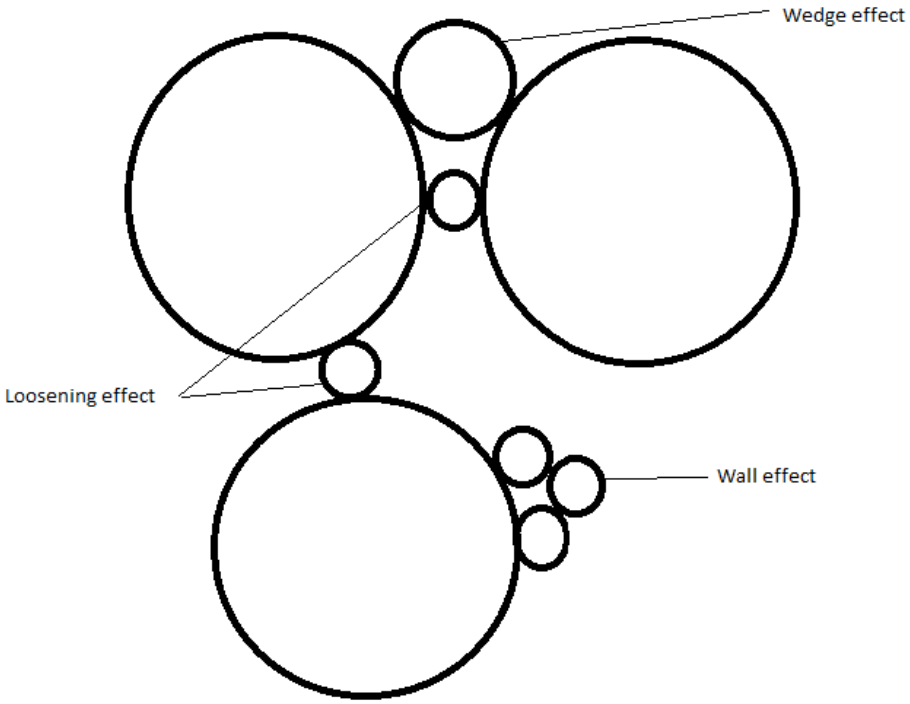

Figure 2-1: Packing parameters of bed voidage modelling

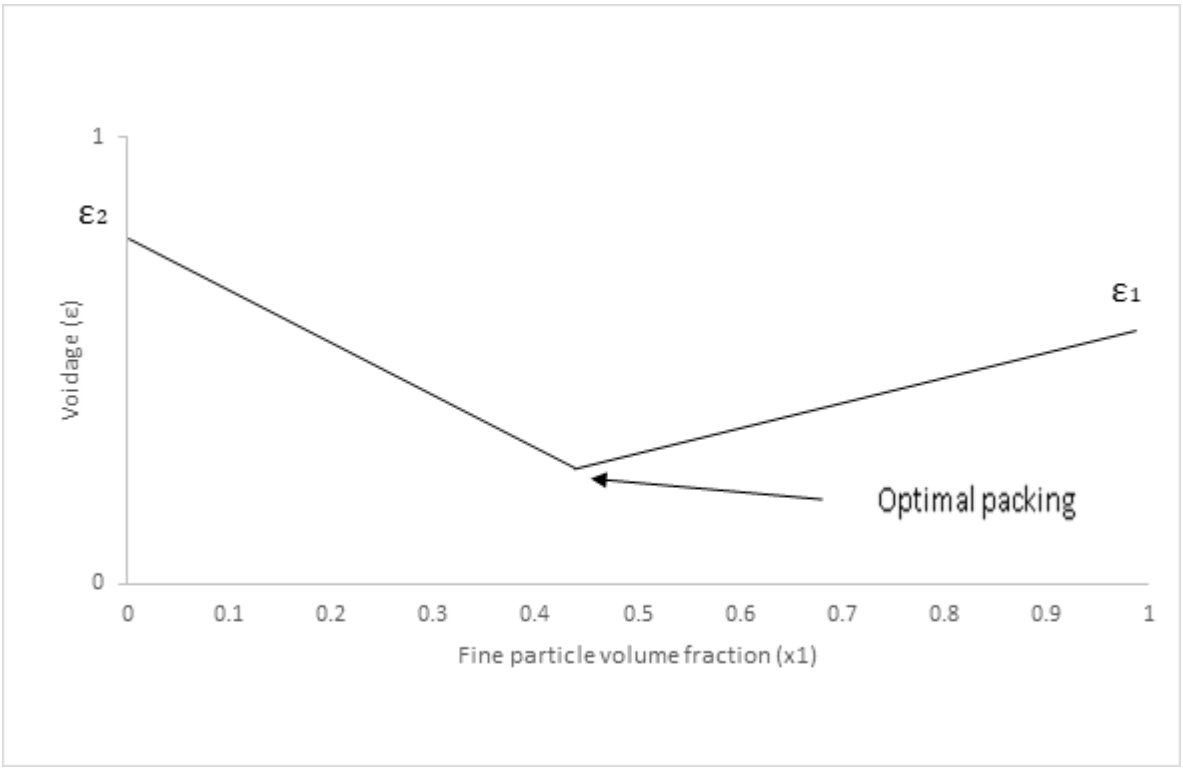

Figure 2-2: Binary voidage diagram and model parameters

Table 2-6: Linear bed voidage models for binary mixtures

Model name	Equation	
Aim & Golf minimum ε of size 1	$\varepsilon_1 = (1 + \varepsilon_2)(1 - x_1) - 1$	**2-11**
Aim & Golf minimum ε of size 2	$\varepsilon_2 = (1 + \varepsilon_1)(1 - x_1)b_{AGM} - 1$	**2-12**
Aim & Golf wall effect b_{AGM}	$b = 1 + 0.9s$	**2-13**
Aim & Golf minimum ε of mixture	$\varepsilon_{min} = \max(\varepsilon_i)$	**2-14**
LPD minimum ε of certain particle size j	$\varepsilon_j^* = \left[1 - x_j \sum_{j=i+1}^{n} \left(1 - \frac{\varepsilon_j}{1+\varepsilon_i} - b_{LPD}\frac{\varepsilon_j}{1+\varepsilon_i}\right) - x_j \sum_{j=1}^{i=1}(1 - a_{LPD}\frac{1+\varepsilon_j}{1+\varepsilon_i})\right]$	**2-15**
a_{LPD}: Loosening effect parameter	$a_{LPD} = 1 - (1-s)^{3.3} - 2.8s(1-s)^{2.7}$	**2-16**
b_{LPD}: wall effect parameter	$b_{LPD} = 1 - (1-s)^2 - 0.4s(1-s)^{3.7}$	**2-17**
s: Characteristic diameter ratio	$s = \frac{d_i}{d_j}\ ,\ i < j$	**2-18**

Toufar considered the wall effect between spherical particles in binary mixtures and developed the non-linear Toufar model. The wall effect parameter of the Toufar model is a function of the voidage values of the mono-sized batches from which the binary mixtures are composed of and the solid volume fraction. Previous studies have shown that the Toufar model performed well for particles with diameters up to 16mm (Jones, 2001). The Toufar model's modelled values, however, have large deviations when the volume fraction of the fine particles are small (Liu *et al.*, 2020). The Toufar model is shown in Table 2-7.

Table 2-7: Toufar voidage model

Model/parameter name	Equation	
Toufar model voidage ($\varepsilon_{\mathrm{TM}}$)	$\varepsilon_{TM} = (1 + \varepsilon_1)x_1 + (1 + \varepsilon_2)x_2 + k_d b_{TM} \varepsilon_2 x_2 - 1$	**2-19**
k_d	$k_d = \frac{d_2 - d_1}{d_2 + d_1}$	**2-20**
b_{TM}	$b_{TM} = 1 - \frac{1 + 4z}{(1 + z)^4}$	**2-21**
z	$z = \frac{(1 + \varepsilon_1)x_1}{\varepsilon_2 x_2}$	**2-22**

The Toufar model only considered the wall effect packing parameter. The wall effect of the Toufar model is a function of the finer particles' initial voidage and the volume fractions of both the fine and coarse particles. The Toufar model, however, tended to deviate significantly at lower s values. The modified Toufar model performed slightly better than the original Toufar model when tested with quartz sand. The modified Toufar model increased the model performance at lower s values. For some binary mixtures, the modified Toufar model's accuracy was slightly lower than the original Toufar model at higher s values. The s values for the binary mixtures ranged between $0.248 \leq s \leq 0.500$ in this study. The performance of the Toufar model and the Modified Toufar model is expected to decrease further for s values higher than 0.5 (Liu *et al.*, 2020).

A general problem for the binary voidage models was that the experimental and modelled values differed significantly when the solid volume fraction and the optimum volumetric fraction values were close to each other. Kwan considered wedging, wall and loosening effect parameters for spherical binary mixtures to minimise these differences. The particle type that Kwan considered to test his model were spherical glass beads up to 15.73mm in diameter (Kwan *et al.*, 2013). The Kwan model (KM) related the wedging effect to the solid volume fraction and modified the expressions. The Kwan model does not relate the wedging effect to the optimal voidage ratio. The empirical loosening, wall and wedging effect expressions were then further modified through regression analysis to create the modified Kwan model. The loosening effect's value for the modified Kwan model is usually higher than the original Kwan model's. The modified Kwan model's performance was generally good for quartz particles (Liu *et al.*, 2020). The Kwan model and modified Kwan models are shown in Table 2-8.

Table 2-8: Kwan and modified Kwan voidage models

Model/parameter name	Equation	
Minimum ε_{KM} of size 1	$\varepsilon_1^* = (1 + \varepsilon_1)x_1 + (1 + \varepsilon_2)x_2 - (1 - a_{KM})(1 + \varepsilon_1)x_1\left[1 - c_{KM}\left(\frac{x_1}{x^*}\right)^2\right] - 1$	**2-23**
Minimum ε_{KM} of size 2	$\varepsilon_2^* = (1 + \varepsilon_1)x_1 + (1 + \varepsilon_2)x_2 - (1 - b_{KM})\varepsilon_2 x_2\left[1 - c_{KM}\left(\frac{x_2}{1 - x^*}\right)^2\right] - 1$	**2-24**
a_{KM}	$a_{KM} = 1 - (1 - s)^{3.3} - 2.6s(1 - s)^{3.6}$	**2-25**
b_{KM}	$b_{KM} = 1 - (1 - s)^{1.9} - 2s(1 - s)^6$	**2-26**
c_{KM}	$c_{KM} = 0.322\ tanh\ (11.9s)$	**2-27**
ε_{KM}	$\varepsilon_{KM} = max(\varepsilon_i^*)\,, i = 1{,}2$	**2-28**
Minimum ε_{MKM} of size 1	$\varepsilon_1^* = (1 + \varepsilon_1)x_1 + (1 + \varepsilon_2)x_2 - (1 - a_{MKM})(1 + \varepsilon_1)x_1[1 - c_{MKM}(3.8^{x_1} - 1)] - 1$	**2-29**
Minimum ε_{MKM} of size 2	$\varepsilon_2^* = (1 + \varepsilon_1)x_1 + (1 + \varepsilon_2)x_2 - (1 - b_{MKM})(\varepsilon_2 x_2)x_1[1 - c_{MKM}(2.6^{x_2} - 1)] - 1$	**2-30**
a_{MKM}	$a_{KM} = 1 - (1 - s)^5 - 1.s(1 - s)^{3.1}$	**2-31**
b_{MKM}	$b_{KM} = 1 - (1 - s)^{1.9} - 2.1s(1 - s)^{10.5} - 0.2(1 - s)^{7.6}$	**2-32**
c_{MKM}	$c_{KM} = 0.335\ tanh\ (26.9s)$	**2-33**
ε_{MKM}	$\varepsilon_{KM} = max(\varepsilon_i^*)\,, i = 1{,}2$	**2-34**

The study of (Liu *et al.*, 2020) made use of the root mean squared error (RMSE) to determine the models' accuracy. Equation 2-35 shows how the RMSE is calculated.

$$RMSE = \sqrt{\frac{\sum_{i=1}^{n}(experimental\ value - modelled\ value)^2}{n}} \quad \textbf{2-35}$$

Table 2-9 shows RMSE results of Equations 2-11 to 2-34 with spherical particles and quartz sand.

Table 2-9: Linear voidage model RMSE comparison

Model	Particle type	Average RMSE
AG	Quartz sand	0.086
LPD	Quartz sand	0.056
Toufar	Quartz sand	0.039
Kwan	Quartz sand	0.033
Modified Kwan	Quartz sand	0.027
Kwan	Glass beads	0.022
Modified Kwan	Glass beads	0.034

(Liu *et al.*, 2020)

The particles tested in Table 2-9 ranged between 0.075 – 0.2 mm. The voidage values modelled ranged between 0.24 – 0.76. All models produced relatively satisfactory results. The AGM's RMSE increased as the value for s increased. This indicates that the AG model becomes less accurate with a wider PSD. The average RMSE for the LPD model stayed relatively constant for $0.0 < s < 0.5$ and quartz sand. The RMSE values of the TM, KM and MKM was also relatively constant for $0.0 < s < 0.5$ and quartz sand. The MKM's average RMSE was less than the KM for spherical particles (Liu *et al.*, 2020).

Wong derived a voidage model for ternary mixtures by modifying models originally developed for binary mixtures. Most binary models assume that a bed's specific volume is a linear function of the volumetric size ratios of the bed's particles. The specific volume is the ratio of the bulk volume of a bed to the volume of the particles. Wong derived 2 separate models. The first model only considered loosening and wall effects. The second model included wedging effects along with loosening and wall effects. Wong's model does not assume that correlation is linear. Wong's models were tested using spherical glass beads ranging from 1.43mm to 15.73mm. This model does not assume voidage to be a linear function of volumetric fractions and works on the basis of a dominant particle class. The 2-parameter model that Wong derived

had a maximum relative error of 9.03%. The 2-parameter model generally overestimated the voidage values from experimental results. Wong's 3-parameter model generally overestimated the modelled values in relation to the experimental values with a maximum relative error of 2.69%. The 3-parameter model performed much better than the 2-parameter model Wong's ternary model is shown in Table 2-10 (Wong & Kwan, 2014).

Table 2-10: Wong voidage model

Model/parameter name	Equation	
ε_{WM} if fine size class is dominant	$\frac{1}{\varepsilon_1^*} = \frac{1}{\varepsilon_T} - (1-b_{12})(1-\varepsilon_2)\frac{x_2}{\varepsilon_2}[1-c_{12}(2.6^{x_2+x_3}-1)] - (1-b_{13})(1-\varepsilon_3)\frac{x_3}{\varepsilon_3}[1 - c_{13}(2.6^{x_2+x_3}-1)]$	**2-36**
ε_{WM} if intermediate size class is dominant	$\frac{1}{\varepsilon_2^*} = \frac{1}{\varepsilon_T} - (1-a_{12})(1-\varepsilon_2)\frac{x_1}{\varepsilon_1}[1-c_{12}(3.8^{x_1}-1)] - (1-b_{23})(1-\varepsilon_3)\frac{x_3}{\varepsilon_3}[1-c_{23}(2.6^{x_3}-1)]$	**2-37**
ε_{WM} if coarse size class is dominant	$\frac{1}{\varepsilon_3^*} = \frac{1}{\varepsilon_T} - (1-a_{13})\frac{x_1}{\varepsilon_1}[1-c_{13}(3.8^{x_1}-1)] - (1-a_{23})(1-\varepsilon_{23})\frac{x_2}{\varepsilon_2}[1-c_{23}(3.8^{x_2}-1)]$	**2-38**
ε_T	$\frac{1}{\varepsilon_T} = \frac{x_1}{\varepsilon_1} + \frac{x_2}{\varepsilon_2} + \frac{x_3}{\varepsilon_3}$	**2-39**
R_{ij}	$s = \frac{d_i}{d_j}, \ i < j$	**2-40**
a_{ij}	$a_{ij} = 1-(1-s)^{3.3} - 2.6s(1-s)^{3.6}$	**2-41**
b_{ij}	$b_{ij} = 1-(1-s)^{1.9} - 2s(1-s)^{6}$	**2-42**
c_{ij}	$c_{ij} = 0.322\ tanh\ (11.9s)$	**2-43**

De Larrard proposed a discrete voidage model for aggregate mixtures. The de Larrard (DL) model considers particle size interactions, loosening, and wall effects. The loosening and wall effects are defined differently from the previous models for the DL model. The DL model, with its loosening and wall effects, is shown in Table 2-11. A prerequisite for the DL model is that

d_{min}/d_{max} > 0.1. The DL model could predict lab scale voidage results for limestone aggregates with an error of 2.5% and a standard deviation of 2%. (García-Cortés *et al.*, 2022).

Table 2-11: De Larrard voidage model

Model/parameter name	Equation	
ε_{DL}^{*}	$\varepsilon_i^* = \frac{\varepsilon_i}{1 - \sum_{j=1}^{i-1}\left[1 - \varepsilon_i + b\varepsilon_i\left(1 - \frac{1}{\varepsilon_j}\right)\right]x_j - \sum_{j=i+1}^{n}\left[1 - a\frac{\varepsilon_i}{\varepsilon_j}\right]x_j}$	**2-44**
a_{ij}	$a = \sqrt{1 - \left(1 - \frac{d_j}{d_i}\right)^{1.02}}$	**2-45**
b_{ij}	$b = 1 - \left(1 - \frac{d_i}{d_j}\right)^{1.50}$	**2-46**
ε_{DL}	$\varepsilon_{DL} = min(\varepsilon_i^*), i = 1,2,3$	**2-47**

For mixtures with wide particle size distributions, the voidage decrease as the finer particles fill the gaps between the coarse particles. The overall performance of the DL model was good. The maximum percentage error tested was 5% and with a mean percentage error of lower than 2%. These tests were conducted with natural limestone and electric arc furnace slag aggregates. The mixtures consisted of particles ranging from 4mm – 22mm. (García-Cortés *et al.*, 2022).

Chang et al. developed a voidage model which also incorporated the loosening and wall effects. Chang's model also considers a dominant particle size for voidage modelling. The model was tested for glass beads and sand. The glass beads' diameters ranged from 1.43mm – 15.73mm. The sand particles' diameters ranged from 0.089nm – 4.47mm. This showed that Chang's model worked for a wide range of particle sizes. This model is also derived from a linear model but is itself not a linear model. The maximum percentage error of the linear model from which Chang derived his model was 8.65%. The maximum percentage error of Chang's model for glass beads and sand particles was 2.58%. Chang's model showed a significant improvement from the linear model from which it was derived. Chang's model slightly under-predicted its overall voidage results. Table 2-12 shows the Chang model (Chang & Deng, 2018).

Table 2-12: Chang's voidage model

Model/parameter name	Equation	
ε^*_{Chang}	$\varepsilon_i^* = \sum_{j=1}^{i-1}[\varepsilon_j - a\varepsilon_j]x_j + \varepsilon_i x_i + \sum_{j=i+1}^{n}[\varepsilon_j - b(\varepsilon_j + 1)]$	**2-48**
a_{ij}	$a = 1 - \left(1 - \frac{d_j}{d_i}\right)^p \; for\; d_i > d_j$	**2-49**
	$a = 0\; for\; d_i \leq d_j$	
b_{ij}	$b = 1 - \left(1 - \frac{d_i}{d_j}\right)^q \; for \; for\; d_i < d_j$	**2-50**
	$b = 0\; for\; d_i \geq d_j$	
ε_{Chang}	$\varepsilon = \max(\varepsilon_i^*)\,, i = 1,2,3$	**2-51**

Chang's model regressed the values for p and q as 2.4 and 1.5, respectively, for the spherical ball bearings. The regressed values for p and q for non-spherical glass beads were found to be 3.08 and 1.88. The regressed values for p and q for non-spherical sand particles were found to be 2.53 and 2.3, respectively (Chang & Deng, 2018).

The models discussed up to this point were derived for spherical particles. Most of the models were also tested on slightly less spherical particles and shown to still perform satisfactory. These models however have not been tested for particles with sphericity values of much lower than 1. Equation 2-52 show a correlation by Brownell et al. to determine bed voidage using sphericity. The sphericity and voidage ranges used for this correlation included $0.15 < \phi < 1.0$ and $0.25 < \varepsilon < 1.0$.

$$\varepsilon = 1.0 - 0.8648\phi + 0.2745\phi^2 \qquad \textbf{2-52}$$

Another study by Koekemoer et al. derived a model to determine voidage using the average particle diameter and PSD of the packed bed. The model was validated using coal, charred coal and ash. Equation 2-53 show the correlation between voidage and particle diameter and PSD. The Δd parameter is calculated using Equation 2-54. Values for a, b and c is shown in Table 2-13.

$$\varepsilon = a + bd_{psm} + c\Delta d \qquad \textbf{2-53}$$

$$\Delta d = \frac{d_{max} - d_{min}}{d_{psm}} \quad \textbf{2-54}$$

Table 2-13: Parameter values for Koekemoer's voidage equation

Particle type	a	b	c
Coal	0.430	0.061	-0.030
Charred coal	0.455	0.116	-0.039
Ash	0.494	0.055	-0.023

Table 2-14 show information regarding previously mentioned models and the particle types that was used for initial testing. Overall the models showed satisfactory results with modelling errors of less than 10%. Table 2-15 show the modelling performance of the same models for less spherical particles. The studies rarely, if ever give information on the sphericities of the particles they used. The models generally performed better for the more spherical particles they were derived for.

Table 2-14: Voidage models information

Model	Voidage range	Size range (mm)	D/d_p	Particle type	Modelling errors
AGM	0.12 – 0.40	Not mentioned	3 - 10	Spherical grains	< 9%
LPDM	0.60 – 0.85	6 - 28	Not mentioned	Spherical grains	< 10%
TM	TBA	TBA	TBA	Spherical grains	TBA
KM and MKM	0.58 – 0.75	1.43 – 15.73	13 - 140	Spherical grains	< 8%
WM	0.58 – 0.84	1.43 – 15.73	13 - 140	Spherical glass beads	< 1%
CPM	0.64 – 0.82	0.2 - 12	14 - 800	Aggregates Sand-slit	< 5%
CM	0.60 – 0.84	0.089 – 15.73	< 140	Ball bearings Steel shots Glass beads Sand	< 10%
BM	0.30 – 0.95	3.29 – 25.4	Not mentioned	Clay saddles Nickel Saddles Clay rings	< 11 %
KM	0.36 - 0.50	2.36 – 53.0	5.7 – 127.1	Coal Char Ash	< 3%

Table 2-15: Voidage models performance for other particles

Model	Voidage	D/d_p	Particle diameter (mm)	Particle type	Mean modelling error
Aim-Goff	0.28 - 0.76[a]	Not mentioned	0.075 - 2[a]	Quartz sand	16.1%
LPDM	0.28 - 0.76[a] 0.62 - 0.88[b]	Not mentioned	0.075 - 2[a] 6 - 28[b]	Quartz sand Spherical grains and aggregates	10.3%
TM	0.28 - 0.76[a]	Not mentioned	0.075 - 2[a] 2 - 16[a]	Quartz sand coarse aggregates	10.6%
KM and MKM	0.28 - 0.76[a]	13 - 140[c]	0.075 - 2[a]	Quartz sand	
	0.58 - 0.84[c]		1.43 - 15.73[c]	Glass beads	7.1%
WM	0.58 - 0.84[c]	12 - 140[c]	1.43 - 15.73[c]	Glass beads	0.35%
CPM	0.5 - 0.7[d]	7 - 75[d]	2 - 22[d]	Limestone aggregates	6.2%
BM	0.4 - 1	TBA	TBA	TBA	TBA
KM	0.36 - 0.50	5.7 - 127.1	2.36 - 53.0	Coal Char Ash	< 5%

2.4 PARTICLE SPHERICITY

A particle's sphericity is an indication of how closely a particle resembles a perfect sphere. According to Equation 2-5, the pressure drop over a packed bed decreases as a particle's sphericity increases. Sphericity is a value between 0 and 1, which is calculated using Equation 2-55 (Liauchuk & Kovalev, 2017):

$$\varphi_s = \frac{\pi^{\frac{1}{3}}(6V_p)^{\frac{2}{3}}}{A_p} \qquad \textbf{2-55}$$

The volume of a particle is usually determined through the volume displacement of either solids, liquids, or gases. However, a particle's volume and surface area can become difficult to define. This makes Equation 2-55 less convenient to use in practice for a bed of particles. Different materials have different outer and inner characteristics. One of these characteristics is the particle's porosity. Porosity complicates the way researchers define a particle's characteristics, such as volume and surface area.

The envelope characteristic of a particle includes the sections of solid mass and voids within the particle. Envelope volume could be described as the volume of a particle if it was enveloped within a thin film. The skeletal volume includes the volume of closed pores within a particle but does not include the volume of open pores in a particle. The true volume of a particle does not include the volume of any voids within a porous particle. These volumes are represented in Figure 2-3 (Webb, 2001).

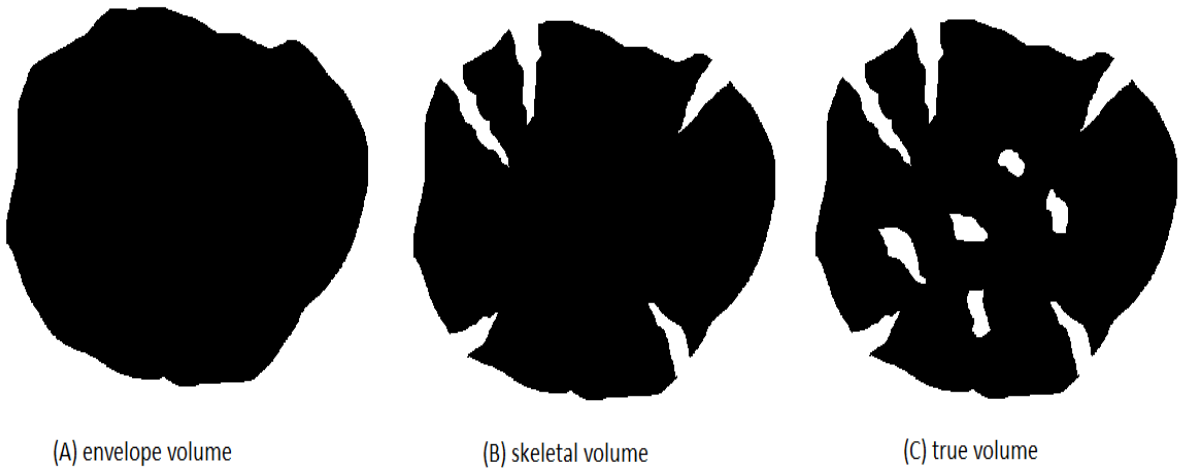

Figure 2-3: Different volume types

The envelope volume of a particle will influence the bed voidage of a fixed bed the most. Biomass particles, such as charcoal, have micropores (Pan *et al.*, 2019). These micropores do not make significant contributions to the packing density of fixed beds, as the pores are much smaller than the particles. This is why the true volume and skeletal volume of particles are not parameters of concern when studying bed voidage. A particle's envelope volume and (Webb, 2001) surface area are of more importance for determining the bed voidage and sphericity of a bed packed with particles with micropores. Determining the envelope volume of lightweight porous particles is challenging.

Density determination using the pycnometer for porous charcoal particles will determine its skeletal density; thus, it can't be used to determine the bed voidage of a bed packed with charcoal. The BET (Brunauer, Emmet, Teller) method is a common surface area determination method, but this method only determines a particle's skeletal surface area; thus, it can't be used to determine the sphericity of charcoal particles (Walter & Morse, 1984). A suitable method to define sphericity for microporous particles is by using intercept sphericity. The intercept sphericity is determined by Equation 2-56 (Zheng *et al.*, 2020).

$$\varphi = \left[\frac{d_2 d_3}{(d_1)^2}\right]^{\frac{1}{3}} \qquad \textbf{2-56}$$

Equation 2-56 make use of 3 dimensions through a particle where $d_1 > d_2 > d_3$. These 3 dimensions are at right angles to each other (Zheng *et al.*, 2020). Intercept sphericity is an indication of the volume relationship between a reference ellipsoid to a circumscribing sphere. Particle dimensional analysis is a convenient way of defining a particle's shape characteristics through image analysis. A particle's intercept sphericity can be obtained relatively easy with the aid of image analysis (Cruz-Matías *et al.*, 2019).

The Kozeny-Carman (KC) equation is used in fluid mechanics used to model a flowing fluid's pressure drop through fixed beds. The KC equation is shown in Equation 2-57:

$$\frac{\Delta P}{L} = \frac{180(1-\varepsilon)^2}{\varepsilon^3}\frac{\mu U}{(\varphi_s d_p)^2} \qquad \textbf{2-57}$$

Equation 2-57 is only valid for very low Reynolds numbers below 1, also known as creep flow. The KC equation is commonly used to back calculate sphericity with experimental pressure drop values (Flint & Selker, 2003).

Table 2-16 show sphericity values by studies conducted for biomass, biochar and coal materials. The sphericities for biomass and biochar are generally in lower ranges of < 0.6. Materials with flake shapes can have sphericities lower than 0.3.

Table 2-16: Biomass particles sphericities

Particle type	Particle size (mm)	Sphericity
Poplar	0.25 – 1.4	0.29 – 0.59
Pulverised wood	0.43 – 1.4	0.44 – 0.65
Wheat straw	0.43 – 1.4	0.33 – 0.55
Ground wood chips	3.2 – 12.7	0.44 – 0.73
Shredded wood chips	10	0.4
Mica flakes	Not mentioned	0.28
Coarse ground fiber	0.34	0.24
Fine ground fiber	0.21	0.46
Coarse ground rachis	0.71	0.27
Rice	1	0.36
Coffee husks	1.6	0.42
Coal	5 – 90	0.73 – 0.84
Charred coal	2.5 – 46.0	0.71 – 0.79
Ash	2.5 – 46.4	0.66 – 0.81

2.5 POLYNOMIAL MODELLING

In mathematics and statistics, polynomial functions are useful tools for non-fundamental modelling. Simple trends can be identified just by observing the shape of a curve relating a dependant variable to an independent variable. The Ergun equation states that pressure drop is a function of numerous different independent variables. Pressure drop is a quadratic function of particle diameter (Koekemoer & Luckos, 2015). Pressure drop can then be modelled as a polynomial function of these variables in the form of Equation 2-55:

$$f(x) = a_n x^n + a_{n-1} x^{n-1} + \ldots + a_1 x^1 + a_0 \qquad \textbf{2-55}$$

Another useful polynomial for quadratic approximations is the Padé polynomial. The Padé polynomial is in the form of 2-56.

$$f(x) = \frac{a_0 + a_1 x^1 + a_2 x^2 + \ldots + a_n x^n}{1 + b_1 x^1 + b_2 x^2 + \ldots + b_n x^n} \qquad \textbf{2-56}$$

3. METHODOLOGY

The methodology chapter describes the techniques used for particle characterisation, the experimental plan and the test models used.

3.1 MATERIALS

Charcoal was chosen to be the material for the pressure drop experiments. The charcoal was obtained from Ignite, which has offices in Johannesburg. Ignite's wattle lump wood charcoal consists of batches made from only a single type of wood.

3.2 SAMPLE PREPARATION

The charcoal was crushed with a jaw crusher and sieved into 5 size ranges that were used to make particle mixtures. The samples were then washed with tap water to get rid of dust accumulated on the particles' surfaces. The size ranges are shown in Table 3-1. The column for which the pressure drop experiments were used has an inner diameter (D) of 104mm.

Table 3-1: Batch particle sieve sizes

Batch no.	Particle sizes (mm)	Sample size (kg)
1	-4.75 +2.36	19
2	-6.70 +4.75	13
3	-9.50 +6.70	15
4	-11.2 +9.50	15
5	-13.2 +11.2	15

Binary and ternary mixtures were made from the 5 size ranges. These mixtures were varied of compositions made of multiplications of 10% for each size range. A total of 5 mono-sized batches, 90 binary mixtures and 360 ternary mixtures can be used for experiments in this configuration. Voidage experiments were done for all 455 of the mixtures and batches to compare and test the models from Table 2-5 to Table 2-11 for non-spherical particles.

3.3 PARTICLE SHAPE CHARACTERISATION

Debtech's Rhovol machines were used to characterise the particles' shape factors, such as the average particle diameter and intercept sphericity. The Rhovol fines model from the NWU campus and the coarse model on the De Beers Johannesburg campus was used. The Rhovol makes use of calliper values to determine a particle's shape characteristics. The Rhovol is self calibrated. Table 3-2 shows how the Rhovol calculates a particle's intercept sphericity (compactness), elongation and flatness.

Table 3-2: Rhovol Equations

Particle characteristic	Equation
Flatness	$\frac{b}{c}$
Elongation	$\frac{a}{b}$
Compactness/Sphericity	$\left(\frac{bc}{a^2}\right)^{\frac{1}{3}}$

(Debtech, 2022)

The relative standard deviation (RSD) was used to determine the variability of these values for each batch of particles. The RSD is calculated using Equation 3-1 (Kruisz *et al.*, 2021).

$$Relative\ Standard\ Deviation\ (RSD) = \frac{Sample\ Standard\ Deviation}{Mean} * 100 \qquad \textbf{3-1}$$

3.4 BED VOIDAGE DETERMINATION

The test column for the pressured drop experiments was also used for the voidage determination of the char particles. Bed voidage was obtained by filling the 104 mm x 1000 mm column with particles. The bed was only submerged halfway with water to prevent the bed from rising/floating. The submerged particles were left for 30 minutes to allow the particles' pores to saturate with liquid. Water was removed from the column and captured in a bucket of known mass. The bucket was then weighed to determine the weight of the water that occupied the space between the particles. The weight was then converted to volume to determine the voidage of the particle bed. The column was filled with char to a height of 1m, but only 0.5m of the bed was filled with water since the char particles have an SG value lower than 1. The particles were then removed from the column, left to dry, and sieved into their original size ranges.

3.5 PRESSURE DROP EXPERIMENTS

Pressure drop experiments were done on mixtures while varying the gas velocity between 0.05 m/s and 0.30 m/s. The 104 mm x 1000 mm column was filled completely with particles The experimental setup's instruments are shown in Table 3-3. A PFD of the setup is shown in Figure 3-1.

Table 3-3: Experimental setup instrument list

Equipment	Manufacturer	Unit	Range	Tolerance
Flow regulator and filter (MSB4)	Festo	-	-	-
Flow meter (SFAB-50U)	Festo	l/min	0 – 50	± (3% of measured value + 0.15)
Flow meter (SFAB-200U)	Festo	l/min	0 – 250	± (3% of measured value + 0.75)
Differential pressure cell (DPTH221)	Teren	Pa	0 – 125	± 0.625
Differential pressure cell (DPTH221)	Teren	Pa	0 – 1000	± 5

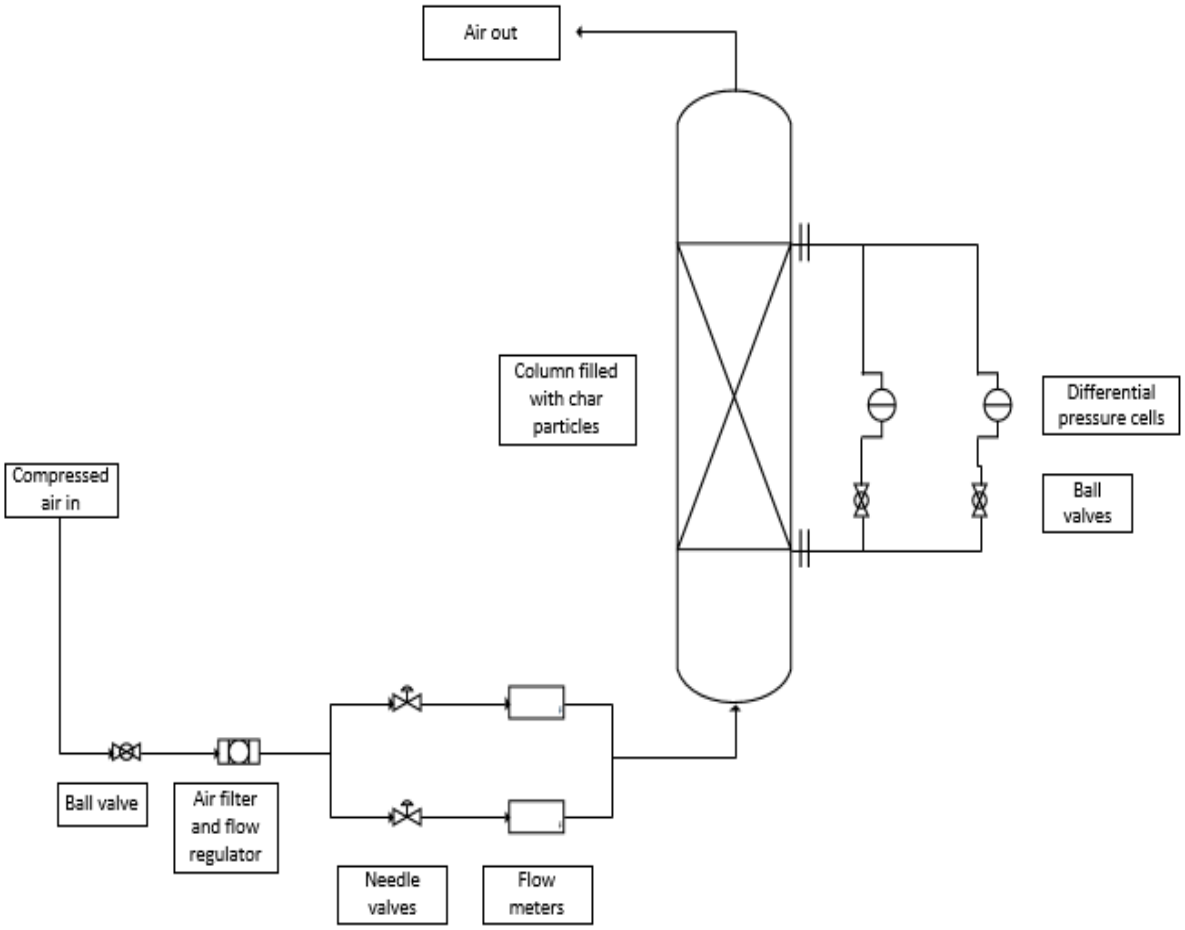

Figure 3-1: Pressure drop experimental setup

3.6 BINARY VOIDADE TEST MODELS

Seven models were tested for bed voidage. Four of the models were used for binary mixtures, and three models were used for ternary mixtures. The first two models for the binary mixtures are the Aim-Golf (AG) and LPD approximations. Their models are shown in Equations 2-11 to 2-14 and 2-15 to 2-18. The AG and LPD approximations are linear voidage models. The third and fourth models for the binary mixtures are the Toufar and Modified Kwan approximations. Their models are shown in Equations 2-19 to 2-22 and 2-29 to 2-34. Toufar and Modified Kwan approximations are non-linear voidage models. These Equations compare the performance of the linear and non-linear models for voidage modelling. The LPD model considers wall and loosening effects, while the AG model only considers the wall effect. The Toufar model only considers the wall effect. The modified Kwan model considers the loosening, wall and wedging effects. From all of these models, the consideration of these effects can be compared to the models' performances.

3.6 TERNARY VOIDADE TEST MODELS

The final three models were used to modelle the voidage for ternary mixtures. The Wong is shown in Equations 2-36 to 2-43. The DL is shown in Equations 2-44 to 2-47. The Chang model is shown in Equations 2-48 to 2-51. The Wong model considers loosening, wall and wedging effects. The DL and Chang model only consider the loosening and wall effects. The performance of the models and the consideration of some and all of these effects is discussed in Chapter 4.

3.7 PRESSURE DROP PER METER TEST MODELS

The pressure-drop models include the Ergun equation shown in Equation 2-5. The Ergun modifications used from Table 2-4 include the Tallmadge, KTA and Foscolo models. The models were chosen because they were previously proved to work for similar ε, D/d_p and Reynolds number values of the char samples.

3.8 VOIDAGE AND PRESSURE DROP REPEATABILITY AND UNCERTAINTY

Binary mixtures and mono-sized batches were used to determine the uncertainty levels of the voidage results. The uncertainty is calculated using Equation 3-2 :

$$Uncertainty = \frac{Max\ (range) - Min(range)}{Mean} * 100 \qquad \textbf{3-2}$$

For the voidage uncertainty, experiments were repeated 5 times using identical particles. After each experiment, the particles were removed from the column, and the same mixture was added to the column again to ensure that the particles' packing changed between the experiments.

4. RESULTS & DISCUSSION

This chapter shows and discusses the particle characterisation results. The performance of the models used to model voidage for mono-sized, binary and ternary char mixtures is also discussed. This chapter also shows the results for the models used to model fixed bed pressure drop for binary and ternary char mixtures.

4.1 PARTICLE CHARACTERISATION RESULTS

Table 4-1 shows the results of the Rhovol analysis of the particle batches.

Table 4-1: Particle characterisation results of the Rhovol analysis

Particle size range (mm)	MCD (mm)	MSS (mm)	Intercept sphericity (dimensionless)	Elongation (dimensionless)	Flatness (dimensionless)
-4.75 +2.36	4.50	3.65	0.559	1.93	2.01
-6.70 +4.75	6.72	5.45	0.575	1.74	2.13
-9.50 +6.70	8.16	6.62	0.553	1.96	2.11
-11.2 +9.50	10.8	9.01	0.578	2.02	1.72
-13.2 +11.2	13.0	10.8	0.584	1.83	1.89
Average	-	-	0.570	1.90	1.97

The elongation and flatness factors of all the particle batches had values ≈ 2. This suggests that the MCD values are so high relative to the actual minimum sieve that was used during sample preparation. The most extreme result, for example, was the MCD value of the -6.70 mm +4.75 mm range. The MCD value was 6.72, which is the only value higher than the top sieve that was used at 6.70 mm. This shows that the char particles fell upright through some sieves before falling on their sides on the bottom sieve. For the rest of the batches in the other size ranges, the MCD values were closer to the top sieve's size than the bottom sieve that was used. The sphericity of the particles ranged between 0.553 – 0.584, with an average of 0.570. Appendix B shows the standard deviation values for the Rhovol results in Table B-1. The average standard deviation for the sphericity values for all the particles was 0.128. The standard deviation values for the sphericity were relatively high. Appendix B also shows the relative standard deviation for sphericity in Table B-2.

The average RSD for sphericity of all the char particles was 22.5%, which is quite high. Appendix B illustrates frequency histograms and quantile plots for the particles' sphericities.

The quantile plots show that the sphericity values' z-scores generally lie on the y = x line, indicating strong normal distributions. This means that although the RSD for sphericity is 22.5%, the average sphericity values of each particle batch were a good indication of the sample's sphericity.

4.2 PARTICLE DIAMETER AND SPHERICITY CONFIDENCE INTERVALS

The particle diameter and intercept sphericity values obtained by the Rhovol proved to have satisfactory normal distributions, as shown by Appendix A. As stated before, particle diameter results were obtained using the MCD from the Rhovol. The Rhovol determines the intercept sphericity using Equation 2-56. The KC equation (Equation 2-57) was used to determine sphericity from ΔP experiments. Table 4-2 and Table 4-3 show the 90% confidence intervals of MCD and sphericities.

Table 4-2: Confidence intervals of MCD of biochar particles

d_p(mm)	Mixture	Method	Stdev (mm)	-90% (mm)	+90% (mm)
4.50	Unmixed	Rhovol	0.803	4.36	4.63
6.72	Unmixed	Rhovol	0.836	6.58	6.86
8.16	Unmixed	Rhovol	1.556	7.91	8.41
10.8	Unmixed	Rhovol	1.809	10.7	11.0
13.0	Unmixed	Rhovol	1.664	12.8	13.2

Table 4-3: Confidence intervals of sphericity of biochar particles

d_p(mm)	Mixture	Method	mean	Stdev	-90%	+90%
4.50	Unmixed	Rhovol	0.559	0.129	0.538	0.581
6.72	Unmixed	Rhovol	0.575	0.112	0.556	0.594
8.16	Unmixed	Rhovol	0.553	0.123	0.533	0.572
10.8	Unmixed	Rhovol	0.597	0.134	0.583	0.611
13.0	Unmixed	Rhovol	0.587	0.121	0.571	0.603
13.0	Unmixed	Kozeny-Carman	0.377	0.031	0.347	0.407
4.50	Unmixed	Kozeny-Carman	0.461	0.023	0.439	0.483
6.69	Binary	Kozeny-Carman	0.381	0.015	0.367	0.395
7.71	Ternary	Kozeny-Carman	0.488	0.007	0.481	0.495

The 90% confidence intervals for sphericity determined by the KC equation were determined by conducting 3 ΔP experiments each for 2 unmixed, 1 binary and 1 ternary mixed samples. The sphericity results from the Rhovol and the Kozeny-Carman equation differs quite significantly. The average sphericity results obtained by the Rhovol fell in the range of 0.553 – 597. The sphericity determined by the KC equation were in the range of 0.377 to 0.488, which is significantly lower than the Rhovol's results.

From Table 4-2, the MCD results from the unmixed samples show that the 90% confidence intervals all differ less than 0.2 mm from the mean values. From Table 4-3, the difference between the 90% confidence intervals and the mean values of sphericity for both the Rhovol and KC equation were quite similar. The difference between the mean sphericity and the confidence intervals for both methods were < 0.03.

Figure 4-1 and Figure 4-2 show the sphericity results obtained using the Rhovol and KC equation. The Rhovol results yielded sphericity values ranging from 0.211 – 0.909. The sphericity from the Rhovol had a very wide range, especially when compared to the values in Table Table 2-16. The KC equation yielded sphericity values ranging from 0.374 – 0.645. The sphericity values from the KC Equation were less distributed. The results from the KC equation were similar to pulverised wood, wheat straw and ground wood chips from Table 2-16.

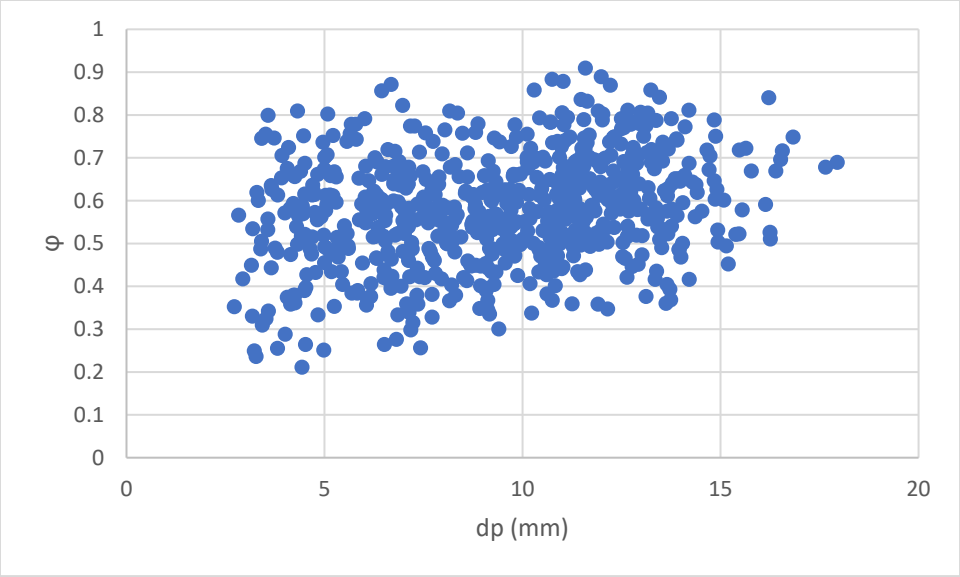

Figure 4-1: Rhovol intercept sphericity results on individual particles

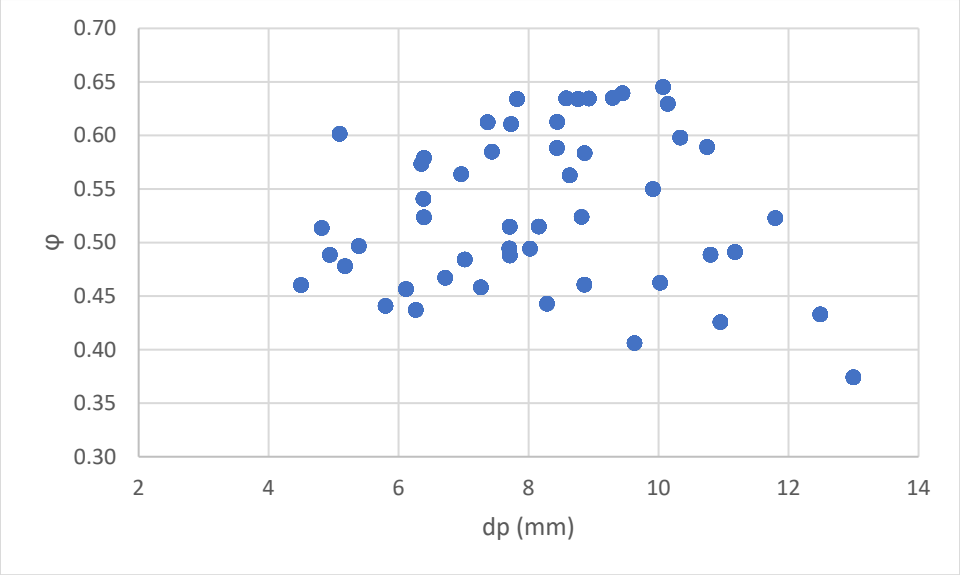

Figure 4-2: Sphericity results obtained using the KC equation on fixed beds of biochar particles

4.3 VOIDAGE AND PRESSURE DROP REPEATABILITY AND UNCERTAINTY RESULTS

Table 4-4 shows the results for the voidage experiments' uncertainty levels. Batch no. 3 had the highest level of uncertainty and RSD, at 5.58% and 2.79%, respectively. The bed voidage increased as expected when the particles' diameters increased for the mono-sized batches. Table 4-4 shows that the voidage of the mono-sized batches ranged from 0.521 – 0.564.

Table 4-4: Voidage uncertainty levels

Vol % d_p = 4.50 mm	Vol % d_p = 6.72 mm	Vol % d_p = 8.16 mm	Vol % d_p = 10.8 mm	Vol % d_p = 13.0 mm	Mean	Standard Deviation	Uncertainty %
1	0	0	0	0	0.521	8.32E-3	3.07
0	1	0	0	0	0.525	8.02E-3	3.05
0	0	1	0	0	0.538	1.50E-2	5.58
0	0	0	1	0	0.562	1.53E-3	0.53
0	0	0	0	1	0.564	5.29E-3	1.77
0.5	0	0	0	0.5	0.513	9.71E-3	2.44
0.2	0	0	0	0.8	0.519	9.74E-3	2.31
0.8	0	0	0	0.2	0.490	1.40E-2	3.47

Comparing the voidage of all the binary and ternary mixtures, it was found that bed voidage does not necessarily increase as the bed's average particle diameter increases. This was expected as previous studies came to the same conclusion.

For the pressure drop repeatability, the gas velocity was varied between 0.05m/s – 0.30m/s, for two mono-sized batches, one binary and one ternary mixture. Each batch/mixture was removed from the column and added back again to get a total of 3 tests. Figure 4-1 to Figure 4-6 shows plots of the mean ΔP vs U graphs with the standard deviation as limit bars. Since ΔP increases while U increases, the standard deviation also increases. The RSD values for the ΔP experiments ranged between 3.18% - 7.75%. The RSD values indicate that the ΔP experiments' repeatability was satisfactory.

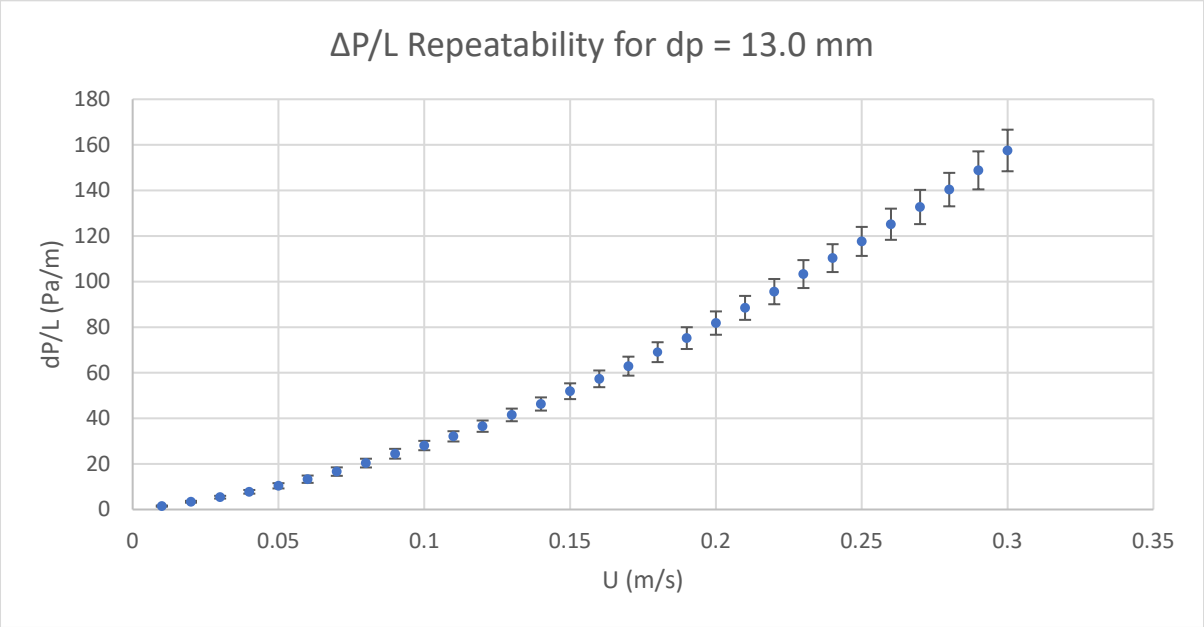

Figure 4-3: Pressure drop repeatability for the unmixed batch of particles where dp = 13.0mm

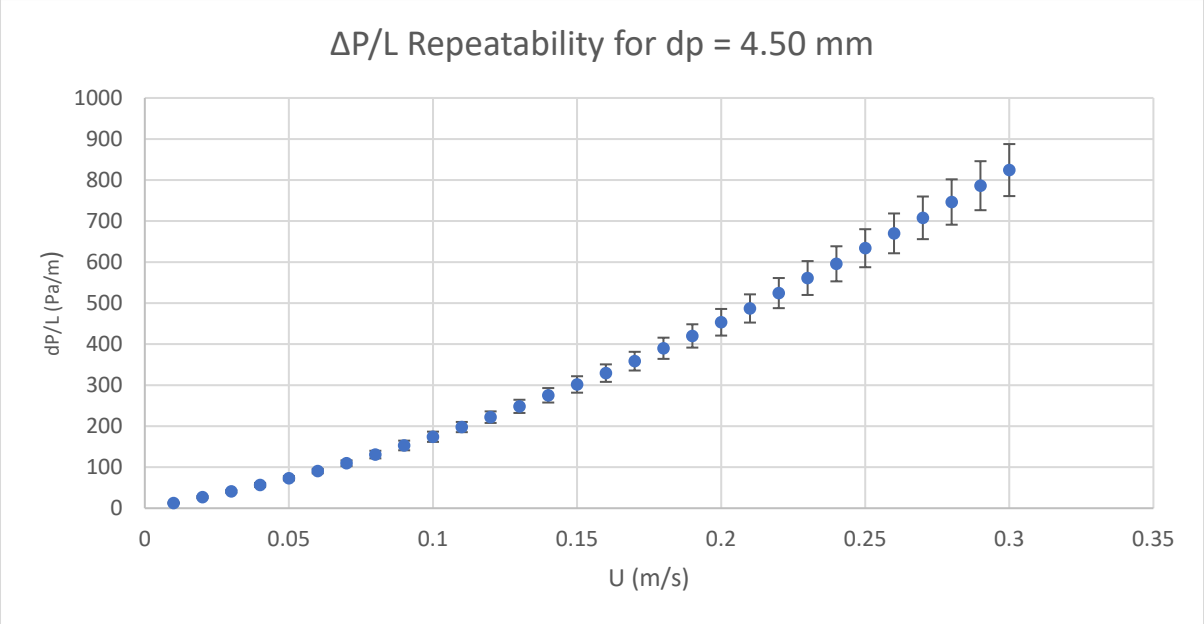

Figure 4-4: Pressure drop repeatability for the unmixed batch of particles where dp = 4.50mm

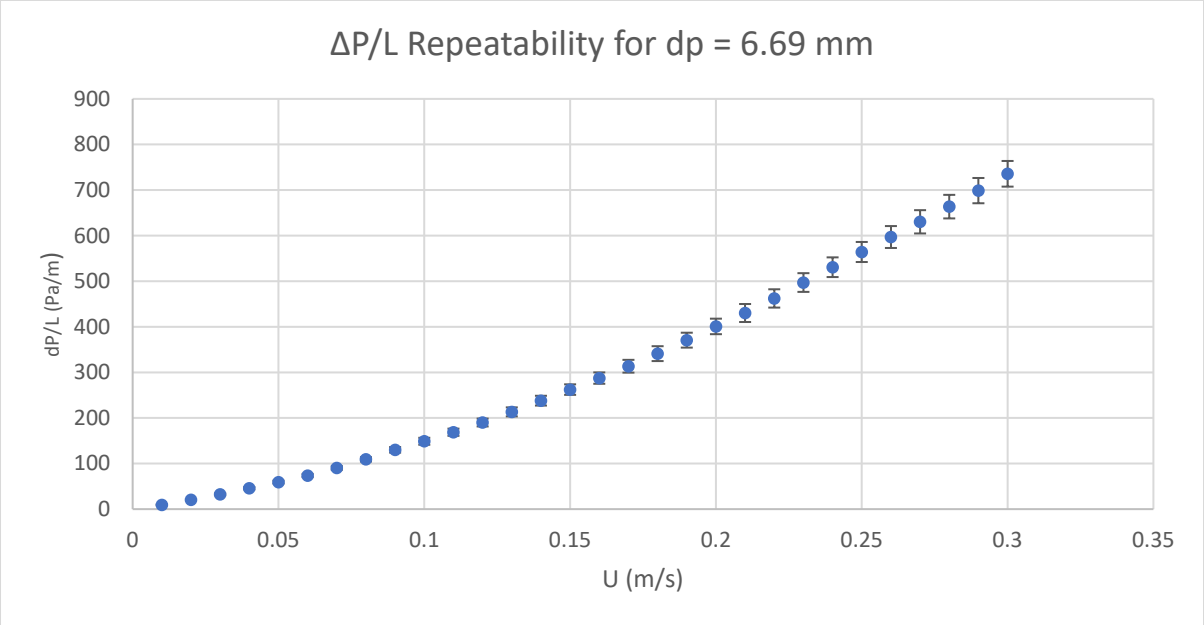

Figure 4-5: Pressure drop repeatability for a binary mixture of particles where dpsm = 6.69mm

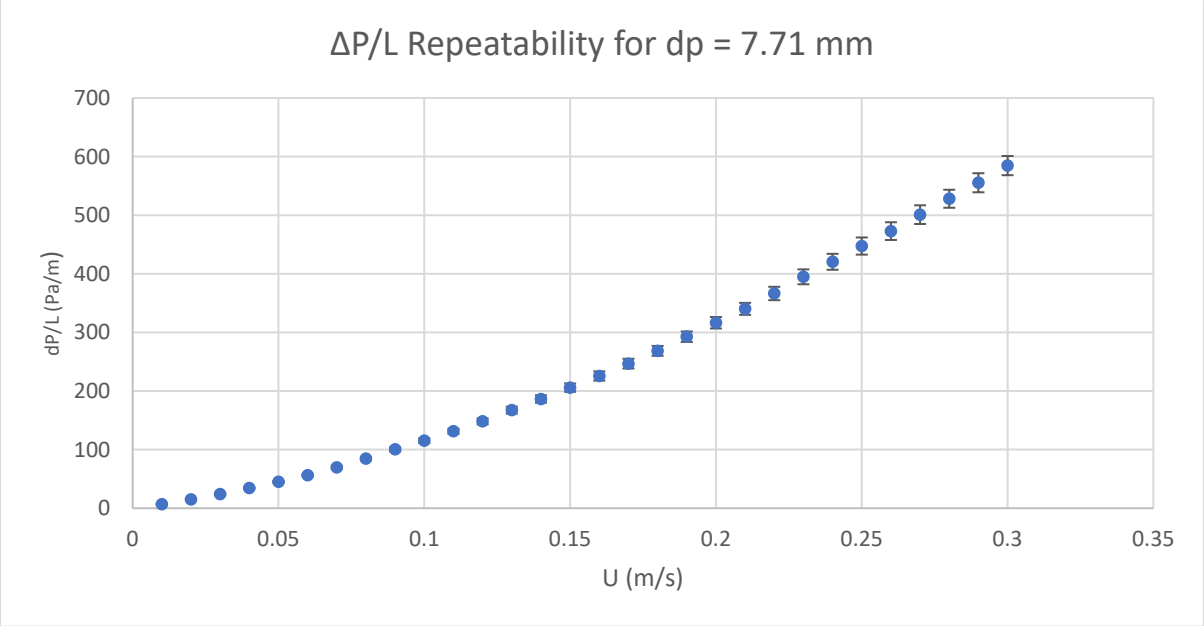

Figure 4-6: Pressure drop repeatability for a ternary mixture of particles where dpsm = 7.71mm

4.4 BINARY VOIDAGE MODELS PREDICTION PERFORMANCE

Figure 4-7 shows voidage vs. sauter mean diameter for binary mixtures. The results show the voidage results for binary mixtures had some variance. The binary mixture voidage results ranged between 0.425 – 0.528. The highest voidage value from Table 4-4 was 0.562.

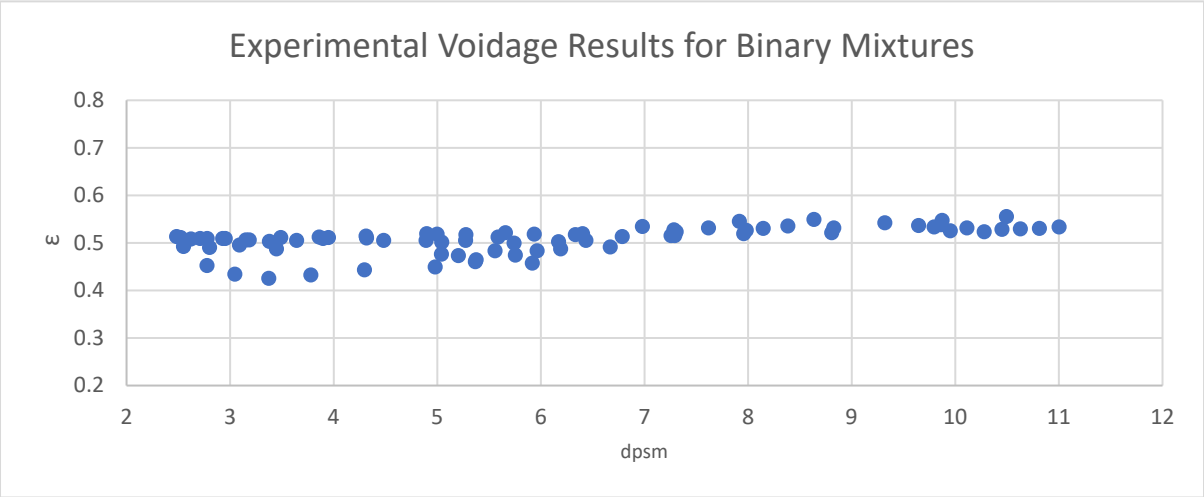

Figure 4-7: Voidage measurements for binary mixtures

Between sauter mean diameters of 5mm – 6mm, the voidage results varied between 0.449 – 0.521. This show that for mixtures with similar sauter mean diameters, voidage can vary up to 13.8%. From Table 2-5, the voidage results of biochar were in the range of almond shells, sugarcane bagasse, milled wheat straw pellets, activated carbon and granular activated carbon.

Equation 4-1 shows how the wall effect parameter of the AG model was used to improve the fit of the model for the char particles. Table 4-5 shows how the char particles' regression compared with the study by (Liu et al., 2020). The value for B_{AGM} was more than 60% higher for char particle than the original study. The wall effect was thus much more prominent for less spherical particles for the AG model. Figure 4-9 shows the parity plot for the AG model of the binary mixtures, and illustrates how the AG model performed for its best and worst predicted mixture. The average percentage error of the model with the new regressed wall effect constant was 4.99%. Figure 4-10 shows the binary mixtures for which the model performed the best, which were for the mixtures where d_1 = 6.72 mm and d_2 = 8.16 mm.

$$b_{AGM} = 1 + B_{AGM}s \qquad \textbf{4-1}$$

Table 4-5: AG regression for char particles

Parameter	Original regression	Regressed for char particles
B_{AGM}	0.9	1.45

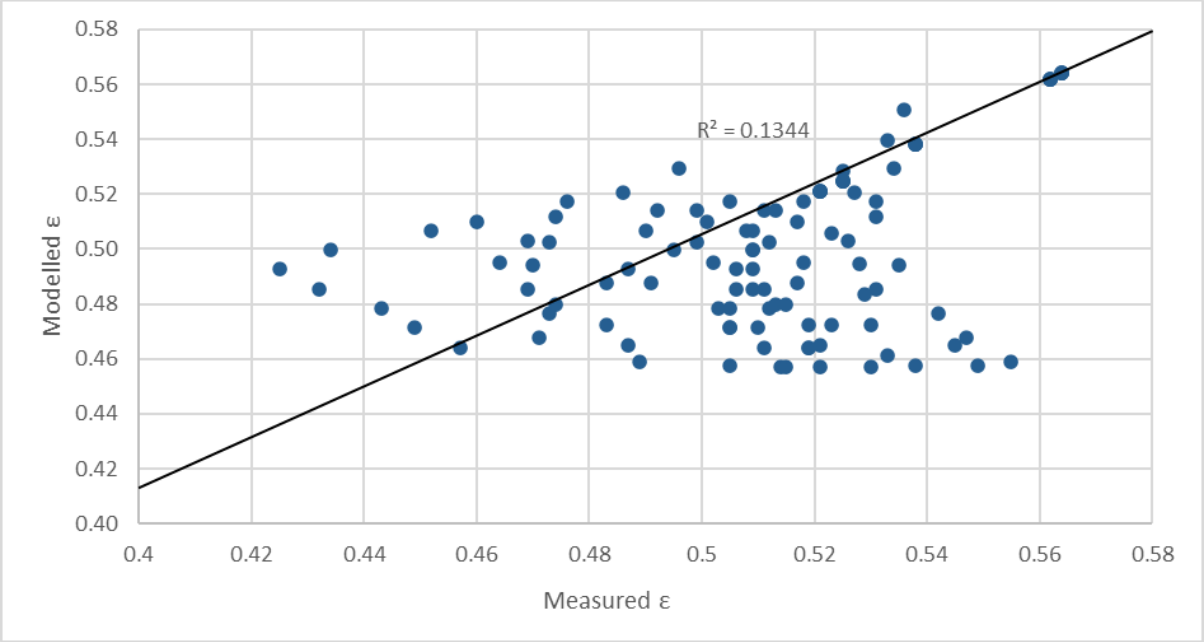

Figure 4-9: Parity plot for the Aim-Golf model with new regressed empirical constants

Figure 4-10 shows that the AG model modelled the optimum packing fraction for too-low values of x_1. This was the case for each of the char mixtures. It should be noted that although the average percentage error for the AG model is low, the average error has a wide distribution. The percentage errors of the mixtures range between -16.4 to + 16.3%.

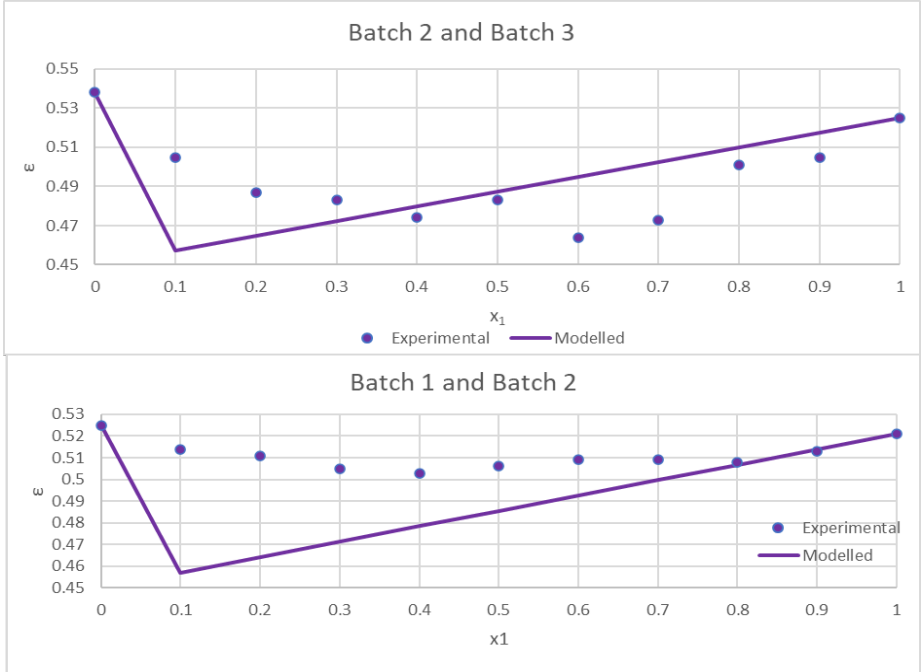

Figure 4-10: Voidage plots for the AG model and binary mixtures

Figure 4-11 shows a comparison of modelled and experimental voidage vs. sauter mean diameter for the AGM. The AGM started to significantly under predict voidage values where d_{psm} > 6.79mm.

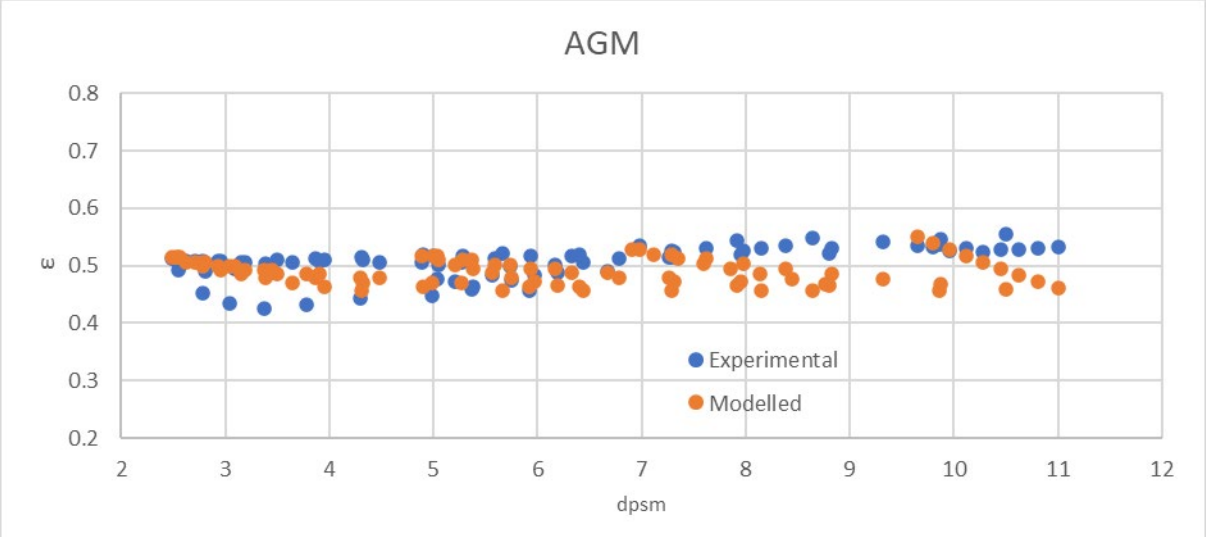

Figure 4-11: AG Model performance

Equations 4-2 and 4-3 show how the loosening wall effect parameters of the LPD model were used to improve the fit of the LPD model and char particles. Table 4-6 shows how the char particles' regression compares with the study by (Liu *et al.*, 2020). The loosening and wall effects were higher for char than for more spherical particles with the LPD model.

$$a_{LPD} = 1 - (1 - s)^{e1} - A_{LPD}s(1 - s)^{e2} \quad \textbf{4-2}$$

$$b_{LPD} = 1 - (1 - s)^{e3} - B_{LPD}s(1 - s)^{e4} \quad \textbf{4-3}$$

Table 4-6: LPD model regression for char particles

Parameter	Original regression	Regressed for char particles
A_{LPD}	2.8	0.3
B_{LPD}	0.4	1.2
$e1$	3.3	21
$e2$	2.7	3.6
$e3$	2.0	7.4
$e4$	3.7	0.1

Figure 4-12 shows the parity plot for the LPD of the binary mixtures. The LPD model had a slightly lower average percentage error than the AG model at 3.82%. This may be due to the LPD model considering loosening and wall effects. Figure 4-12 shows that the LPD model also has a wide distribution of its percentage errors. The percentage errors for the LPD model ranges between -12.9% to +11.4%. The LPD model also has a slightly lower distribution of its percentage errors than the AG model.

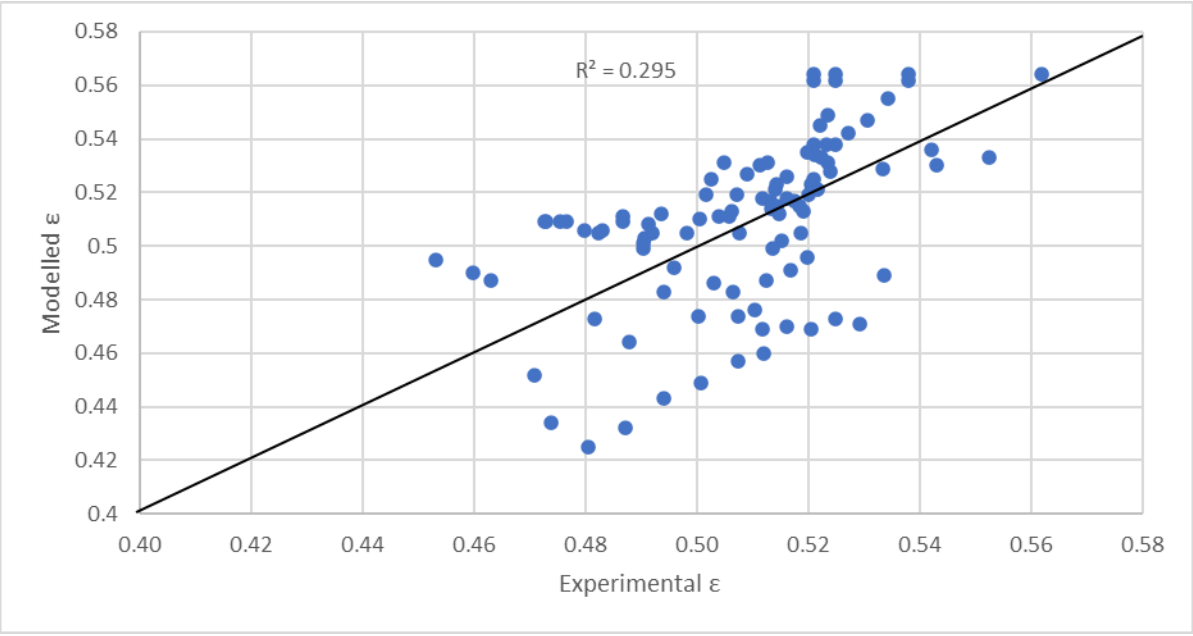

Figure 4-12: Parity plot for the LPD model with new regressed empirical constants

Figure 4-13 shows the best and worse performing mixtures for the LPD model. The LPD model, in contrast to AG, predicted the optimal packing fraction for too high values of x_1 for each binary mixture.

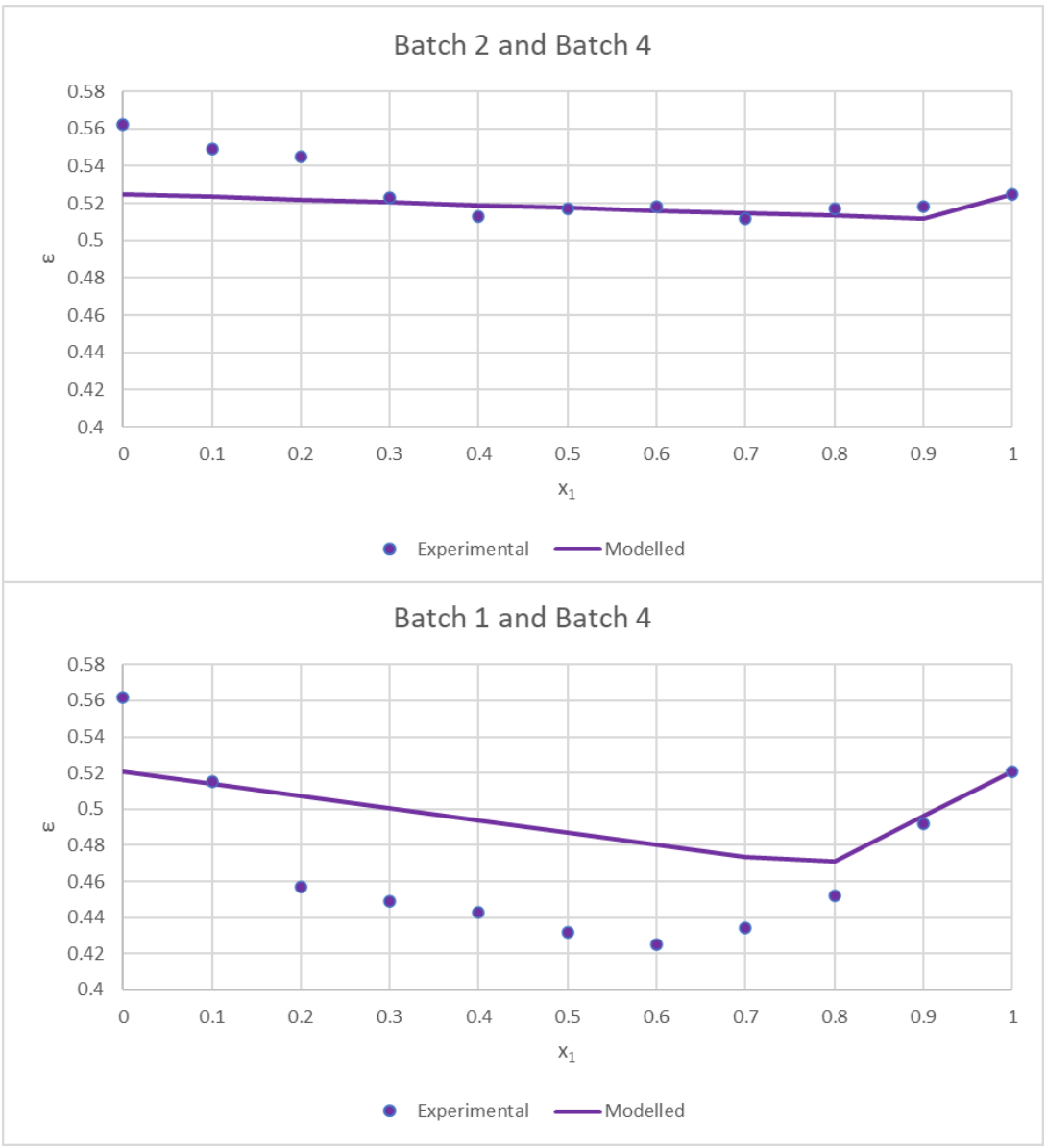

Figure 4-13: Voidage plots for the LPD model and binary mixtures

The mixtures shown in Figure 4-13 showed that for low values for x_1, there are some points where the LPD model under-predicts voidage values for char mixtures. As x_1 becomes larger, the LPD model tends to over-predict the voidage for char mixtures. This was the case for all other binary mixtures and their compositions for the LPD model. The average percentage error for the LPD model with d_1 = 6.72 mm and d_2 = 10.8 mm was 1.82%. This was the mixture for which the LPD model performed the best. The worst performing mixture for the LPD model was for batches d_1 = 4.50 mm and d_2 = 10.8 mm, at an average percentage error of 7.41% for the binary mixtures.

Figure 4-14 shows a comparison of modelled and experimental voidage vs. sauter mean diameter for the LPDM. The LPDM performed seemingly better than the AGM.

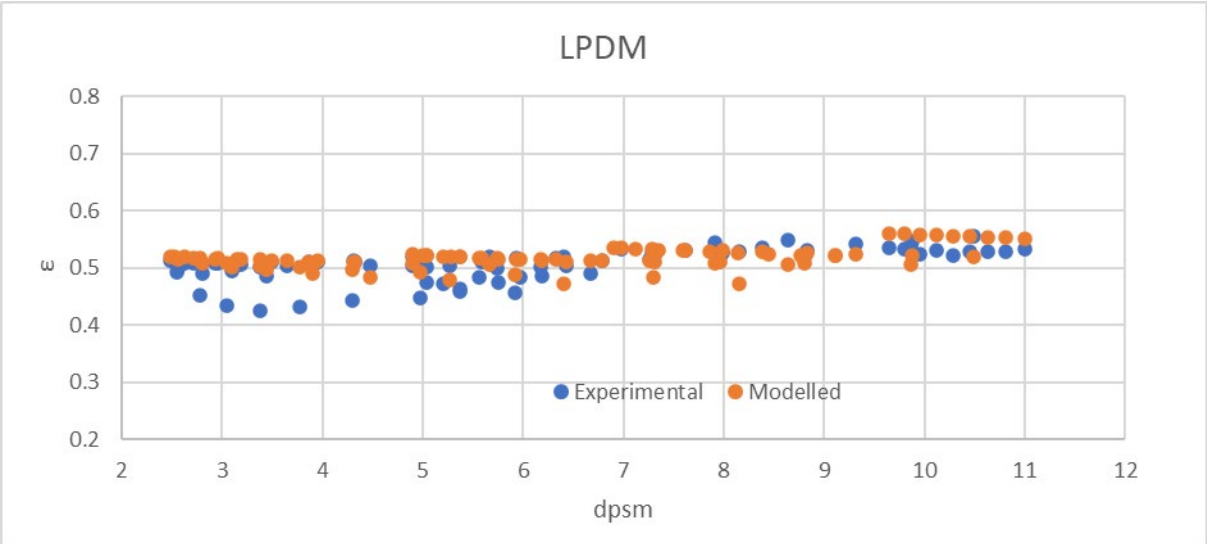

Figure 4-14: LPD Model performance

Equation 4-4 shows how the wall effect parameter of the Toufar model was used to improve the model's fit for the char particles. Table 4-7 shows how the char particles' regression compared with the study by (Liu *et al.*, 2020).

$$b_{TM} = 1 - \frac{1 + xA_{TM}}{(1 + x)^{e1}} \qquad \textbf{4-4}$$

Table 4-7: Toufar regression for char particles

Parameter	Original regression	Regressed for char particles
A_{TM}	4.0	1.1
$e1$	4.0	1.5

The values regressed for char particles in Table 4-7 were significantly lower than the original values. Figure 4-15 shows the parity plot for the Toufar model and the binary mixtures. The Toufar model had an average percentage error of 3.94%. Like the AG model, the Toufar model only considered the wall effect between the particles. The Toufar method had a slightly higher percentage error than the LPD model, but the non-linear models predicted the voidage trends better than the linear models, as seen in Figure 4-16 with d_1 = 6.72 mm and d_2 = 10.8 mm .

Figure 4-16 shows the best and worst performing mixtures for the Toufar model. The average percentage error for the mixture of d_1 = 6.72 mm and d_2 = 10.8 mm was 1.53%, and the percentage error between d_1 = 8.16 mm and d_2 = 10.8 mm was 9.81%. The overall percentage error distribution for the Toufar model ranges from -17.0% to +9.6% . The Toufar model's regressed parameters were significantly lower than the original values. This decreased the wall effect for this model.

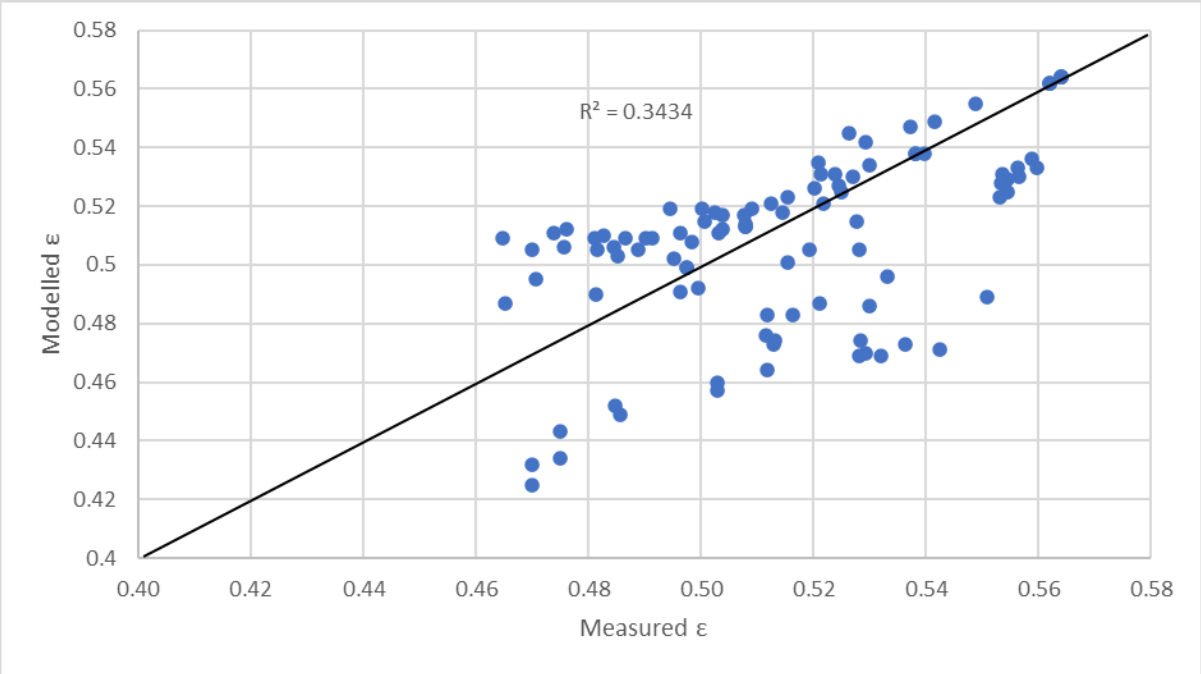

Figure 4-15: Parity plot for the Toufar model with new regressed empirical constants

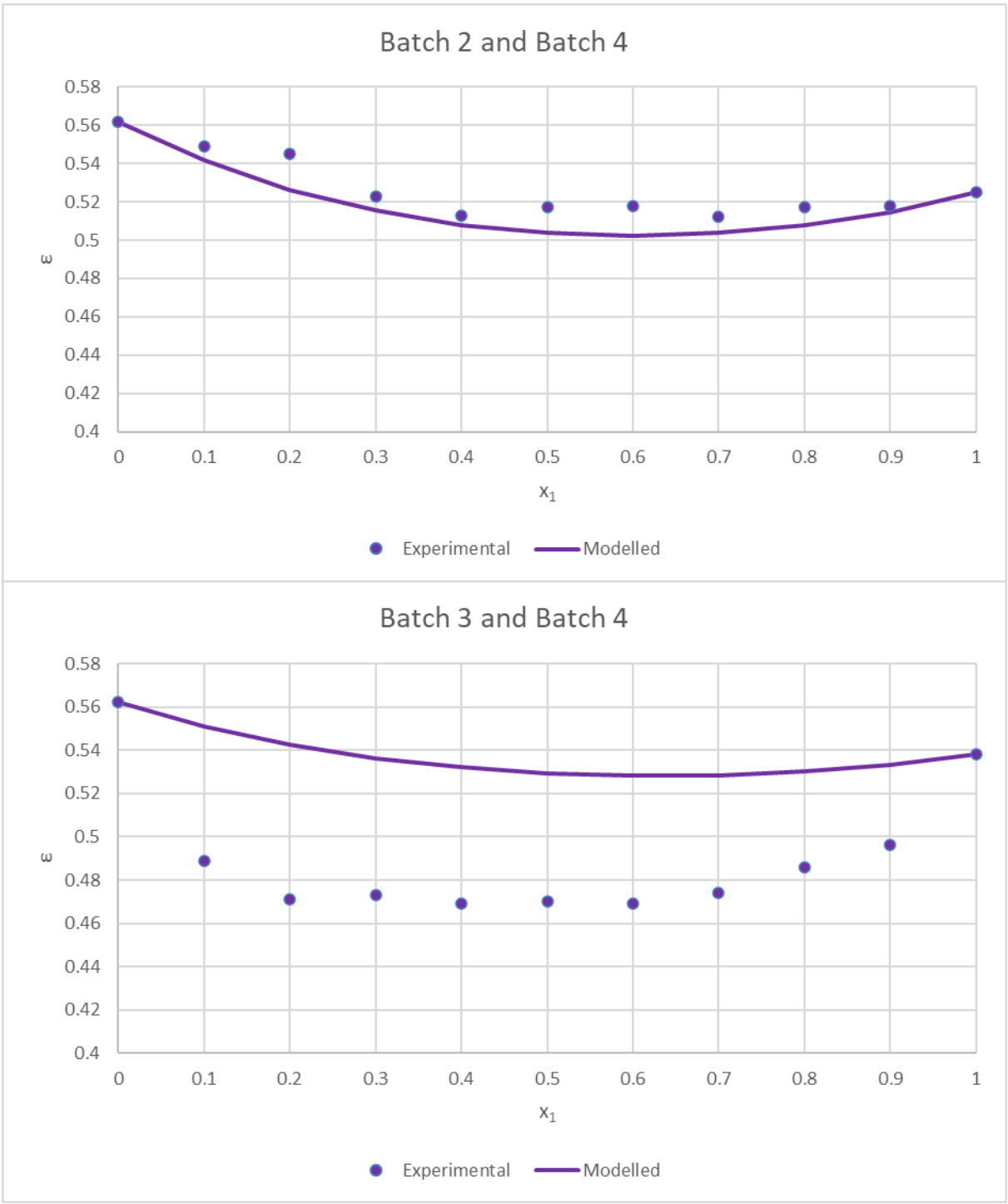

Figure 4-16: Voidage plots for the Toufar model and binary mixtures

Figure 4-17 shows a comparison of modelled and experimental voidage vs. sauter mean diameter for the TM. The figure shows that the TM had a relatively better performance than the AG model and LPD model. The TM was generally close to the range of experimental voidage values. For d_{psm} > 9.65mm, the TM had a tendency to slightly over predict voidage values for binary mixtures.

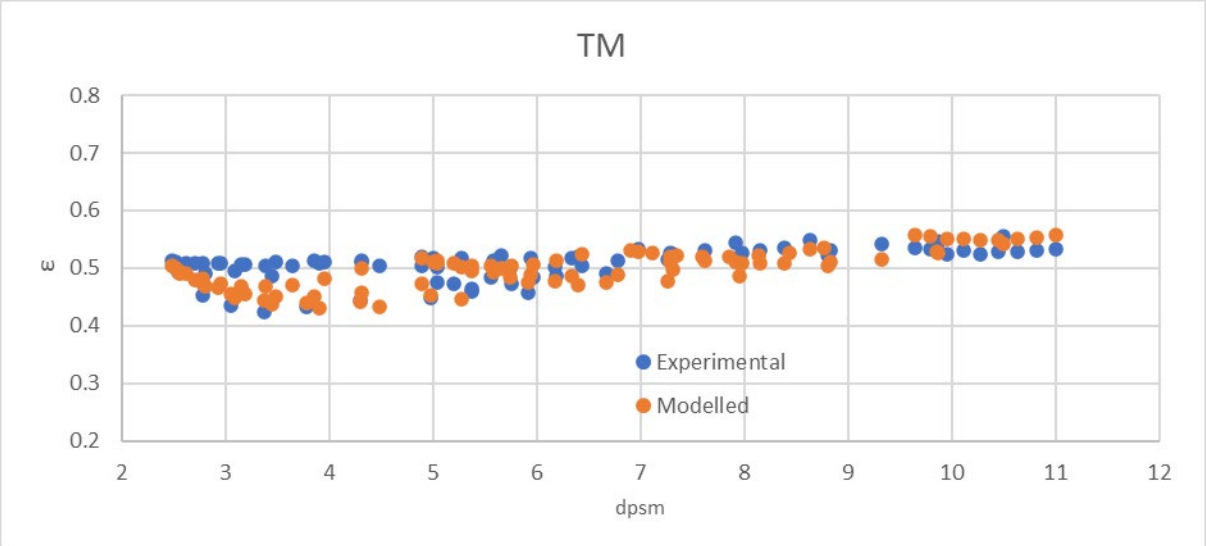

Figure 4-17: Toufar Model performance

Equations 4-5 to 4-9 show how the loosening, wall and wedging effect parameters of the modified Kwan model were used to improve the fit of the model for the char particles.

Table 4-8 shows how the char particles' regression compares with the study by (Liu *et al.*, 2020).

$$\varepsilon_1^* = (1 + \varepsilon_1)r_1 + (1 + \varepsilon_2)x_2 - (1 - a_{MK})(1 + \varepsilon_1)x_1[1 - c_{MK}({A_{MK}}^{x_1} - 1)] - 1 \quad \textbf{4-5}$$

$$\varepsilon_2^* = (1 + \varepsilon_1)x_1 + (1 + \varepsilon_2)x_2 - (1 - b_{MK})(\varepsilon_2 x_2)x_1[1 - c_{MK}({B_{MK}}^{x_2} - 1)] - 1 \quad \textbf{4-6}$$

$$a_{KM} = 1 - (1 - s)^{e1} - C_{MK}s(1 - s)^{e2} \quad \textbf{4-7}$$

$$b_{KM} = 1 - (1 - s)^{e3} - D_{MK}s(1 - s)^{e4} - E_{MK}(1 - s)^{e5} \quad \textbf{4-8}$$

$$c_{KM} = F_{MK} \tanh(G_{MK}s) \quad \textbf{4-9}$$

Table 4-8: Modified Kwan model regression for char particles

Parameter	Original regression	Regressed for char particles
A_{MK}	3.8	1.1
B_{MK}	2.6	2.0
C_{MK}	1.9	2.1
D_{MK}	2.1	0
E_{MK}	0.2	0
F_{MK}	0.335	0.996
G_{MK}	26.9	42.6
$e1$	5	37.6
$e2$	3.1	1.6
$e3$	1.9	2.1
$e4$	10.5	30.8
$e5$	7.6	19.5

The D_{MK} and E_{MK} were regressed to 0 for the char particles. This increased the values for the wall effect of the MK model for char. The values for F_{MK} and G_{MK} were higher for char particles than for more spherical particles. This indicate that the wedging effect increased for char particles. Figure 4-18 shows the parity plot for the modified Kwan and the binary mixtures. The model had an average percentage error of 4.25% with a distribution between and -15.9% +10.9%. Figure 4-19 show the best and worst performing mixture for the modified Kwan model.

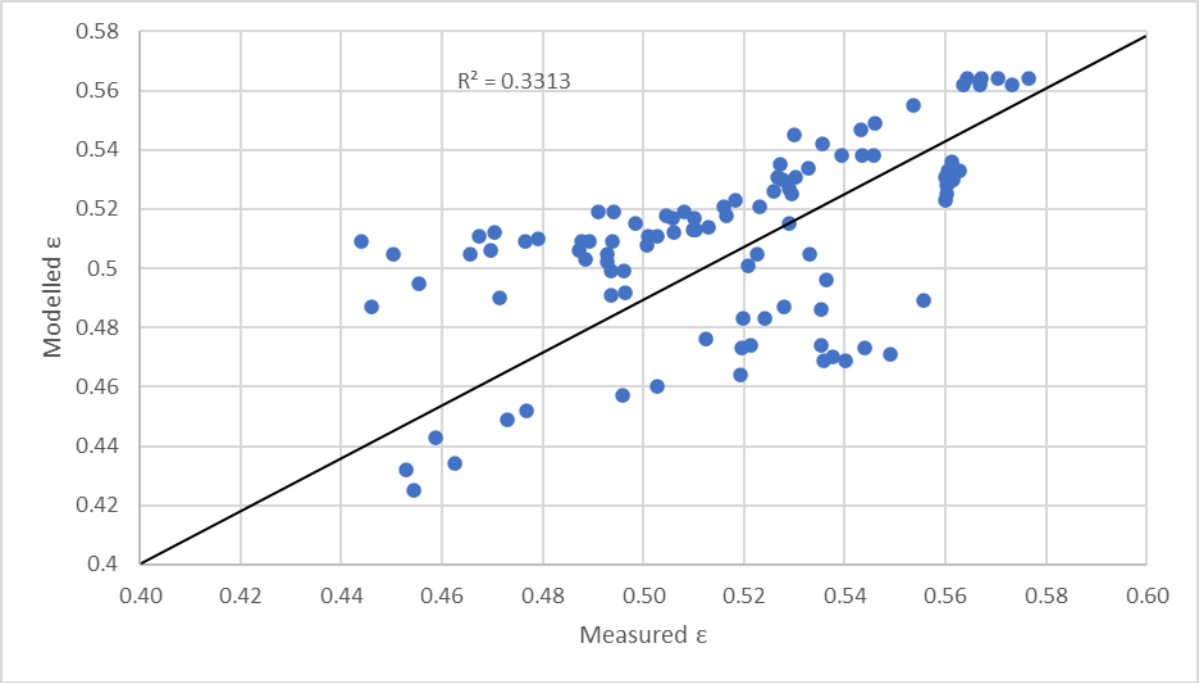

Figure 4-18: Parity plot for the modified Kwan model with new regressed empirical constants

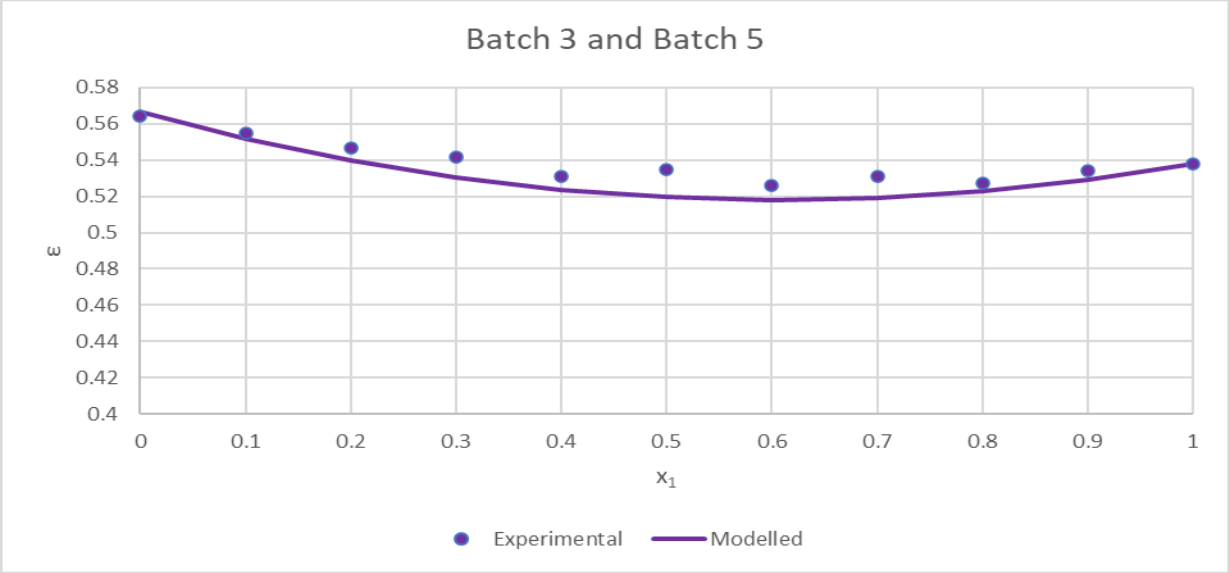

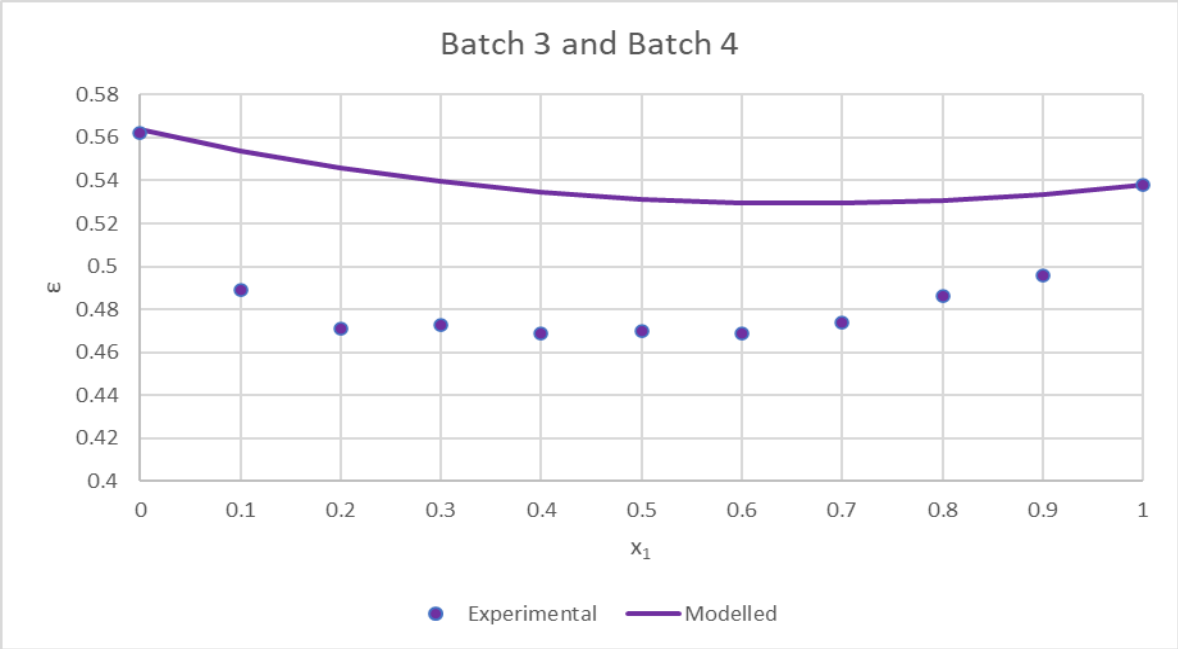

Figure 4-19: Voidage plots for the best and worst performing mixtures of the Kwan model

Table 4-8 shows that the modified Kwan model's loosening, wall and wedge effect parameters were also larger than the original values used for more spherical quartz particles. Figure 4-20 shows a comparison of modelled and experimental voidage vs. sauter mean diameter for the MKM. The MKM was generally close to the range of experimental voidage values. Similair to the TM, for d_{psm} > 9.65mm, the TM had a tendency to slightly over predict voidage values for binary mixtures.

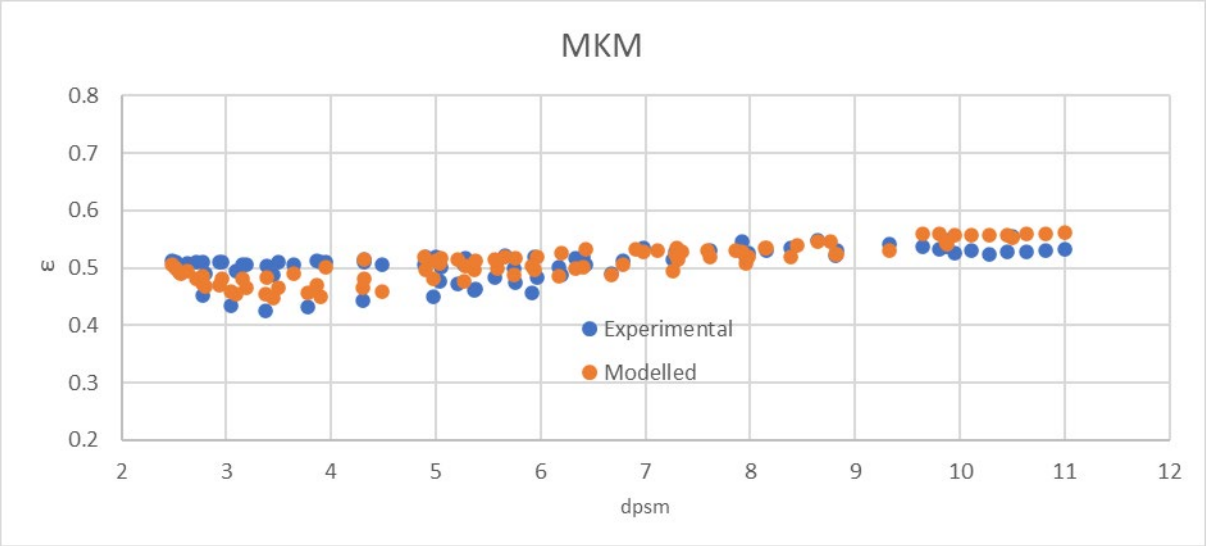

Figure 4-20: MKM Model performance

Figure 4-21 shows the relationship between the RMSE and each binary mixture's s value. The RMSE values of the linear models were much higher than the non-linear models' when s = 0.2. The RMSE of all the models does not tend to stabilise as the s value increases or decreases. For most of the s value range, the non-linear models had a lower RMSE. Only in the range of 0.71 < s < 0.85 did the RMSE of the AG model become lower than the other models.

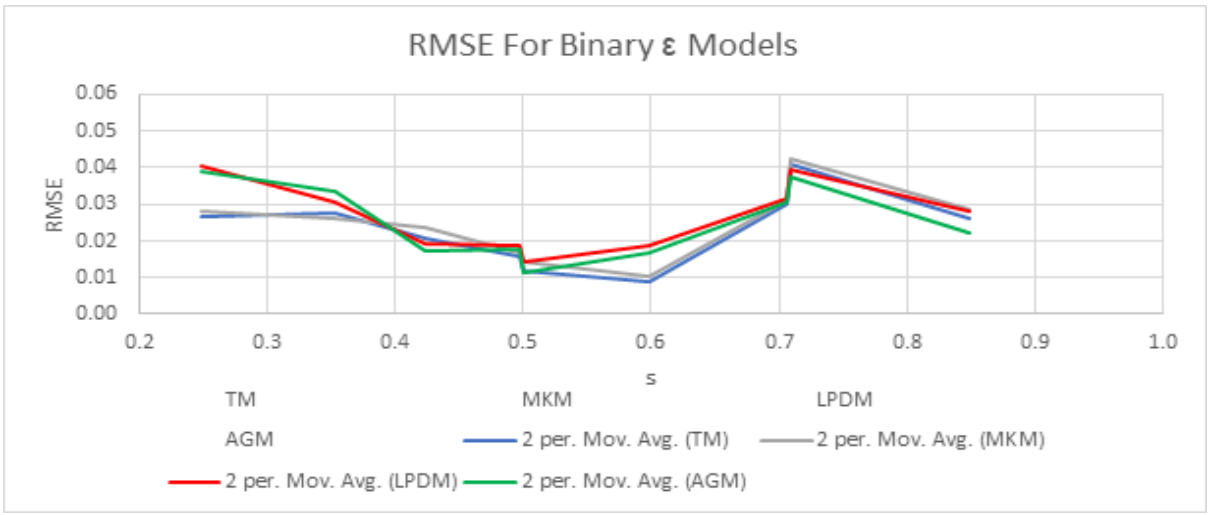

Figure 4-21: Root mean squared error for binary voidage models

4.3 TERNARY VOIDAGE MODELS PREDICTION PERFORMANCE

Figure 4-22 show voidage vs sauter mean diameter for the ternary mixture results. The figure show that the ternary results also showed significant variance. Sauter mean diameters between 3mm – 4mm had voidage values between 0.422 – 0.484. This variance show that mixtures with similar sauter mean diameters can vary up to 12.8%. This variance percentage is very similar to the binary mixtures' variance of 13.8%. The voidage values for ternary mixtures were in the range of 0.406 - 0.506, which according to Table 2-5, is similar to almond shells, milled straw pellets and crushed charred spruce.

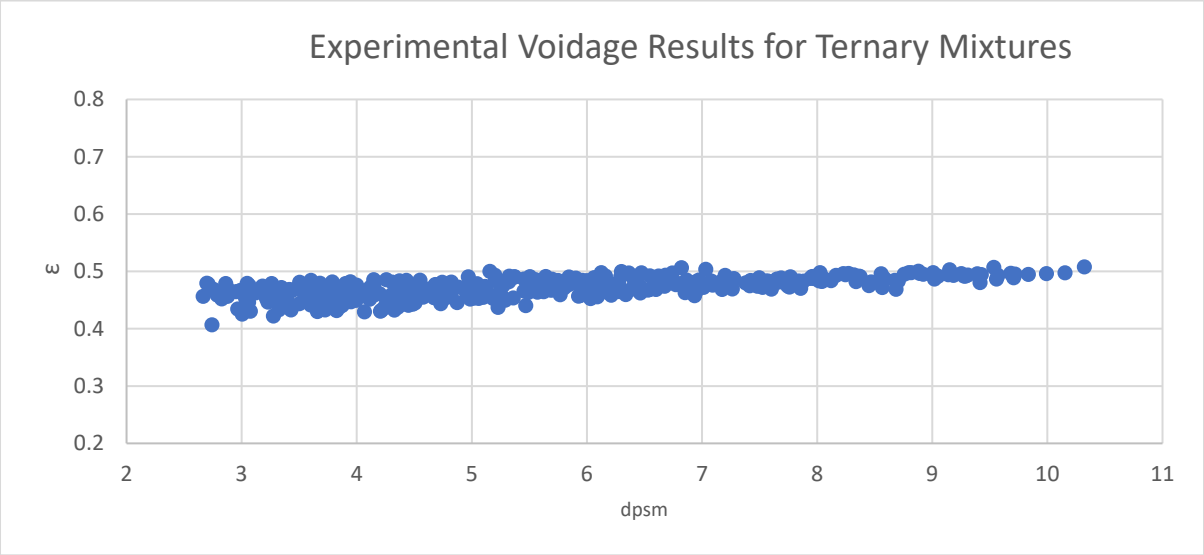

Figure 4-22: Voidage results for ternary mixtures of biochar

Figure 4-23 and Figure 4-24 show the results of the ternary voidage experiments. A clear trend from these results was that the voidage tends to be higher for binary mixtures and mono-sized batches than for ternary mixtures. This may be due to finer particles filling the gaps between coarse particles in mixtures and thus decreasing voidage. The voidage increased as the average d_p for the bed increased. The colours of the last 2 graphs (for mixtures where d_1 = 6.72 mm, d_2 = 10.8 mm d_3 = 13.0 mm and where d_1 = 8.16 mm, d_2 = 10.8 mm d_3 = 13.0 mm) were lighter than the first 2 graphs (d_1 = 4.50 mm, d_2 = 6.72 mm d_3 = 8.16 mm and where d_1 = 4.50 mm, d_2 = 6.72 mm d_3 = 10.8). This phenomenon was to be expected as also seen in (Wong, 2014), as the absence of finer particles lead to voidage increasing between larger particles.

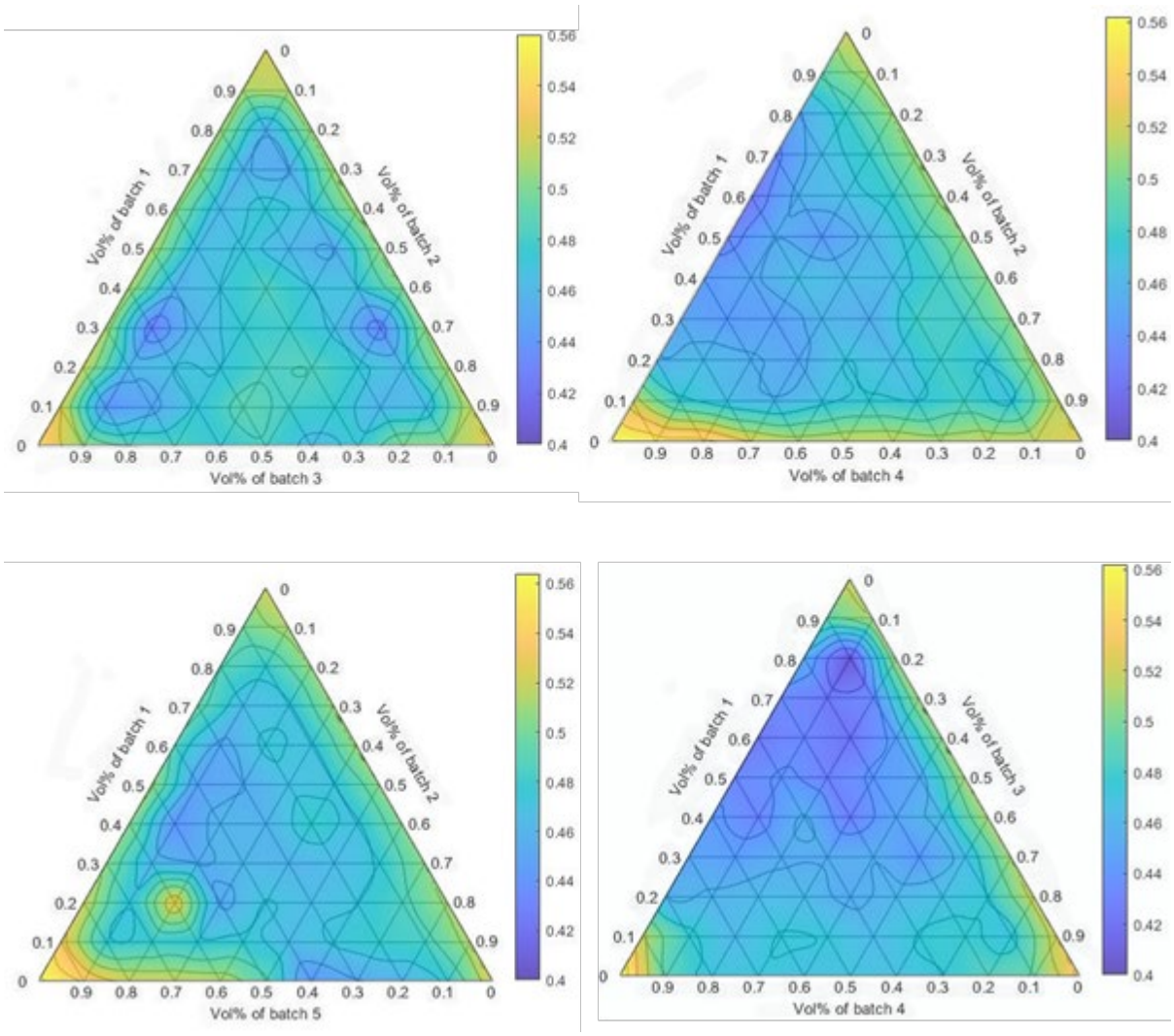

Figure 4-23: Voidage diagrams for ternary mixtures

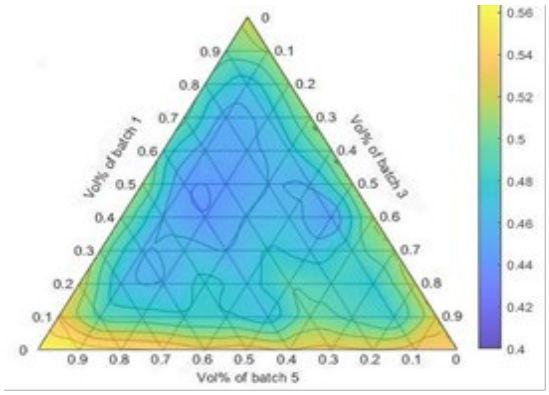

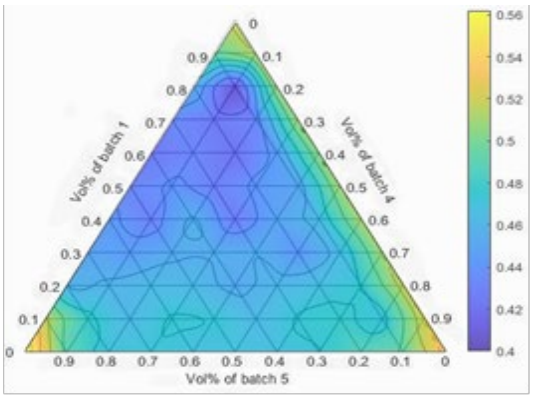

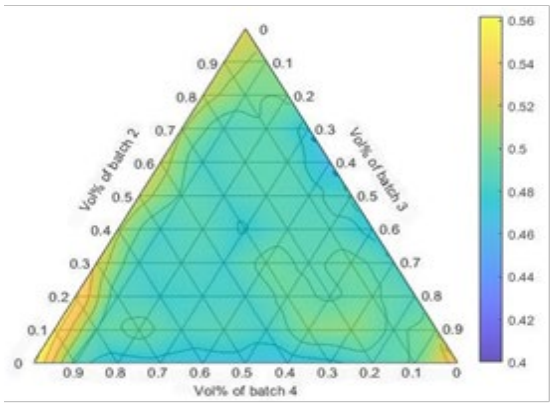

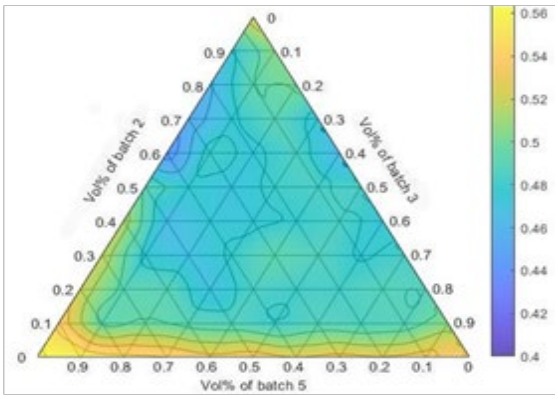

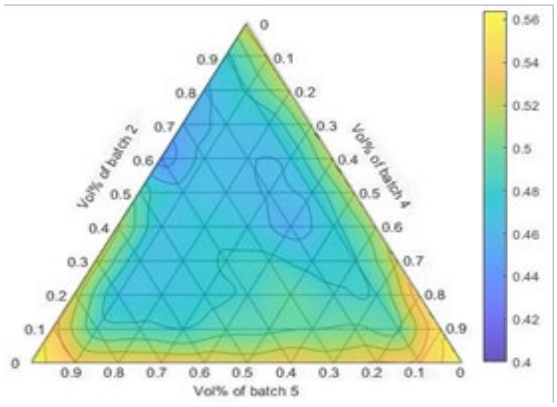

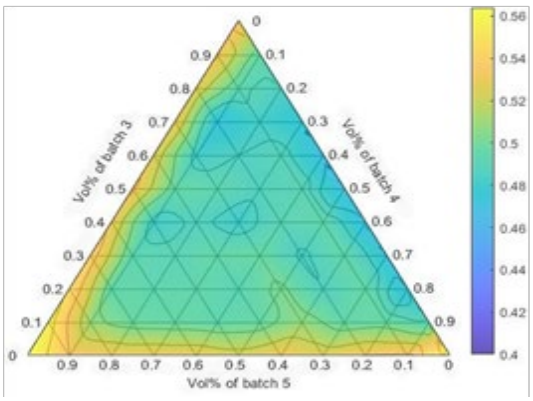

Figure 4-24: Voidage diagrams for ternary mixtures

Figure 4-25 shows the parity plot for Wong's model and ternary mixtures. The average percentage error for the Wong model was 9.25%, with a standard deviation of 3.49%.

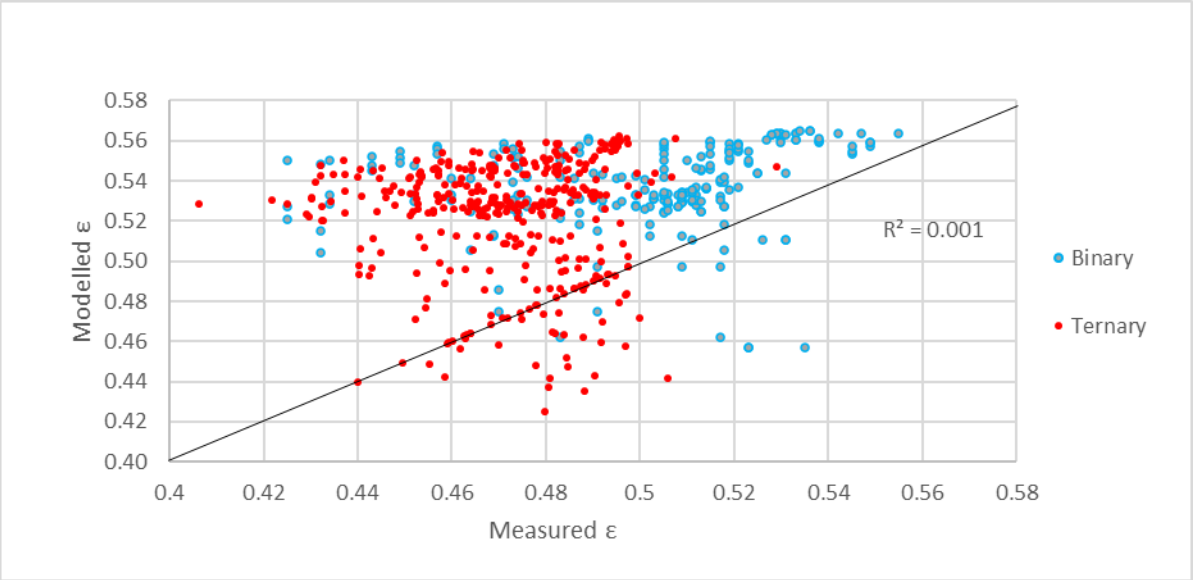

Figure 4-25: Voidage parity plot for Wong's model and ternary mixtures

Figure 4-25 shows that the Wong model tend to overpredict the voidage values for binary and ternary mixtures. Equations 4-10 to 4-15 and Table 4-9 show how the loosening, wall and wedging effects were regressed to fit the char particles. The G_{WM} and H_{WM} terms for Wong's model were lower than the original values. The I_{WM} and J_{WM} terms for Wong's model and char were higher than the original values regressed for spherical particles. This indicate that the loosening, wall and wedging effects became more prominent for char particles than the original more spherical particles.

Table 4-10 and Table 4-11 show the best and worst performing mixtures in terms of percentage error for the Wong model. The ternary mixture where Wong's model performed best was with d_1 = 8.16 mm, d_2 = 10.8 mm d_3 = 13.0 mm, with an average percentage error of 8.22%. The mixture where Wong's model performed the worst, was where d_1 = 4.50 mm, d_2 = 10.8 mm and d_3 = 13.0 mm, with an average percentage error of 13.9%. The mixtures' percentage error where Wong's model performed at its best and worse did not differ significantly, indicating that the overall performance of Wong's model remained relatively constant.

$$\frac{1}{\varepsilon_1^*} = \frac{1}{\varepsilon_T} - (1-b_{12})(1-\varepsilon_2)\frac{x_2}{\varepsilon_2}\left[1 - c_{12}\left({A_{WM}}^{x_2+x_3} - 1\right)\right] - (1-b_{13})(1-\varepsilon_3)\frac{x_3}{\varepsilon_3}\left[1 - c_{13}\left({B_{WM}}^{x_2+x_3} - 1\right)\right] \quad \textbf{4-10}$$

$$\frac{1}{\varepsilon_2^*} = \frac{1}{\varepsilon_T} - (1-a_{12})(1-\varepsilon_2)\frac{x_1}{\varepsilon_1}[1 - c_{12}({C_{WM}}^{x_1} - 1)] - (1-b_{23})(1-\varepsilon_3)\frac{x_3}{\varepsilon_3}[1 - c_{23}({D_{WM}}^{x_3} - 1)] \quad \textbf{4-11}$$

$$\frac{1}{\varepsilon_3^*} = \frac{1}{\varepsilon_T} - (1-a_{13})\frac{x_1}{\varepsilon_1}[1 - c_{13}({E_{WM}}^{x_1} - 1)] - (1-a_{23})(1-\varepsilon_{23})\frac{x_2}{\varepsilon_2}[1 - c_{23}({F_{WM}}^{x_2} - 1)] \quad \textbf{4-12}$$

$$a_{ij} = 1 - (1-s)^{ei} - G_{WM}s(1-s)^{ej} \quad \textbf{4-13}$$

$$b_{ij} = 1 - (1-s)^{ei} - 2H_{WM}(1-s)^{ej} \quad \textbf{4-14}$$

$$c_{ij} = I_{WM}\ tanh\ (J_{WM}s) \quad \textbf{4-15}$$

Table 4-9: Regression parameters for the Wong model

Parameter	Original regression	Regressed for char particles
A_{WM}	2.6	1.3
B_{WM}	2.6	1.9
C_{WM}	3.8	1.8
D_{WM}	2.6	2.5
E_{WM}	3.8	2.5
F_{WM}	3.8	2.4
G_{WM}	2.6	0
H_{WM}	2.0	0.2
I_{WM}	0.322	1.0
J_{WM}	11.9	17.6
$e1$	3.3	43.1
$e2$	3.6	1.4
$e3$	1.9	8.9
$e4$	6	0

Table 4-10: Wong model percentage errors where d_1 = 6.72 mm, d_2 = 10.8 mm, d_3 = 13.0 mm

x_2	Percentage error (%)										
	x_1										
	0	0.1	0.2	0.3	0.4	0.5	0.6	0.7	0.8	0.9	1
0	0	2.9	3.0	4.5	3.7	2.1	1.8	2.7	3.2	2.6	0
0.1	6.3	0.0	0.0	12.9	8.3	1.2	7.7	3.5	0.4	2.1	
0.2	9.9	0.0	13.5	13.2	0.6	5.7	10.8	13.7	3.5		
0.3	10.6	23.5	15.2	11.2	7.1	12.5	21.9	3.4			
0.4	12.4	15.9	12.6	2.3	11.7	12.7	3.1				
0.5	8.5	13.8	7.9	11.2	16.2	3.1					
0.6	4.9	13.9	9.4	11.7	4.1						
0.7	8.6	14.8	16.3	3.7							
0.8	5.0	15.2	2.6								
0.9	4.6	2.1									
1	0										

Table 4-11: Wong model percentage error where d_1 = 4.50 mm, d_2 = 10.8 mm, d_3 = 13.0 mm

x_2	Percentage error (%)										
	x_1										
	0	0.1	0.2	0.3	0.4	0.5	0.6	0.7	0.8	0.9	1
0	0	5.5	6.9	9.0	8.1	2.3	6.4	6.7	8.2	5.7	0
0.1	5.8	0.0	0.0	25.9	23.9	12.0	20.4	23.4	16.0	7.2	
0.2	6.3	0.0	19.4	21.5	12.1	19.9	22.4	20.0	17.9		
0.3	6.5	15.7	21.0	19.7	17.9	25.1	19.0	23.7			
0.4	6.7	17.8	18.9	4.9	24.2	24.9	26.9				
0.5	12.6	15.8	1.4	9.1	26.7	24.9					
0.6	3.8	15.7	4.1	13.0	23.0						
0.7	3.6	8.1	7.8	22.3							
0.8	5.1	1.3	21.1								
0.9	5.4	8.3									
1	0										

Table 4-10 and Table 4-11 show that for both cases of the Wong model's percentage error increased for the compositions of the ternary mixtures. Table 4-11 show that the percentage error for Wong's model was relatively high for the binary mixture where d_1 = 4.50 mm and d_2 = 10.8 mm.

Figure 4-26 shows a comparison of modelled and experimental voidage vs. sauter mean diameter for the WM. In the range where 3.33 mm < d_{psm} < 9.29 mm, the WM approximated voidage relatively close to the experimental values.

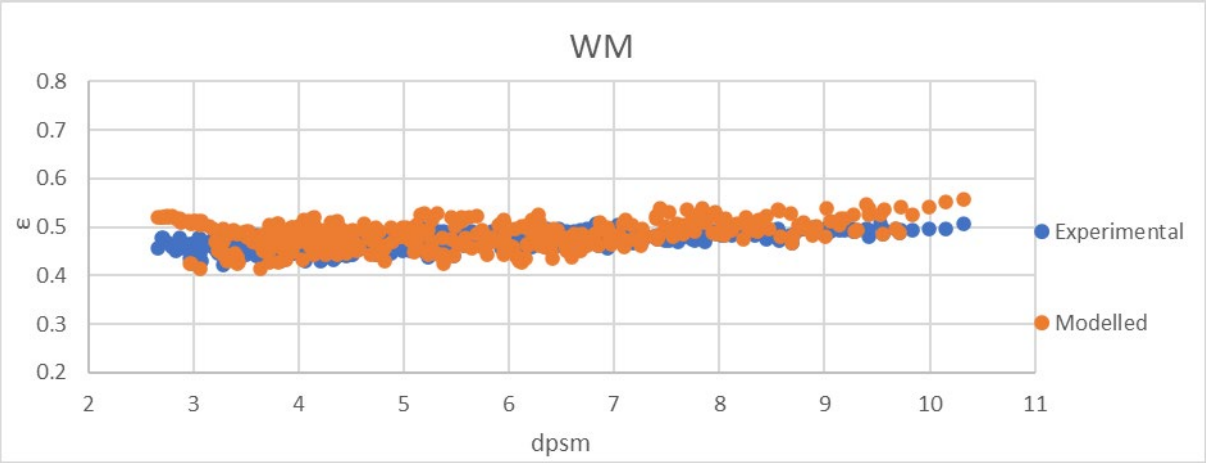

Figure 4-26: Wong model performance

Outside that range the WM had a tendency to over predict voidage values. The D/d_p ratio for this study was between values 8.0 – 44.1. Previous studies for the wong model had ratios between 12 – 140. The particle sizes used in previous studies were between 1.43mm – 15.73mm. The char particles used in this study yielded D/d_p and sizes mostly within the ranges of previous studies. The exception was that for this study, the D/d_p was a bit lower than previous studies. Particles that the Wong model was tested for only included spherical glass beads. The Wong model is one of the more comprehensive voidage models. The model includes loosening, wall and wedging effects, particle volumetric ratios, size ratios and voidage values for unmixed particle batches. Overall the Wong model did not model voidage to a satisfactory degree. The R^2 value of Figure 4-25 is near zero, which means that the model's prediction performance has too much variance.

Figure 4-27 shows the parity plot for the CM. Chang's model had an average percentage error of 9.95% with a standard deviation of 1.6% for all ternary mixtures. Chang's model had a tendency to over-predict all voidage values for the ternary mixture but overpredicted and underpredicted the voidage for many binary mixtures. Chang's model was regressed with the p and q values from Equations 2-49 and 2-50. Table 4-12 shows the original values for p and q and the regressed values for the char particles. The mixture for which Chang's model performed the best was for d_1 = 4.50 mm, d_2 = 6.72 mm and d_3 = 13.0 mm and had an average percentage error of 7.42%. The mixture for which Chang's model performed the worst was for d_1 = 4.50 mm, d_2 = 10.8 mm and d_3 = 13.0 mm, with an average percentage error of 13.62%. Table 4-13 and Table 4-14 shows the percentage error of each of the previous mixtures. Table 4-13 show that Chang's model predicted voidage best for binary mixtures where d_1 = 4.50

mm, d_2 = 6.72 mm and d_3 = 13.0 mm. Table 4-14 show that Chang's model did not model voidage adequately for binary mixtures where d_1 = 4.50 mm, d_2 = 10.8 mm and d_3 = 13.0 mm. For this mixture, Chang's model predicted voidage better for ternary mixtures than for binary mixtures. Overall the CM did not yield satisfactory modelling results, with an R^2 value of 0.0127 for the parity plot.

The p and q values for Chang's model were significantly higher for char particles than the values of the original model. This means that for Chang's model, the loosening and wall effects become more prominent the less spherical the particles are.

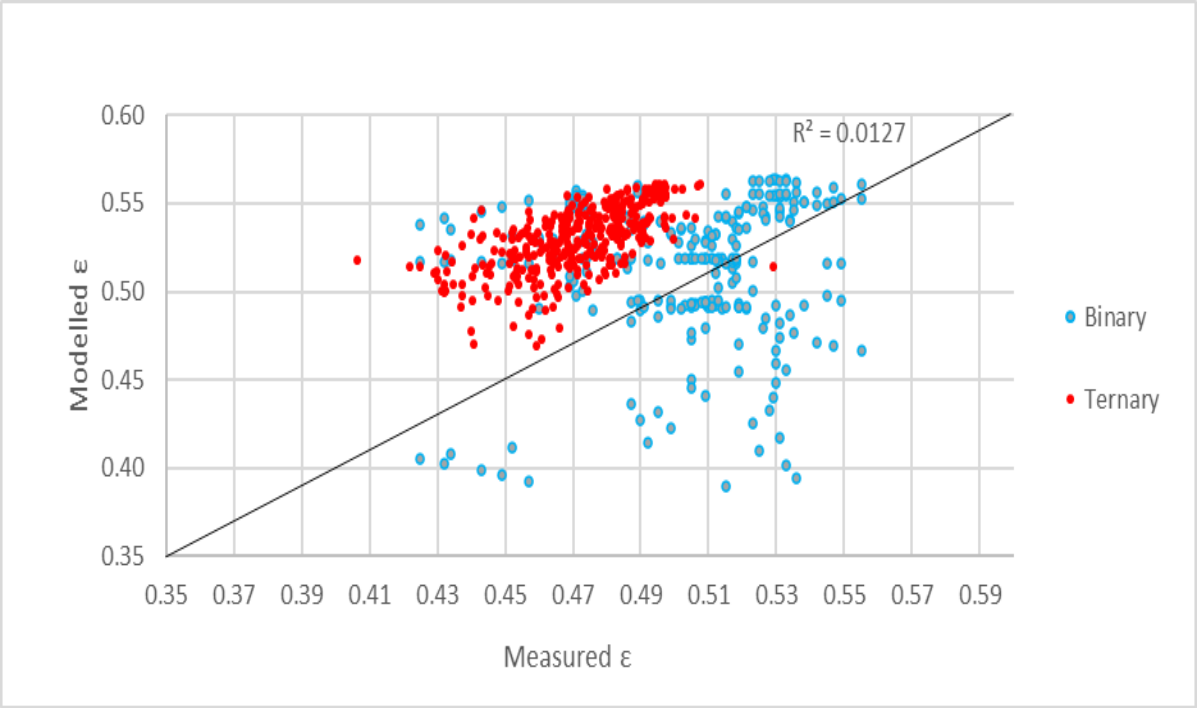

Figure 4-27: Voidage parity plot for Chang's model and ternary mixtures

Table 4-12: Regression parameters for Chang's model

Parameter	Original regression	Regressed for char particles
p	2.53	9.42
q	2.3	7.3

Table 4-13: Chang's model percentage errors for d_1 = 4.50 mm, d_2 = 6.72 mm, d_3 = 13.0 mm

x_2	Percentage error (%)										
	x_1										
	0	0.1	0.2	0.3	0.4	0.5	0.6	0.7	0.8	0.9	1
0	0	11.5	8.5	4.9	3.8	3.5	2.0	1.4	3.6	2.8	0
0.1	12.8	13.6	11.9	12.1	10.7	7.1	6.5	6.3	6.5	1.1	
0.2	8.9	9.9	2.8	12.6	14.3	8.2	8.1	6.3	2.1		
0.3	7.4	7.9	8.8	6.0	9.5	9.9	8.8	1.9			
0.4	5.7	8.5	2.7	15.8	6.7	9.6	1.9				
0.5	0.1	19.2	16.8	12.7	11.5	2.5					
0.6	1.0	17.2	11.2	11.5	3.2						
0.7	0.7	13.2	11.4	2.8							
0.8	10.4	9.5	1.6								
0.9	7.9	1.0									
1	0										

Table 4-14: Chang's model percentage errors for d_1 = 4.50 mm, d_2 = 10.8 mm, d_3 = 13.0 mm

x_2	Percentage error (%)										
	x_1										
	0	0.1	0.2	0.3	0.4	0.5	0.6	0.7	0.8	0.9	1
0	0	13.4	12.4	10.9	11.8	13.4	10.4	12.8	12.8	15.3	0
0.1	14.5	10.4	11.5	12.4	6.8	12.5	15.9	17.8	11.8	15.7	
0.2	15.4	7.1	7.9	6.2	23.3	13.9	15.2	14.3	8.9		
0.3	16.7	5.8	7.1	2.3	10.5	16.2	11.8	5.9			
0.4	18.0	5.5	2.9	14.3	20.3	15.9	4.7				
0.5	18.7	13.7	17.2	14.7	16.8	6.9					
0.6	21.4	13.6	18.0	14.5	10.0						
0.7	22.0	13.9	16.1	11.9							
0.8	24.6	14.3	14.1								
0.9	26.5	24.4									
1	0										

Figure 4-28 shows a comparison of modelled and experimental voidage vs. sauter mean diameter for the CM. The CM performed best for smaller d_{psm} values of d_{psm} < 5mm. For d_{psm} > 5mm, the CM started to over predict voidage from experimental results.

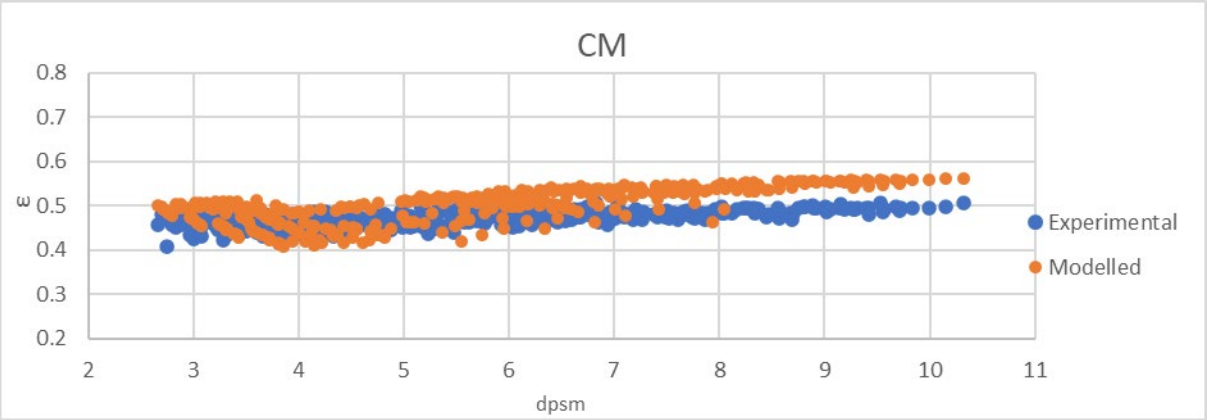

Figure 4-28: Chang model performance

As previously stated, the D/d_p ratio for this study was between values 8.0 – 44.1. Previous studies for the CM had ratios < 140. The particle sizes used in previous studies were between 0.089mm – 15.73mm. The char particles used in this study yielded D/d_p and sizes mostly within the ranges of previous studies. The least spherical particles the CM was tested for were sand particles. The CM included most of the same parameters as the WM, with the exception of wedging packing effects.

Figure 4-29 shows the parity plot for the De Larrard model. The De Larrard model overpredicted almost all the ternary and binary mixtures combined. The average percentage error for the De Larrard model regressed for char particles was 12.0%, with a standard deviation of 4.2%. De Larrard's model had the worst-performing model for char particles.

Figure 4-30 shows a comparison of modelled and experimental voidage vs. sauter mean diameter for the Del Larrard. For char particles, the De Larrard over predicted voidage for the entire range of d_{psm}.

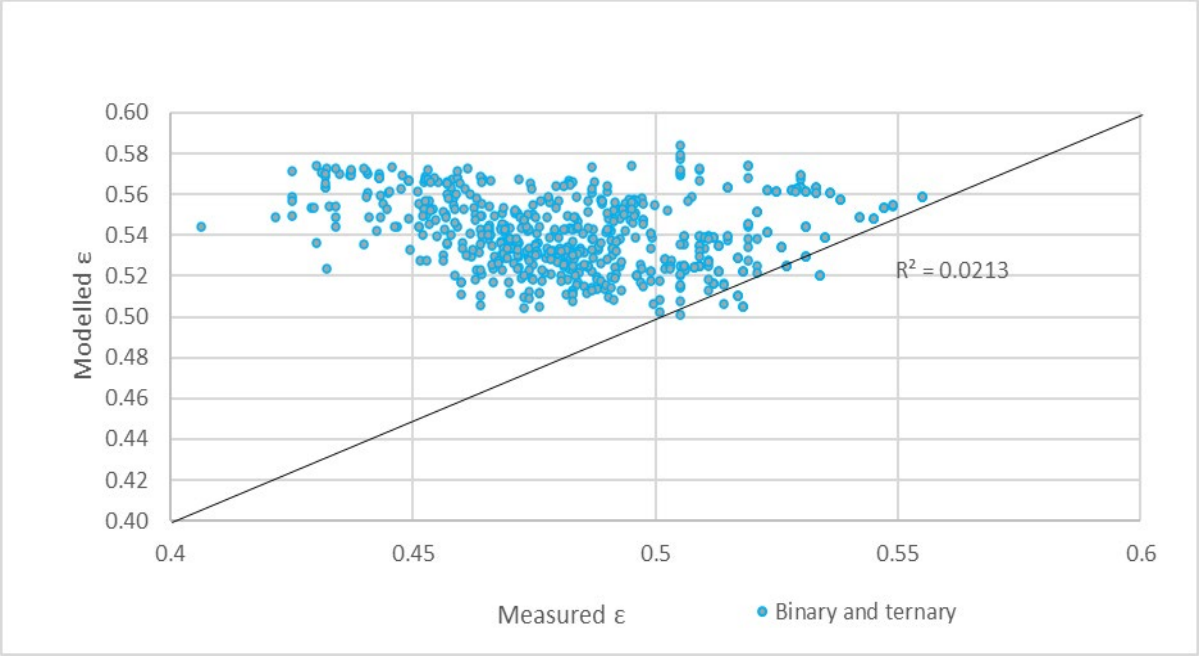

Figure 4-29: Voidage parity plot for the De Larrard model and ternary mixtures

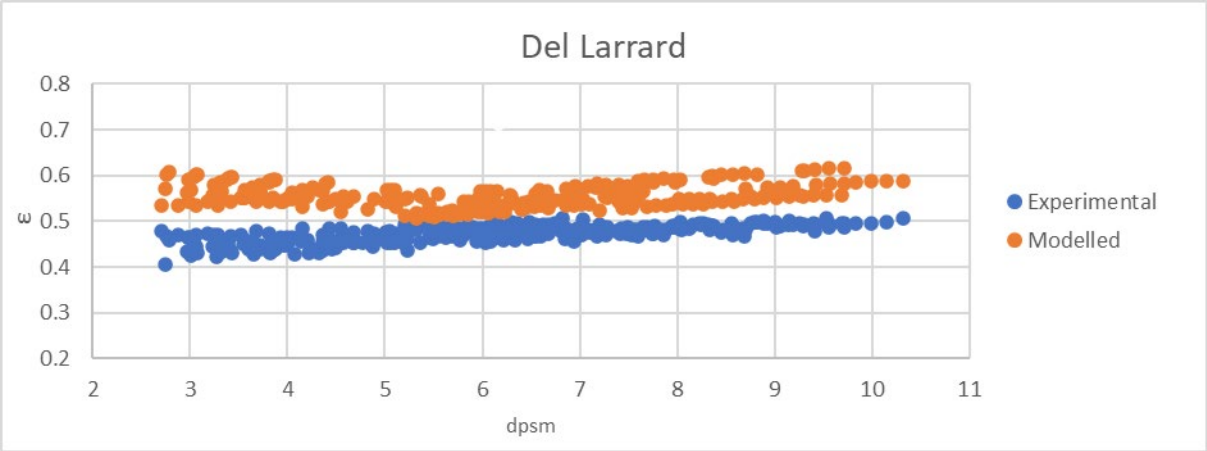

Figure 4-30: Chang model performance

The previous models were originally derived for near spherical particles. Other studies showed that the could produce promising results for less spherical particles. These less spherical particles however did not have sphericity values as low as the biochar particles of this study. Brownell's correlation of equation 2-52 was regressed for biochar particles. The original values for Brownell's equation and the regressed values for biochar is shown in Table 4-15.

Table 4-15: Brownell equation regression parameters

Particle type	a	b
Rings	-0.8648	0.2745
Biochar	-1.2989	0.6325

The values of a and b regressed for biochar in the Brownell equation differed by factors of 1.5 and 2.3 respectively. Sphericity values were obtained from pressure drop experiments at very low velocities using Equation 2-57. The sphericity values of the particle beds range from 0.374 – 0.635. Figure 4-31 show the biochar experiments, original Brownell equation and biochar regressed Brownell results.

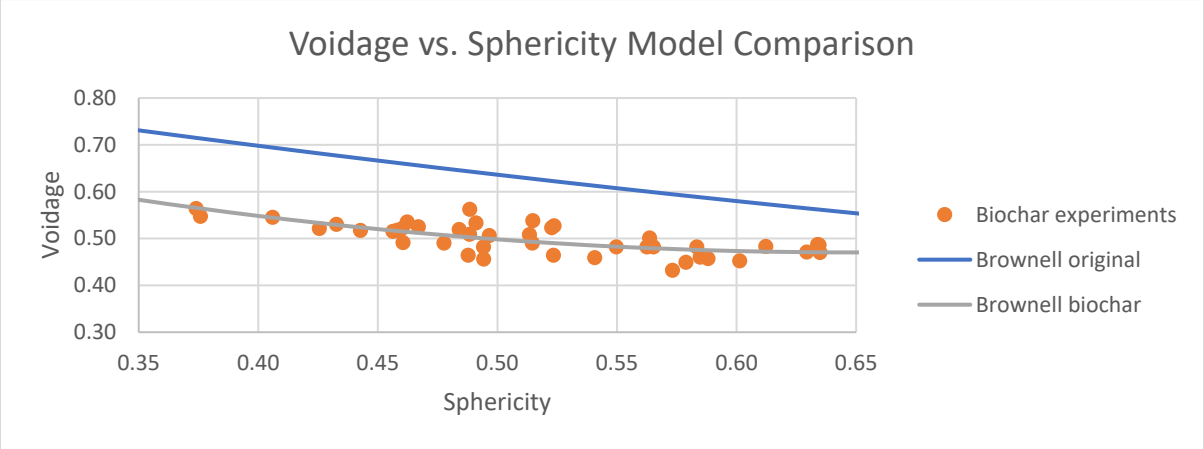

Figure 4-31: Brownell model performance

The original Brownell equation overestimated the voidage results for biochar particles. The Brownell equation with regression performed better, but it's clear that there is still some variance in the model. Figure 4-32 shows the parity plot for the regressed Brownell model. All but 4 data points are outside of the 10% percentage error bounds. The R^2 value of the parity plot is still too low at 0.5049 for satisfactory results.

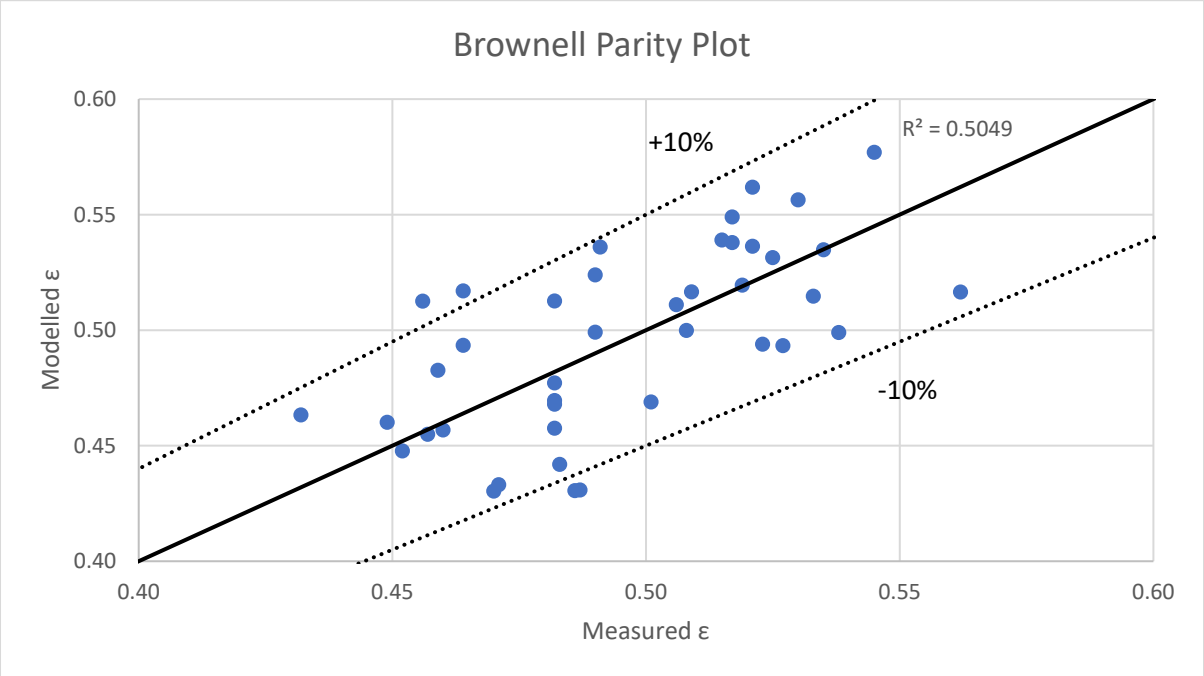

Figure 4-32: Brownell model parity plot

Koekemoer's correlation of Equation 2-53 was regressed for binary mixtures of biochar as well. The original values for Koekemoer's equation and the regressed values for biochar is shown in Table 4-16.

Table 4-16: Koekemoer voidage model parameter values

Particle type	a	b	c
Coal	0.430	0.061	-0.030
Charred Coal	0.455	0.116	-0.039
Ash	0.494	0.055	-0.023
Biochar	0.472	5.108	-0.005

The values regressed for the biochar differed significantly than for coal, charred coal and ash particle beds. The biochar used in this study had significant differences in shape than coal, charred coal and ash. From chapter 2, ash had the lowest sphericity values in the study of Koekemoer et.al. The lowest sphericity value of ash particles were around 0.66. The highest sphericity value for a packed bed of biochar was calculated to be 0.635 (by making use of equation 2-57). The average sphericity of biochar beds were 0.516, with a bed with the lowest sphericity at 0.374. The biochar had significantly lower sphericities than previously tested particles which may lead to the regressed values for Equation 2-53 to differ so much. The parity plot for Koekemoer's equation is shown in Figure 4-33.

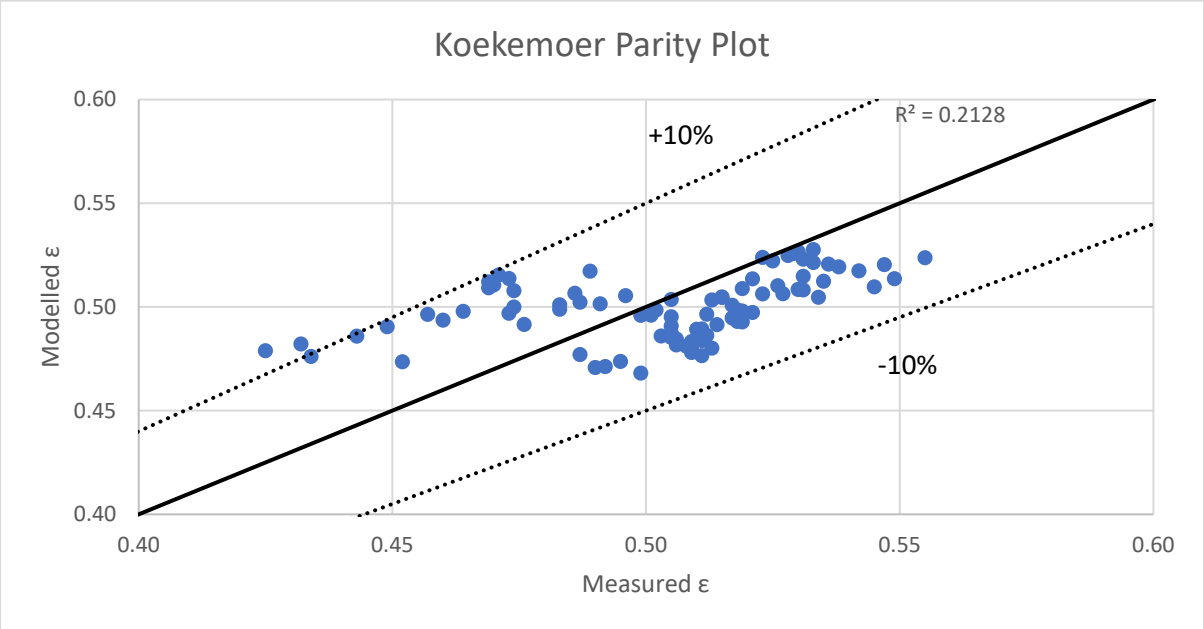

Figure 4-33: Koekemoer model parity plot

All but 2 data points fall outside the 10% percentage error bounds. The model also had a low R^2 value of 0.2128 for its parity plot. Figure 4-34 show the model's performance plotted over the experimental data points.

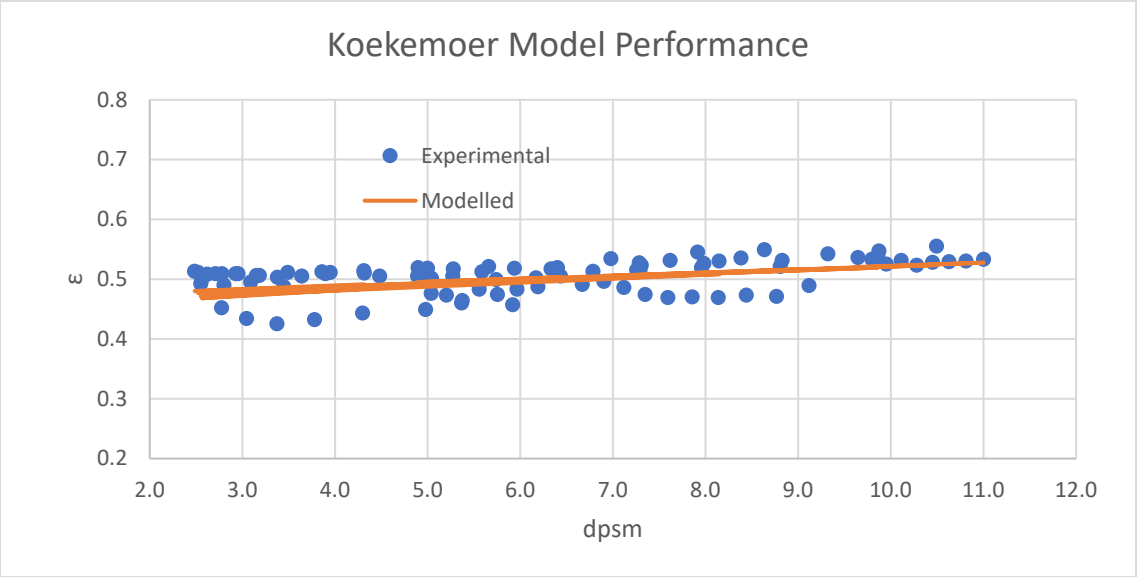

Figure 4-34: Koekemoer model parity plot

Koekemoer's model assumes a linear correlation between voidage and mean particle diameter. The model might predict the overall trend, but in the case where data can have a lot of variance, the model struggles to adequately predict voidage for binary mixtures of biochar.

R^2-value for the parity plots of binary and ternary mixtures gave very low values. The Toufar model had the best, or highest R^2-value, with 0.343. Table 4-17 indicates R^2-values and error percentages for the different models.

Table 4-17: Comparison of voidage models' performances

Model	Mixture type	Original particle type	Percentage error for char	Parity R^2 for char
AGM	Binary	Quartz	4.99	0.134
LPDM	Binary	Quartz	3.82	0.295
TM	Binary	Quartz	3.94	0.343
MKM	Binary	Quartz	4.25	0.331
WM	Ternary	Glass beads	8.22	0.001
CM	Ternary	Aggregate concrete	9.95	0.013
CPM	Ternary	Glass beads	12.0	0.021
	Unmixed	Clay		
Brownell	Binary	And	5.27	0.504
	Ternary	Nickel Saddles		
		Coal		
Koekemoer	Binary	Charred Coal Ash	4.42	0.213

The voidage models generally had satisfactory average percentage error values. This does not mean that they necessarily have good modelling performances. The low parity plot R^2-values indicate that the models' variances were high. This may suggest that the voidage models do not incorporate the correct/enough parameters for char particles. The models make extensive use of empirical correlations. The char particles have very low sphericities and high elongation factors compared to particles such as quartz and glass beads. The study by (Liu *et al.*, 2020) did not give exact values for R^2-values on their parity plots, but it is apparent that their R^2-values were much higher than for char particles. The studies for the ternary voidage models did not give information on R^2-values. Factors such as sphericity and elongation are not commonly used as parameters to model bed voidage for. Figures 4-35 to Figure 4-37 show how the loosening, wall and wedge effects can increase voidage for elongated partilces.

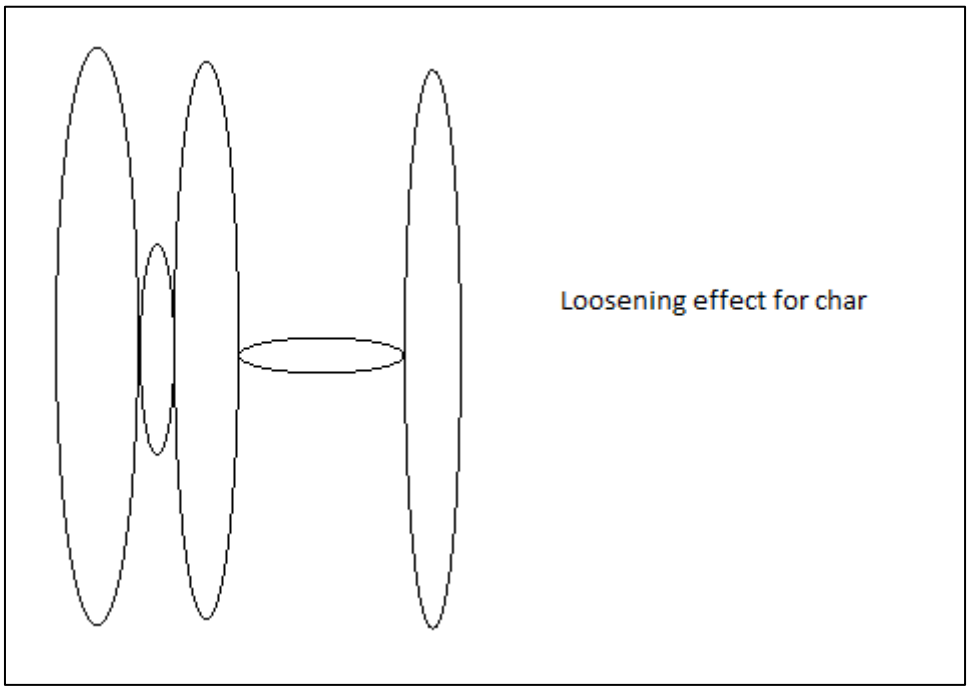

Figure 4-35: Effect of loosening between elongated particles

From figures 35 to 37, a 90˚ change in angle of how a particle packs can have a significant effect on a packed bed's voidage. Current voidage models do not incorporate the angles in which particles are likely to pack. Most voidage models are tesed for near spherical particles in which the angle the particles pack won't make a big difference. For the case of models used for less spherical particles, the models don't include loosening, wall and wedge packing effects. The most encompassing voidage models include packing effects, ratios between the smallest and largest particle, volumetric fractions of the mixtures and the voidage values for the unmixed particles of which a mixture comprise of. Although these models are the most encompassing, they are still heavily reliant on multiple regressed empirical values. This seem to work adequately for more spherical particles, but the models performance drastically deteriorate when particles become elongated. More work needs to be done to see if it is

possible to incorporate an angle in which particles are likely to pack within a bed. This angle will likely affect the way how loosening, wall and wedge effects are modelled.

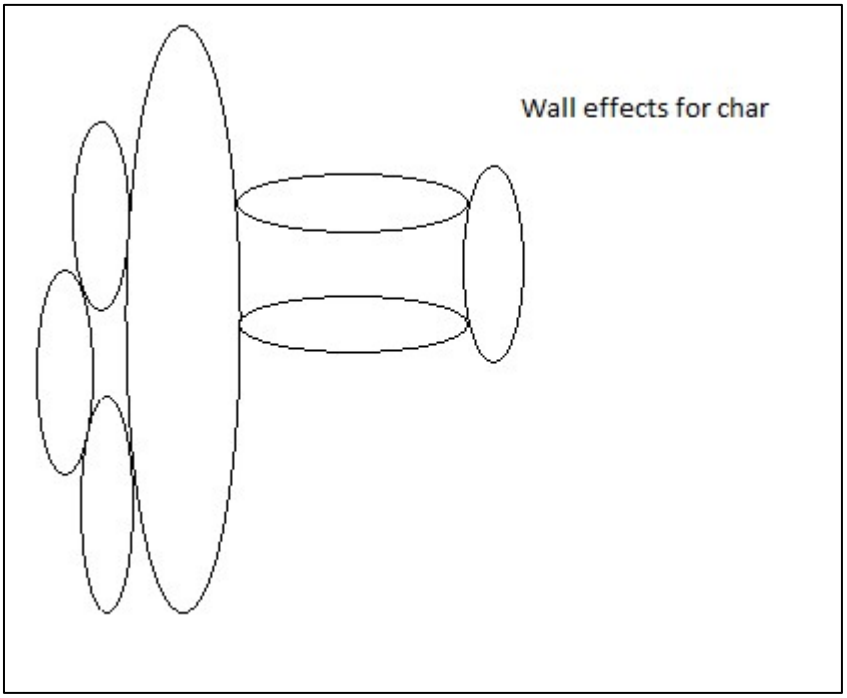

Figure 4-36: Effect of wall effects between elongated particles

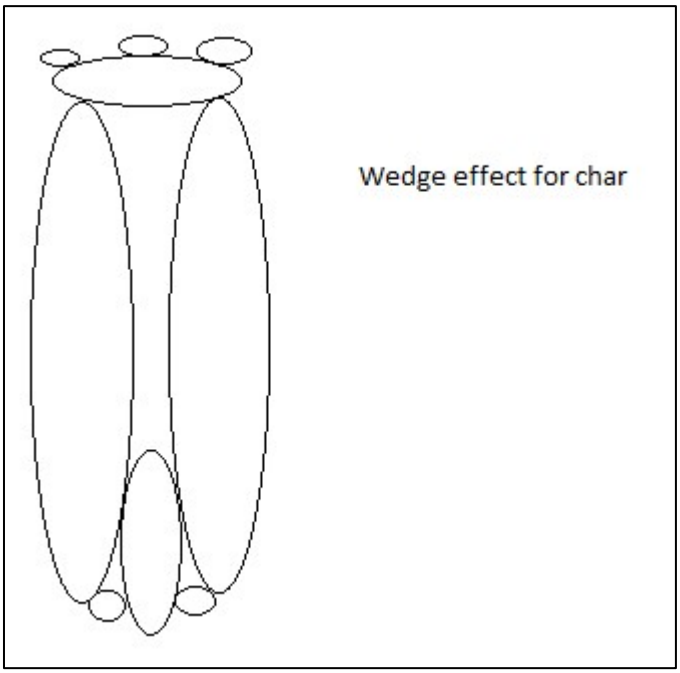

Figure 4-37: Effect of wedging between elongated particles

4.5 PARAMETERS INFLUENCING PRESSURE DROP

Figure 4-38 shows the pressure drop results through the mono-sized char batches.

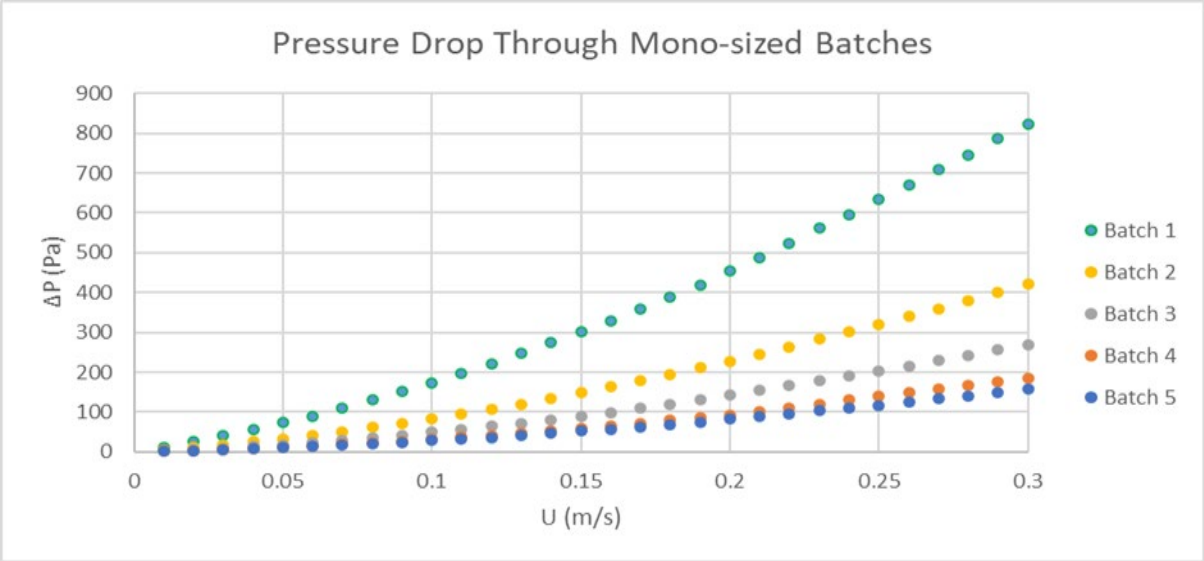

Figure 4-38: ΔP vs. U for unmixed particle batches

From chapter 2, the parameters influencing pressure drop are the particles' diameters, gas velocity and the bed's voidage. Figure 4-38 shows that smaller particle diameters (which give smaller bed voidage values) delivered higher pressure drops.

Figure 4-39 shows the pressure drop vs particle diameter results for mixtures with ε = 0.482

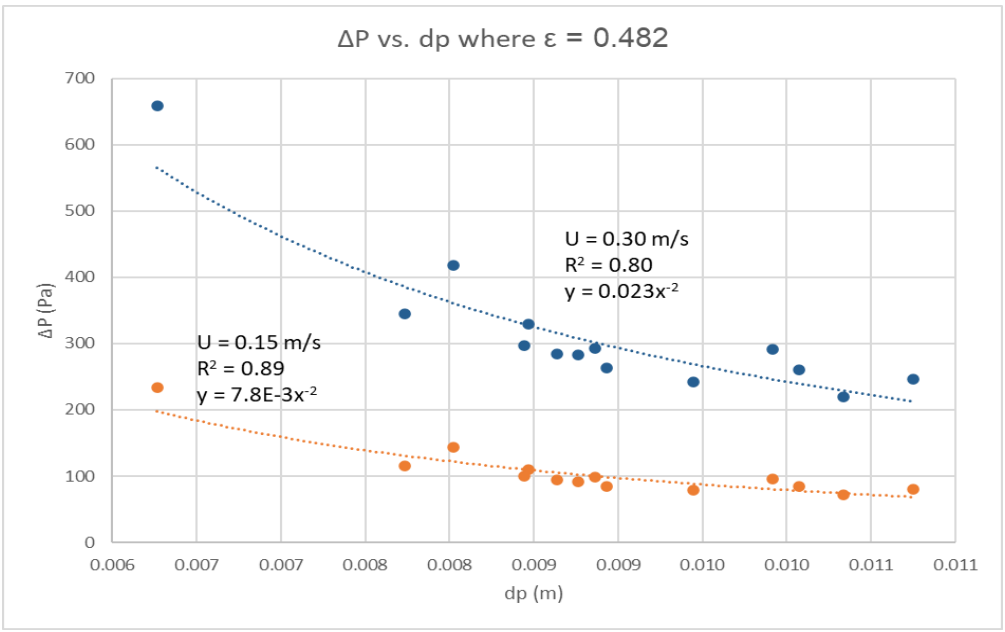

Figure 4-39: ΔP vs. dp at constant gas flow velocity

and for which the fluid velocities were at 0.30 m/s and 0.15 m/s. The overall trends fitted well with $\Delta P \propto dp^{-2}$ correlations, as suggested by literature.

Ergun equation modelling

The Rhovol and KC Equation were used to determine sphericity used in the Ergun Equation. The 2 methods produced considerable different results when used for pressure drop modelling. Figures 4-40 and 4-41 show these results where the A and B values of the Ergun equation were regressed for all mixtures.

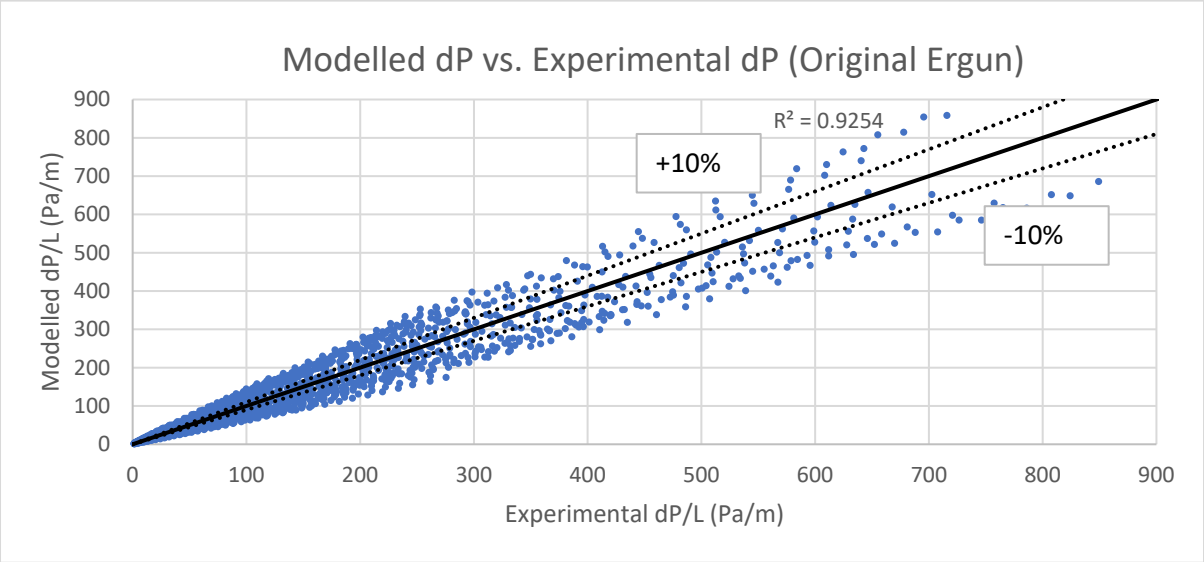

Figure 4-40: Pressure drop modelling using sphericity determined by the Rhovol

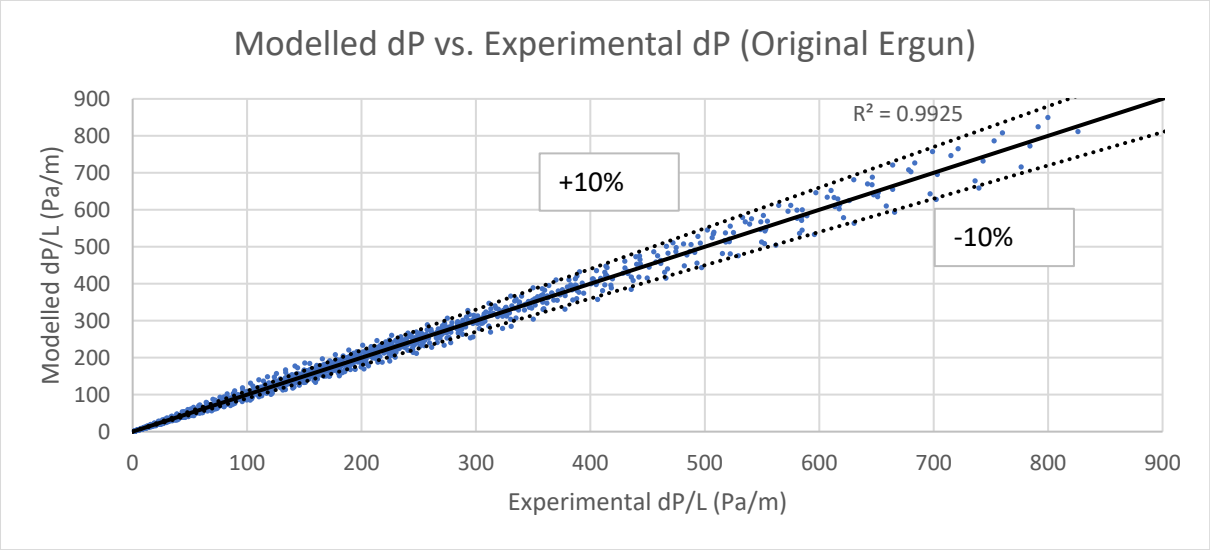

Figure 4-41: Pressure drop modelling using sphericity determined by the KC Equation.

The R^2 values for both graphs seem satisfactory for the Rhovol and KC equation at 0.9254 and 0.9925 respectively. It's clear that the parity plot shown in Figure 4-41 performs better than the plot on Figure 4-40. When looking back at Figures 4-40 and 4-41, the range of sphericity determined with the Rhovol were much larger than determined with the KC equation. Table 4-18 show the A and B values regressed for Figures 4-40 and 4-41. The values for Table 4-18 were regressed using unmixed, binary and ternary mixture results.

Table 4-18: A and B regressed for biochar particles

Sphericity method	A	B
Rhovol	220	2.30
KC	196	2.20

The A and B values shown in Table 4-18 are much higher than the original values of A = 150 and B = 1.75. The difference in modelling performance can possibly be attributed to the way in which the Rhovol and KC equation defines sphericity. From Equation - 2-56, the Rhovol approximates sphericity using 3 dimensions through a particle. The Ergun equation uses the same theoretical part of the KC equation to determine energy losses due to laminar flow. The original empirical values used in the Ergun and KC equations differ with 150 and 180 respectively. The Ergun equation and KC equation is derived from energy losses caused by drag that a fluid experience flowing around the surfaces of particles. The method used by the Rhovol's sphericity does not include the effect of the surface area of a particle. From here onward, sphericity determined by the KC equation will be used for pressure drop models.

The Ergun equation also performed well if a portion of data is used to regress the A and B values with a separate set for data for validation. Unmixed particle batches and binary mixtures used for regression yield satisfactory results when tested with ternary mixtures. Figure 4-42 show the parity plot for the regression set and Figure 4-43 show the parity plot for the validation set of ternary mixtures. The A and B values regressed with the unmixed particles and binary mixtures were A = 205 and B = 2.17, which were similar to the values regressed on all data as seen in Table 4-18. The average modelling error for the regression data was 7.8% and the average modelling error for the test data was 7.3%. The regression data and test data yield satisfactory R^2 values for their parity plots with $R^2 = 0.9945$ and $R^2 = 0.9919$ respectively.

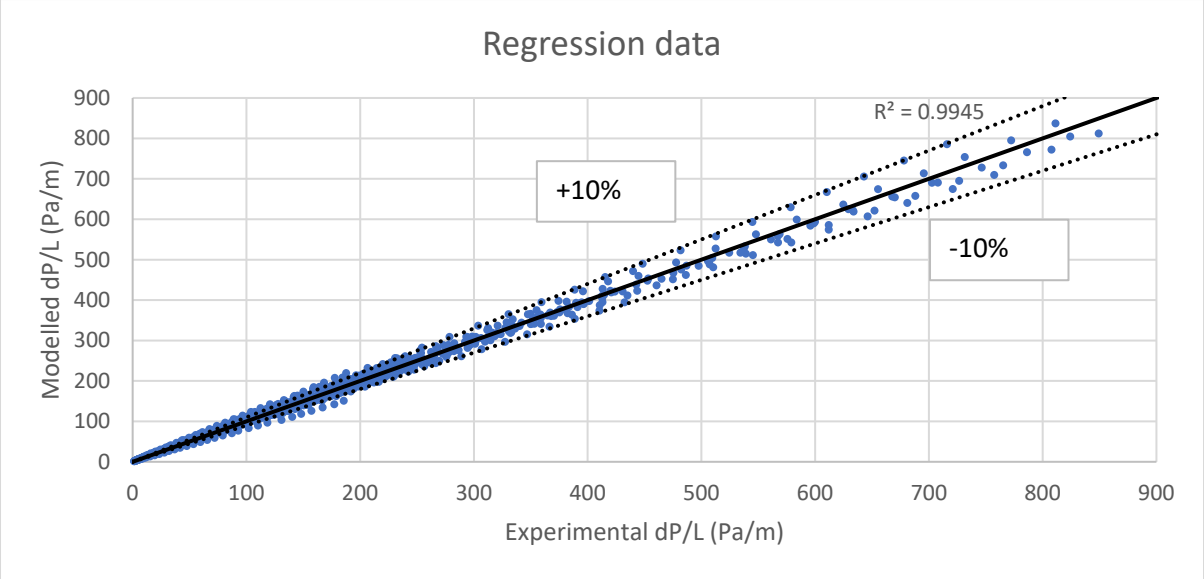

Figure 4-42: Ergun equation results regressed with unmixed batches and binary mixtures

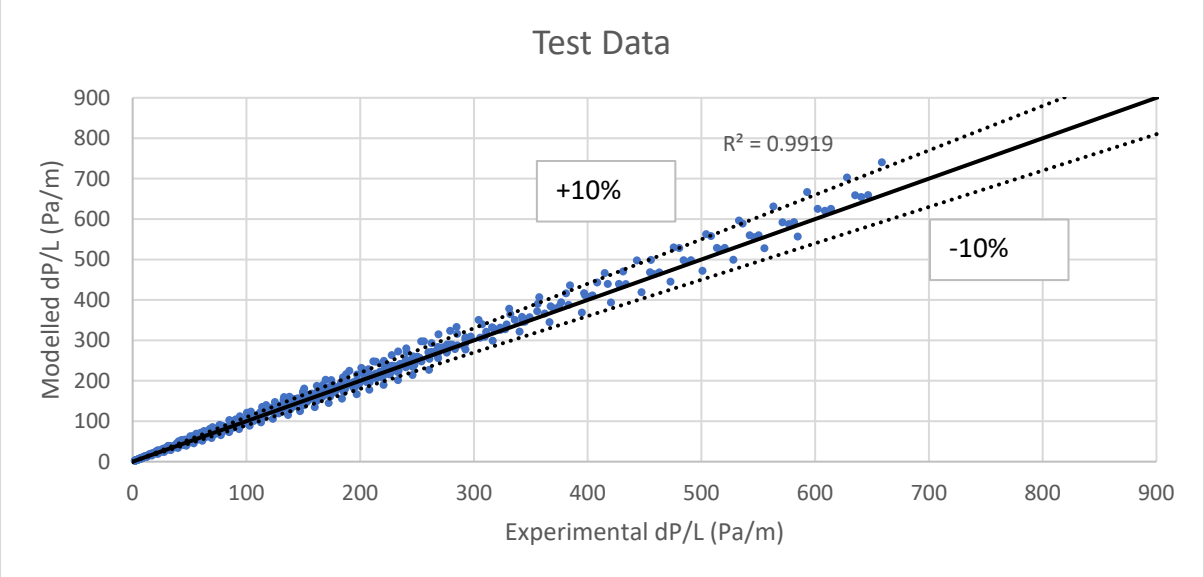

Figure 4-43: Ergun equation results tested with ternary mixtures

4.6 MODIFIED ERGUN MODELS

The Tallmadge, Foscolo and KTA models of Table 2-4 did not incorporate sphericity as the models are typically used for spherical particles in nuclear applications. These models performed well for the biochar particles when sphericity was added as a modelling parameter. The pure and binary mixtures were again used as regression data for the empirical values of the models and the ternary mixtures were used as test data. Table 4-19 show the Foscolo, KTA and Tallmadge models with their empirical values regressed for biochar. Table 4-20 show the percentage error results for the modified Ergun Equation models.

Table 4-19: Modifications of the Ergun Equation incorporating sphericity and the modified Reynolds number

Model	Equation	
Foscolo	$\frac{\Delta P}{L} = 31.2\left(\frac{1-\varepsilon}{\varepsilon^{4.8}}\right)\left(\frac{\mu U}{\left(\varphi_{KC} d_p\right)^2}\right) + 0.507\left(\frac{\rho U^2}{\varphi_{KC} d_p}\right)$	**4-16**
KTA	$\frac{\Delta P}{L} = \left(\frac{3547}{\left(\frac{Re_m}{1-\varepsilon}\right)} + \frac{38}{\left(\frac{Re_m}{(1-\varepsilon)}\right)^{0.1}}\right)\left(\frac{1-\varepsilon}{\varepsilon^3}\right)\left(\frac{U^2}{2\varphi_{KC} d_p}\right)$	**4-17**
Tallmadge	$\frac{\Delta P}{L} = \left(\frac{(1-\varepsilon)^2}{\varepsilon^3}\right)\left(\frac{\mu U}{\left(\varphi_{KC} d_p\right)^2}\right)\left(167 + 5.5 {Re_m}^{0.833}\right)$	**4-18**

Table 4-20: Modified Ergun Equation models' results

Model	Regression data error	Test data error
Foscolo	11.7	15.1
KTA	8.2	7.0
Tallmadge	6.1	6.4

Table 4-20 show that the test data performed as well as the regression data. Figure 4-44 to 4-49 show the parity plots for the Foscolo, KTA and Tallmadge models with the regression and test data.

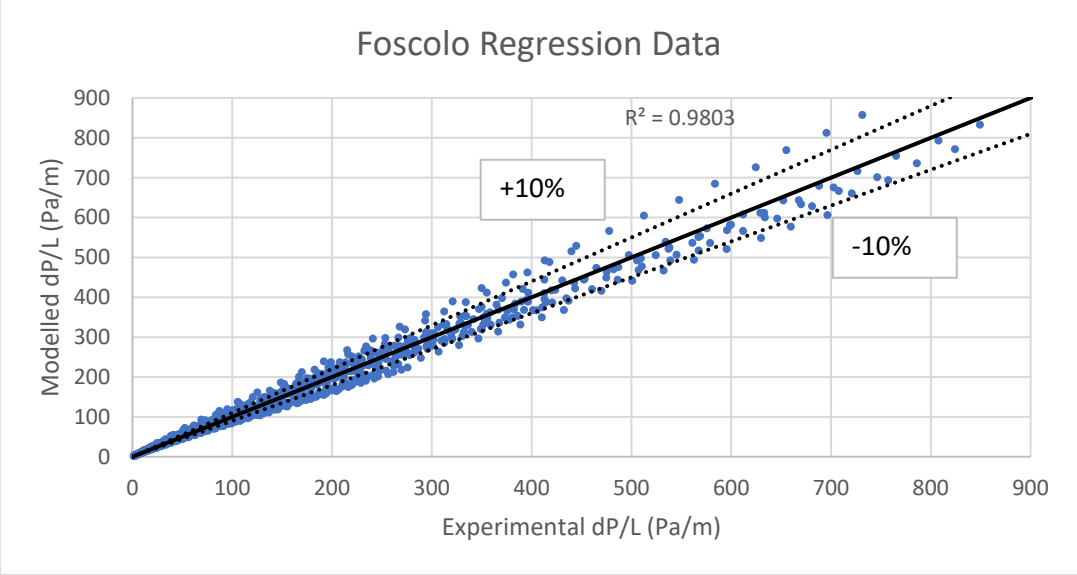

Figure 4-44: Results of the Foscolo model regressed with unmixed batches and binary mixtures

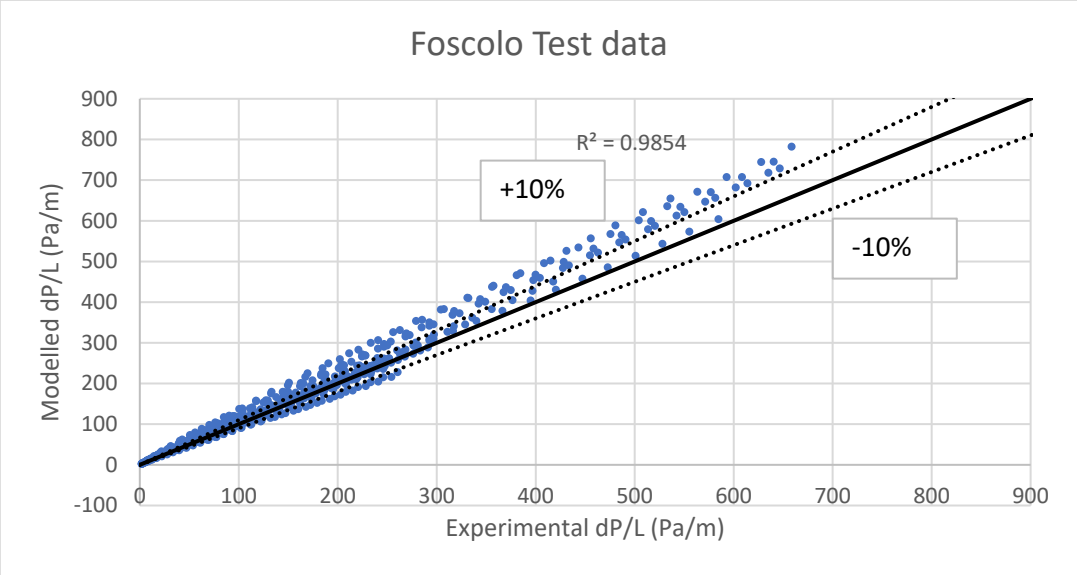

Figure 4-45: Results of the Foscolo model for ternary mixtures

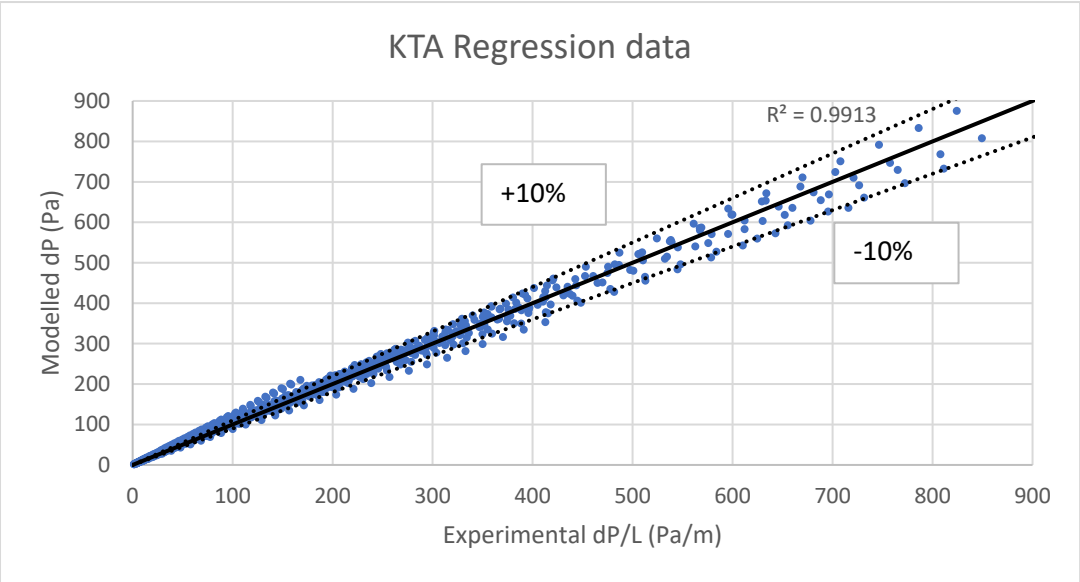

Figure 4-46: Results of the KTA model regressed with unmixed batches and binary mixtures

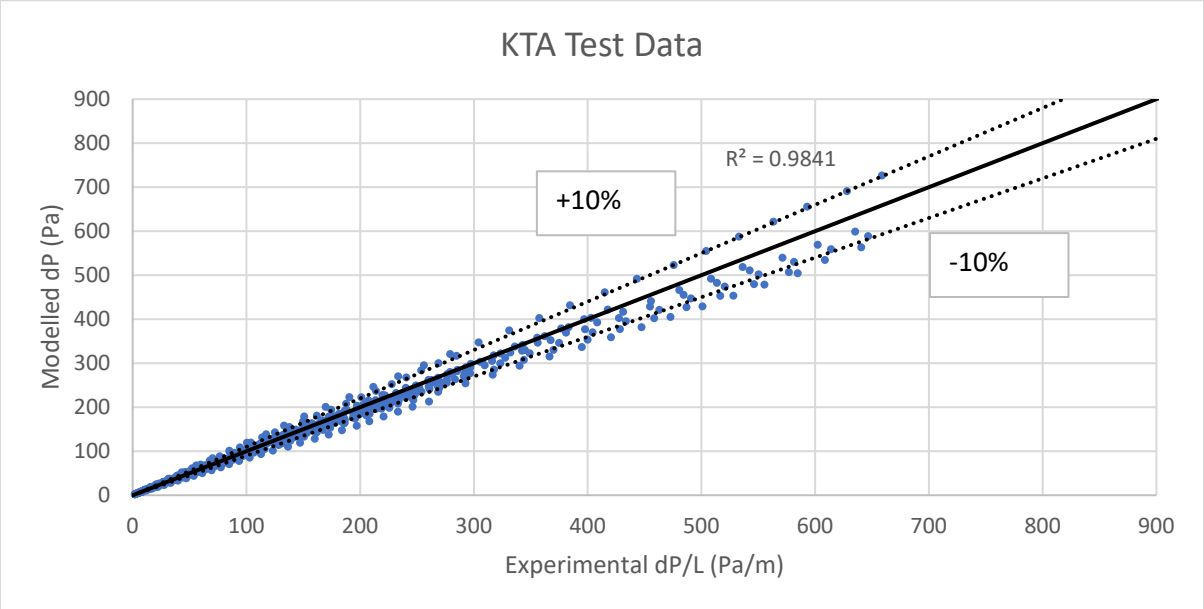

Figure 4-47: Results of the KTA model for ternary mixtures

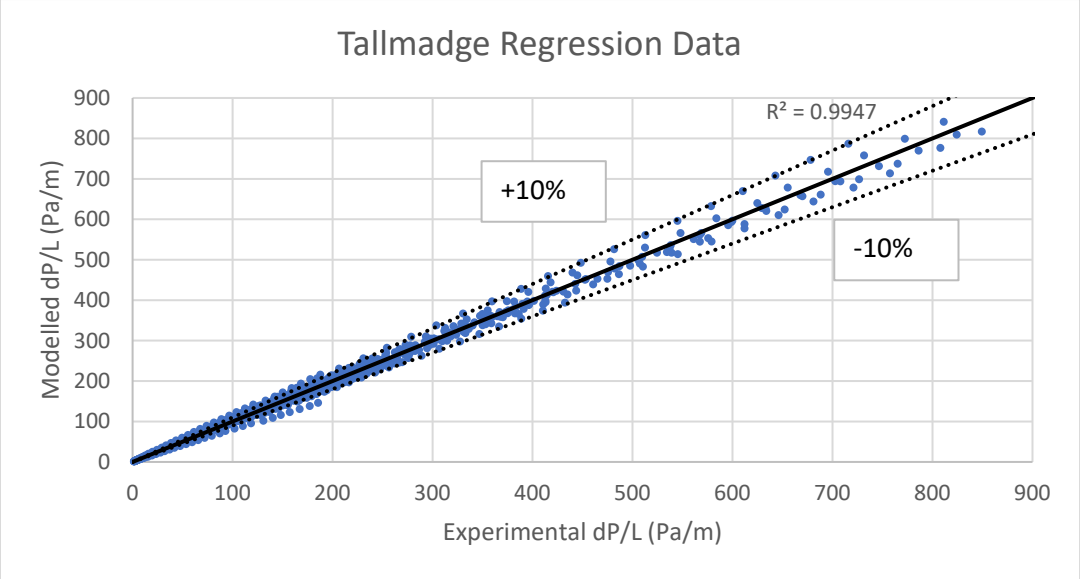

Figure 4-48: Results of the Tallmadge model regressed with unmixed batches and binary mixtures

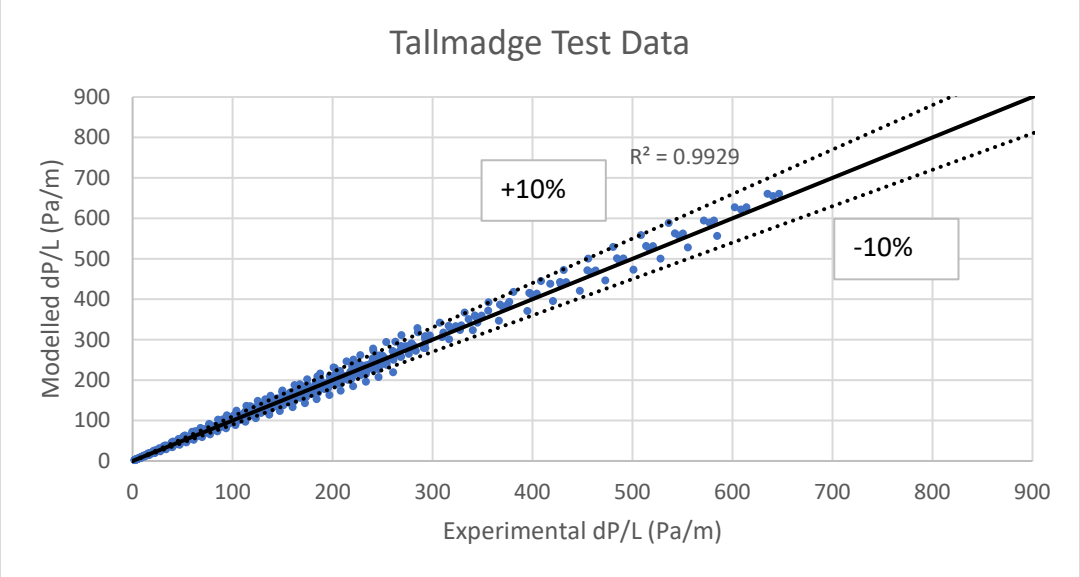

Figure 4-49: Results of the Tallmadge model for ternary mixtures

The Foscolo model performed the worst out of the 3 modified Ergun models. The model over and under predicted ΔP/L yp to > 10% for the regression data set. The Foscolo also over predicted more ΔP/L values for the test data set. The KTA and Tallmadge models performed better with average percentage errors < 10% for the regression and test data sets.

4.7 STATISTICAL MODELLING OF PRESSURE DROP

Sections 4.5 and 4.6 showed that the Ergun equation can be used to adequately model pressure drop for biochar mixtures. The Ergun equation however does not consider the interaction between the particles for the mixtures. Two statistical approximations are shown in equations 4-19 to 4-20 that only considered the interactions between the biochar particle batches and gas velocity. These models were not derived from fundamental principles. The pure batches with binary mixtures were also used to regress the α and β for the statistical models and the ternary mixtures were used for testing. The parity plots for the approximations in Table 4-21: Statistical models' equations are shown in Figure 4-50 to 4-53.

Table 4-21: Statistical models' equations

Approximation	Equation	
Quadratic polynomial	$\frac{\Delta P}{L} = \left(\sum_i \beta_i x_i^2 + \sum_{ij} \beta_{ij} x_i \, x_j \right) U^{1.48}$	**4-19**
Padé polynomial	$\frac{\Delta P}{L} = \left(\frac{\sum_i \beta_i x_i^2 + \sum_{ij} \beta_{ij} x_i \, x_j}{\sum_k \alpha_i x_i} \right) U^{1.48}$	**4-20**

The quadratic and Padé polynomials only considered interactions between 2 particles in a mixture. The fundamental models gave that the pressure drop through the char particles had a quadratic dependency on gas flow velocity. The statistical models suggested that the pressure drop had rather had an exponential dependency on gas flow velocity. Instead of a quadratic dependency, the statistical models fitted better with $\Delta P \propto U^{1.48}$. The statistical models which considered the interactions between the different particles' batches modelled pressure drop with average percentage errors less than 10%. Table 4-23 show the average percentage errors for the statistical models with the regression and test data sets.

The α and β values for the models in Table 4-21 are shown in Table 4-22. Comparing the results from Table 4-23 to the results from the fundamental models show that the consideration of particle interactions can also give good modelling results.

Table 4-22: α and β values for the polynomial models

$\beta_i, \beta_{ij}, \alpha_i$	Quadratic	Padé
β_1	787	193
β_2	1040	179
β_3	1496	216
β_4	2567	183
β_5	4796	549
β_{12}	2329	421
β_{13}	3118	562
β_{14}	5756	925
β_{15}	11388	2106
β_{23}	3498	538
β_{24}	100	100
β_{25}	10628	1615
β_{34}	3779	445
β_{35}	9385	1282
β_{45}	7650	706
α_1	-	0.220
α_2	-	0.167
α_3	-	0.143
α_4	-	0.072
α_5	-	0.117

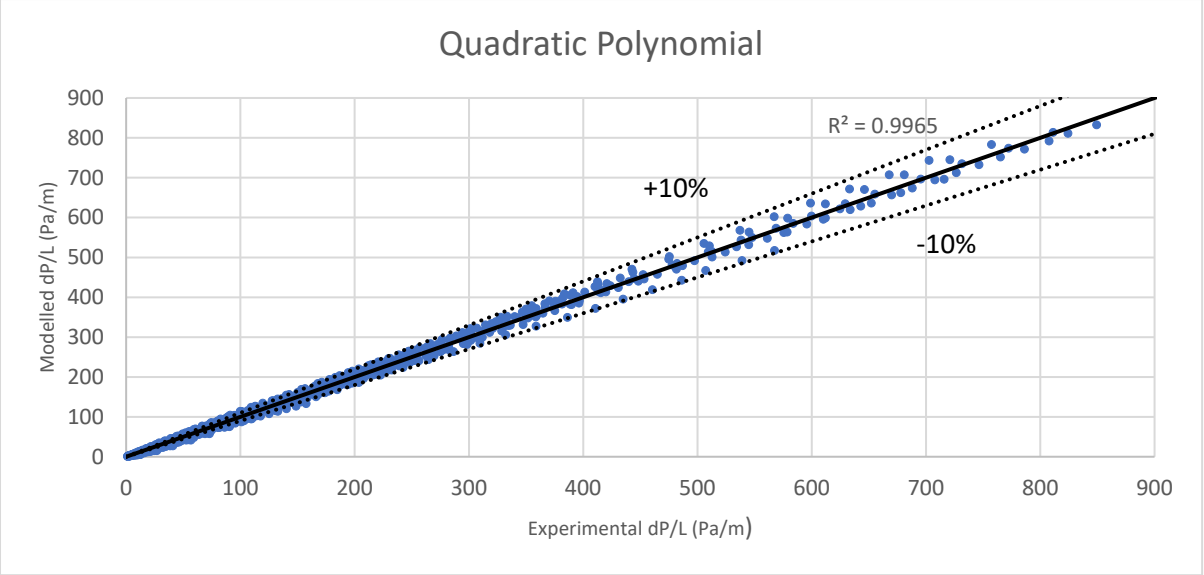

Figure 4-50: Results of the Quadratic polynomial model regressed with unmixed batches and binary mixtures

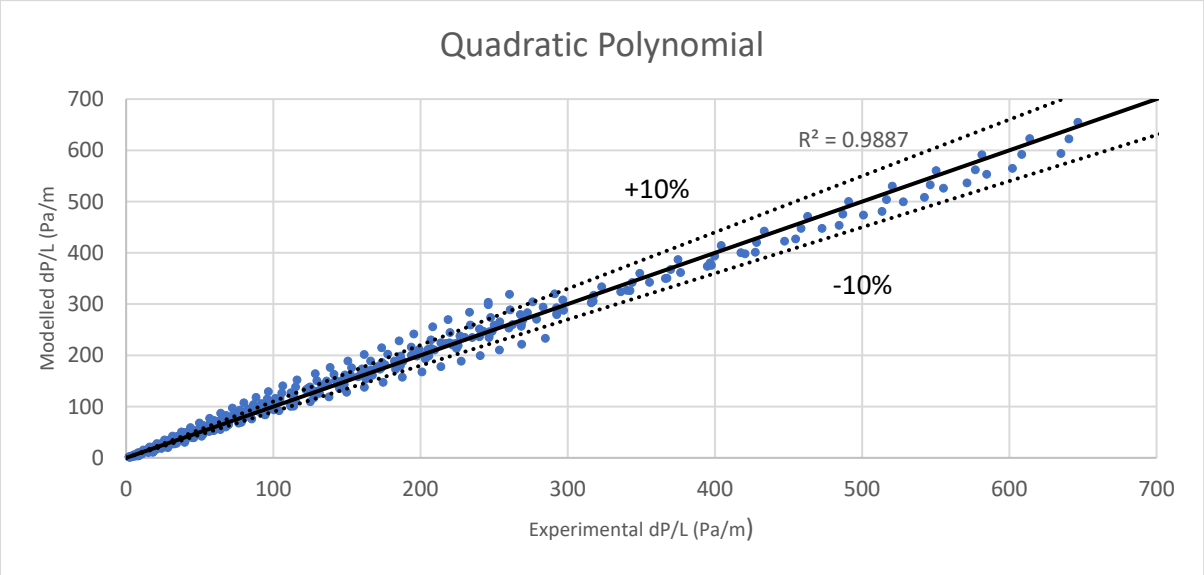

Figure 4-51: Results of the Quadratic polynomial model for ternary mixtures

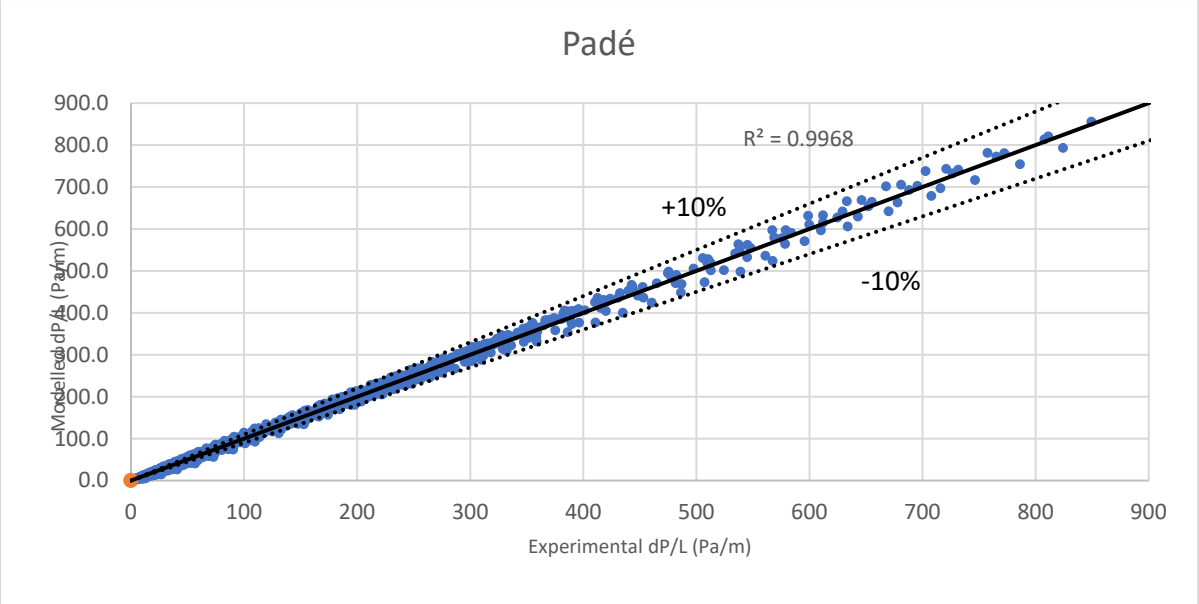

Figure 4-52: Results of the Padé model regressed with unmixed batches and binary mixtures

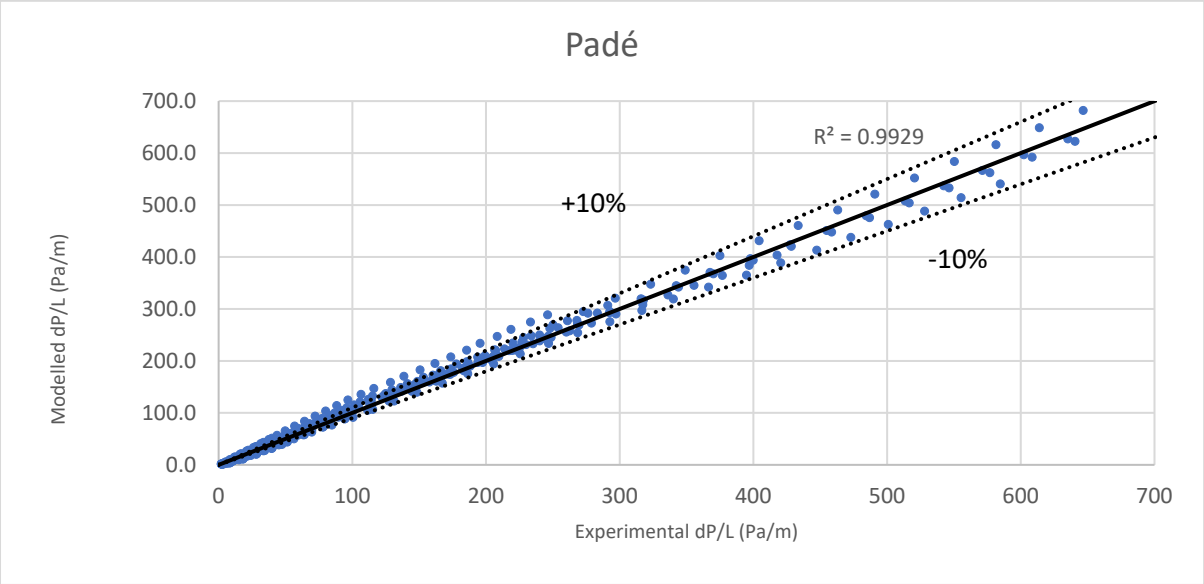

Figure 4-53: Results of the Padé model for ternary mixtures

Table 4-23: Statistical models' performance

Model	Regression data error	Test data error
Quadratic	7.1	11.4
Padé	7.2	10.7

The statistical models yielded good modelling results for the pure batches and binary mixtures with average error percentages of 7.1% and 7.2% respectively. Their performance with the ternary mixtures (test data set) were slightly less satisfactory with 11.4% and 10.7%.

5. CONCLUSION & RECOMMENDATIONS

5.1 CONCLUSION

The aim of this study was to model pressure drop over a fixed bed of biomass char particles by studying the effect of the particles' characteristics on fixed bed structure. Using statistical models, pressure drop through beds of char particles could be modelled with average percentage errors of less than 10%. The statistical models considered the fluid flow velocity and the interactions between mixtures of char particles. Fundamental models could not model pressure drop with the same accuracy.

Objectives:

Determine which of a particle's characteristics influence the bed voidage for different size biomass char particles when packed in binary and ternary mixtures:

Voidage was mainly influenced by the size of the particles and the volumetric ratios of which the mixtures were made of. It was found that linear and non-linear models worked well for binary mixtures with low percentage errors. From the sizes and the volumetric ratios, further parameters, such as loosening, wall and wedging effects, could be calculated. These effect parameters were used to model voidage with average errors of less than 10% for binary and ternary mixtures. Four voidage models were tested for binary mixtures. Two of these were linear models, and the other were non-linear models. The linear models were the AG and LPD models. The non-linear models tested were the Toufar and the modified Kwan models. The AG model yielded a percentage error of 4.99%. The LPD model had a better error percentage of 3.82%. The AG model only considered wall effects, while the LPD model considered wall and loosening effects. The decrease in percentage error of the LPD model compared to the AG model can likely be attributed to the incorporation of the extra packing effect. However, both linear models did not adequately model the general trend of voidage vs x_1. The AG model predicted the optimal packing fraction for too-small values of x_1. The LPD model predicted the optimal packing fraction for too-large values of x_1. The non-linear models predicted the trend of voidage vs. x_1 much better than the linear models. The non-linear models did not perform that much better than the linear models. The Toufar models yielded a percentage error of 3.94%. The modified Kwan model yielded a percentage error of 4.25%. The Toufar model only considered wall effects. The modified Kwan model considered loosening, wall and wedging effects. Non-linear models were also used to model the voidage of ternary mixtures. Two of the three models yielded satisfactory results. The DL model had the highest percentage error of 12.0%. The DL model did, however overestimate nearly all the voidage values. The Wong and Chang models performed adequately. The Chang model only considered loosening and wall effects. Wong's model considered loosening, wall and wedging effects. Chang's model

tended to overestimate voidage for ternary models. Chang's model did, however, have a relatively equal distribution of over- and underestimated voidage results for binary mixtures.

Evaluate the effects of particle and packing characteristics in fixed beds of biomass char on measured and modelled pressure drop values:

Fundamental pressure drop models rely heavily on the particle bed's average particle diameter, sphericity and bed voidage to model pressure drop. As described in literature, pressure drop was found to have similar dependencies on particle diameter. It was found that smaller particle sizes lowered the packed bed's voidage. The pressure drop through beds with smaller particle sizes and bed voidages yielded higher experimental pressure drop values. The widely used Ergun equation could not adequately model the pressure drop through packed beds for binary and ternary mixtures of char particles. The Ergun equation, however, did perform relatively well for mono-sized batch particle beds. The Ergun equation's percentage error for all of the mixtures combined was 20.8%. A percentage error of 20.8% is too high for most engineering applications. Four other fundamental models similar to the Ergun equation was tested. These models included the Tallmadge, Montillet, KTA and Foscolo models. Their percentage errors were 20.4%, 18.6%, 20.6% and 26.1%, respectively. The fundamental models did consider the effects that might occur due to the particles' packing. Three statistical polynomial models were tested. The statistical models only needed the volumetric fractions of the mixtures and the gas flow velocity through the bed. The three statistical models considered were based on a quadratic polynomial, a Padé approximation and a third-order polynomial. Their respective percentage errors were 9.0%, 8.4% and 8.1%. The statistical models performed much better than the fundamental models. The statistical models introduced interaction parameters between the particles of the mixtures, which is not considered in the fundamental models. The fundamental models modelled pressure drop with a correlation of $\Delta P \propto U^2$, however, the statistical models showed that the correlation is closer to $\Delta P \propto U^{1.49}$ for char particles.

5.2 RECOMMENDATIONS

The fundamental pressure drop models assume a homogenous packing arrangement for its voidage parameter. The voidage experiments and modelling results indicate that incorporating packing effects such as loosening, wall, and wedging effects are integral in understanding packing arrangements. The statistical polynomial models mostly used the interactions of the different-sized batches from which mixtures were made. Incorporating these particle interactions within the fundamental pressure drop models might produce better modelling results.

The intercept sphericity data obtained from the Rhovol analysis was used to determine the particles' intercept sphericities. The intercept sphericity is not the same as envelope sphericity. Pressure drop modelling might be improved if the envelope sphericity of the particles were determined. Envelope sphericity determination for a bed of particles can be a time consuming process. If a way of determining a fixed bed's envelope sphericity can be developed, the Ergun equation and its modifications' modelling performance might improve. Further studies on the effect of different ways of modelling sphericity might be useful for fixed bed applications.

The effect that higher fluid flow velocities might have on the Ergun constants with char particles can be studied further. Turbulent flow in fixed beds occur for $Re_M > 2000$. The highest Re_M for this study was 328. Achieving such high Re_M values without causing the bed to fluidise can be achieved by feeding the gas stream from the top of the test column.

The effect that a larger column diameter might have on the Ergun equation can also be studied further. This will increase the D/d_p values of the bed. Most lab scale studies only focus on values of D/d_p ranging from $1 < D/d_p < 100$.

BIBLIOGRAPHY

Allen, K., Von Backström, T. & Kröger, D. 2013. Packed bed pressure drop dependence on particle shape, size distribution, packing arrangement and roughness. *Powder technology*, 246:590-600.

Al-Zareer, M., Dincer, I., Rosen & M. 2000. Production of hydrogen-rich syngas from novel processes for gasification of petroleum cokes and coals. *International journal of hydrogen energy*,

Bock, S., Stoppacher, B., Malli, K., Lammer, M. & Hacker, V. 2021. Techno-economic analysis of fixed-bed chemical looping for decentralized, fuel-cell-grade hydrogen production coupled with a 3 MWth biogas digester. Energy Conversion and Management, 250:114801.

Chang, C.S. & Deng, Y. 2018. A nonlinear packing model for multi-sized particle mixtures. *Powder Technology*, 336:449-464.

Cruz-Matías, I., Ayala, D., Hiller, D., Gutsch, S., Zacharias, M., Estradé, S. & Peiró, F. 2019. Sphericity and roundness computation for particles using the extreme vertices model. Journal of Computational Science, 30:28-40.

Debtech. 2022. *RhoVol - Densimetric Measurement System*. https://www.debtech.com/product-Rhovol.html Date of access: 2022/10/14.

Dukhan, N., Bağcı, Ö. & Özdemir, M. 2014. Experimental flow in various porous media and reconciliation of Forchheimer and Ergun relations. Experimental Thermal and Fluid Science, 57:425-433.

Ergun, S. 1952. Fluid Flow Through Packed Columns. Chemical Engineering Progress, (48):89-94.

Flint, L.E. & Selker, J.S. 2003. Use of porosity to estimate hydraulic properties of volcanic tuffs. Advances in Water Resources, 26(5):561-571.

Fogler, H. 2016. *Elements of chemical reaction engineering*. Boston: Prentice hall.

García-Cortés, V., García Estévez, D. & San-José, J.T. 2022. Assessment of particle packing models for aggregate dosage design in limestone and EAFS aggregate-based concretes. *Construction and Building Materials*, 328:126977.

Gibilaro, L. 2001. *Fluidization dynamics*. Elsevier.

Hamel, S. & Krumm, W. 2008. Near-wall porosity characteristics of fixed beds packed with wood chips. *Powder Technology*, 188(1):55-63.

Jacobs, J. 1976. Analytic and Experimental Techniques for evaluating Compressor Performance Losses. In: Indiana. Purdue e-Pubs.

Jahromi, R., Rezaei, M. & Samadi, S. 2020. Biomass gasification in a downdraft fixed-bed gasifier: optimization of operating conditions. *Chemical Engineering Science*, 231:116249.

Jones, M.R. 2001. Comparison of particle packing models for proportioning concrete constituents for minimum voids ratio. Materials and Structures, 35:301-309.

Kang, Y.A.H.C. 2012. Pressure Drop in a Pebble Bed

Koekemoer, A. & Luckos, A. 2015. Effect of material type and particle size distribution on pressure drop in packed beds of large particles: Extending the Ergun equation. Fuel, 158:232-238.

Kruisz, J., Rehrl, J., Hörmann-Kincses, T.R. & Khinast, J.G. 2021. Effects of signal processing on the relative standard deviation in powder feeding characterization for continuous manufacturing. *Powder Technology*, 389:536-548.

Kwan, A.K.H., Chan, K.W. & Wong, V. 2013. A 3-parameter particle packing model incorporating the wedging effect. Powder Technology, 237:172-179.

Li, Y. & Park, C.-W. 1998. Permeability of packed beds filled with polydisperse spherical particles. *Industrial & engineering chemistry research*, 37(5):2005-2011.

Liauchuk, V. & Kovalev, V. 2017. Supervoxels and Co-occurrence for Tuberculosis CT Image Classification. *Institute of Informatics Problems*,

Liu, Q., Jia, D. & Miao, J. 2020. Study of the linear and nonlinear packing model based on mixing of quartz sand. *Powder Technology*, 366:382-394.

Macdonald, F., El-Sayed, M. & Mow, K. 1979. *Flow through Porous Media-the Ergun equation Revisited*. Ontario.

Mandal, D., Sathiyamoorthy, D. & Vinjamur, M. 2013. Void fraction and effective thermal conductivity of binary particulate bed. *Fusion Engineering and Design*,

Markov, V., Sa, B., Devyanin, S., Grekhov, L., Neverov, V. & Zhao, J. 2022. Numerical analysis of injection and spray characteristics of diesel fuel and rapeseed oil in a diesel engine. *Case Studies in Thermal Engineering*, 35:102129.

Nemec, D. & Levec, J. 2005. Flowthrough packed bed reactors: 1. Single-phase flow. *Chemical Engineering Science*, 60:6947 – 6957.

Pan, J., Zhang, Z., Li, M. & Wu, Y. 2019. Characteristics of multi-scale pore structure of coal and its influence on permeability. *Natural Gas Industry B*, 6(4):357-356.

Perez-Mercado, L.F., Lalander, C., Joel, A., Ottoson, J., Dalahmeh, S. & Vinnerås, B. 2019. Biochar filters as an on-farm treatment to reduce pathogens when irrigating with wastewater-polluted sources. Journal of Environmental Management, 248:109295.

Qian, K., Kumar, A., Zhang, H., Bellmer, D. & Huhnke, R. 2015. Recent advances in utilization of biochar. Renewable and Sustainable Energy Reviews, 42:1055-1064.

Reactor Under High Reynolds Number,. *Nuclear Technology,*, 180(2):159-173.

Salam, A. & Bhattacharya, S. 2006. A comparative study of charcoal gasification in two types of spouted bed reactors. *Energy*, (31):228-243.

Samarawickrama, D., Manoratne, C. & Amunugoda, P. 2020. Production and characterization of black charcoal from Bambusa vulgaris (Yellow Bamboo) and potentiality for advance applications *Advanced materials research*, II(1):28-36.

Sheth, P. & Babu, B. 2009. Experimental studies on producer gas generation from wood waste in a downdraft biomass gasifier. *Bioresource Technology*, 100: 3127–3133.

Stewart, J. 2016. Calculus. In. 8E. Toronto: Cengage. p 27.

Walter, L. & Morse, J. 1984. Reactive surface area of skeletal carbonates during dissolution; effect of grain size. *Journal of Sedimentary Research*, 54(4):1081-1090.

Webb, P. 2001. *Volume and Density Determinations for Particle Technologists*.

Wolfram. 2022. *Padé Approximant*. https://mathworld.wolfram.com/PadeApproximant.html Date of access: 2022/08/14.

Wong, V. & Kwan, A.K.H. 2014. A 3-parameter model for packing density prediction of ternary mixes of spherical particles. *Powder Technology*, 268:357-367.

Yang, W.-c. 2003. Handbook of fluidization and fluid-particle systems. In: CRC press. pp. 37-39.

Zheng, J., Sun, Q., Zheng, H., Wei, D., Li, Z. & Gao, L. 2020. Three-dimensional particle shape characterizations from half particle geometries. *Powder Technology*, 367:122-132.

Zhou, H., Zhou, M., Cheng, M. & Guo, W. 2017. Experimental study and X-ray microtomography based CFD simulation for the characterization of pressure drop in sinter bed. *Applied Thermal Engineering*, 112:811-819.

APPENDIX A: RHOVOL RESULTS AND ANALYSIS

Table A-1: Standard deviation values for Rhovol results

Batch no.	Stdev MCD (mm)	Stdev MSS (mm)	Stdev Sphericity (dimensionless)	Stdev Elongation (dimensionless)	Stdev Flatness (dimensionless)
1	0.807	0.609	0.129	0.823	0.608
2	1.08	0.861	0.126	0.574	0.800
3	1.56	1.23	0.123	1.05	0.753
4	1.75	1.36	0.138	0.942	0.560
5	1.79	1.31	0.124	0.713	0.665

Table A-2: Sphericity Standard Deviation

Batch no.	Stdev (dimensionless)	Mean (dimensionless)	Relative stdev %
1	0.129	0.559	23.1
2	0.126	0.575	21.9
3	0.123	0.553	22.3
4	0.138	0.578	23.9
5	0.124	0.584	21.3

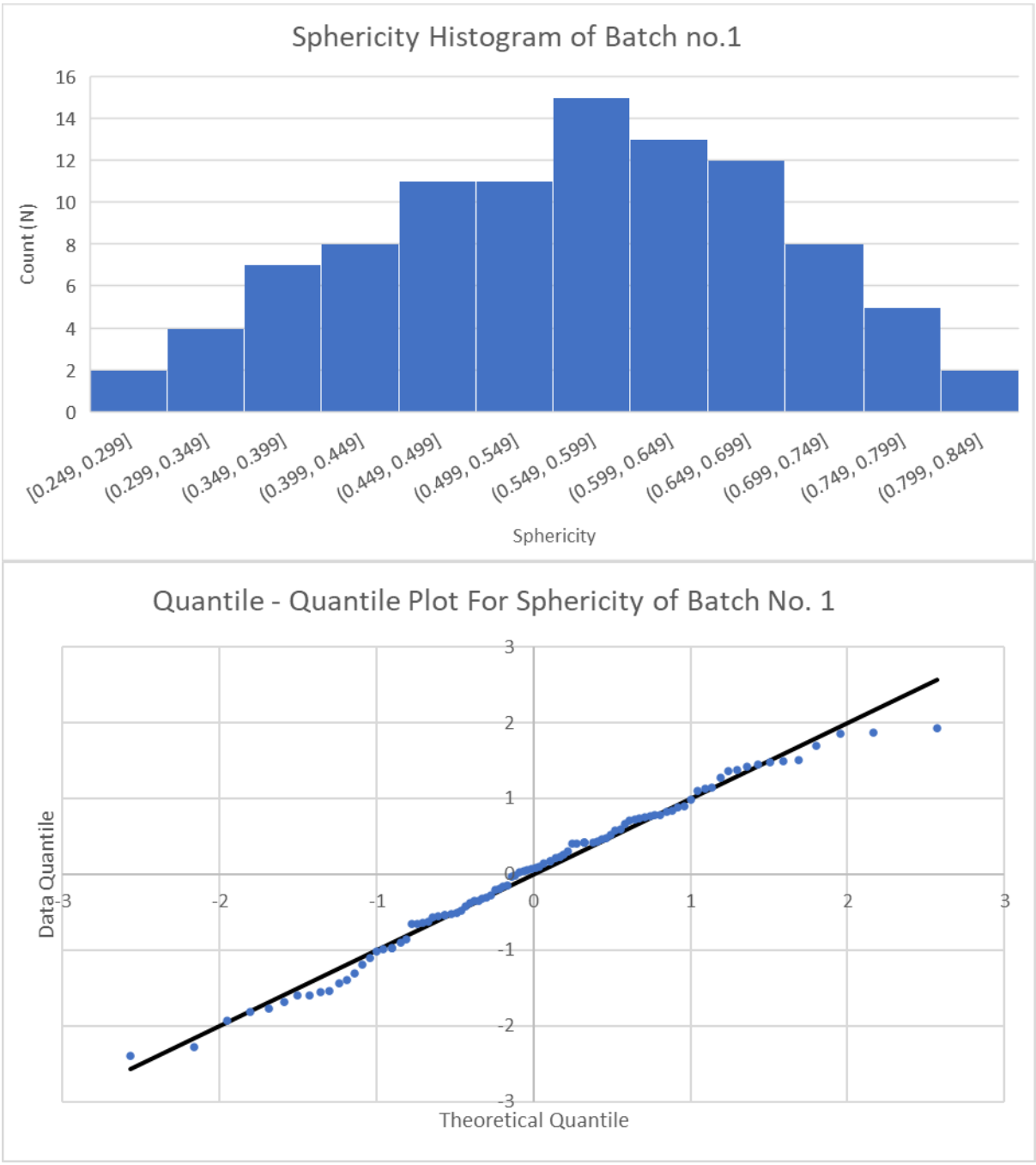

Figure A-1: Histogram and quantile plots for the sphericity of batch 1

The values of the quantile plot correspond well to the y = x line, thus indicating that the sphericity results of batch 1 has a normal distribution.

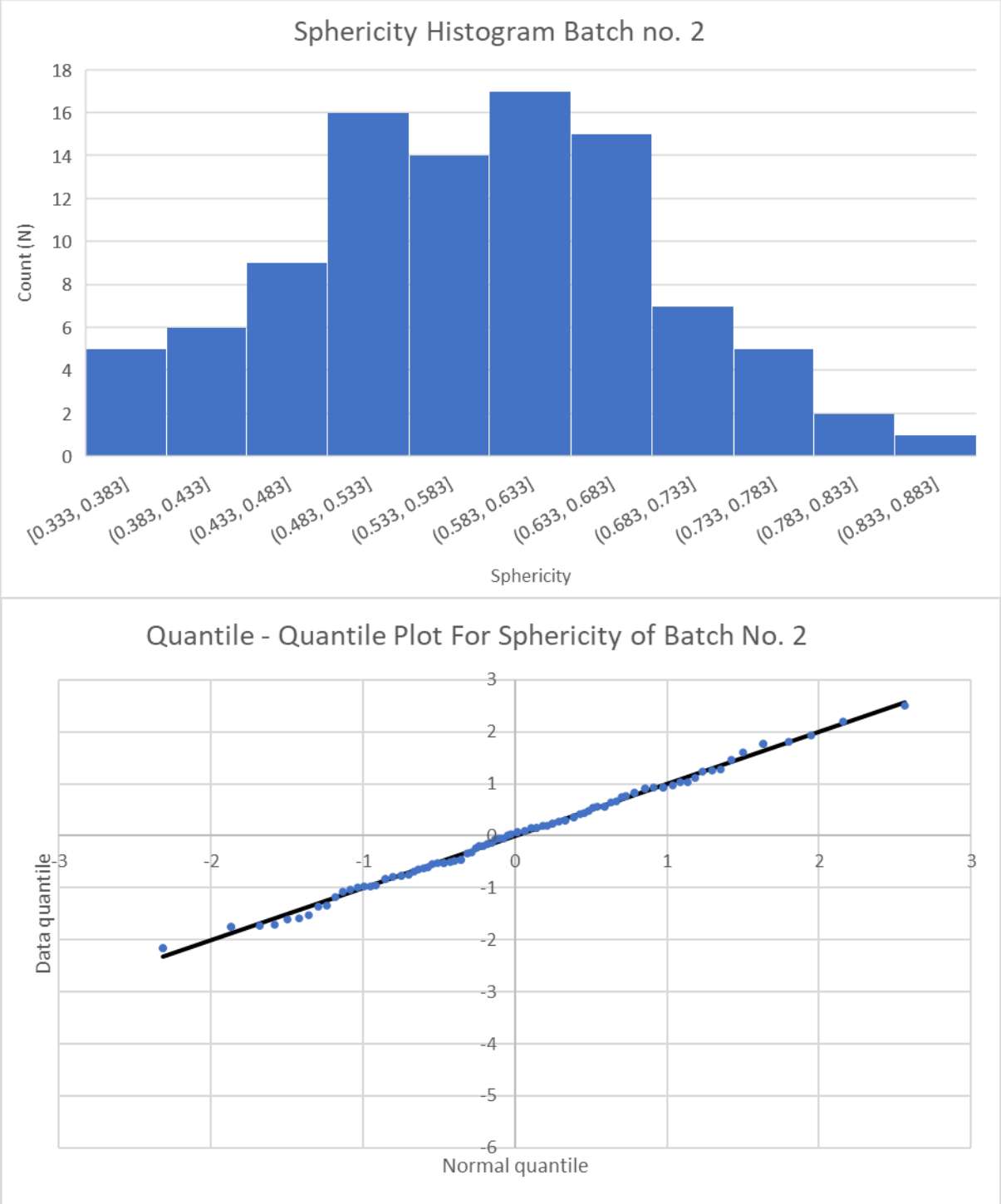

Figure A-2: Histogram and quantile plots for the sphericity of batch 2

The values of the quantile plot correspond well to the y = x line, thus indicating that the sphericity results of batch 2 has a normal distribution.

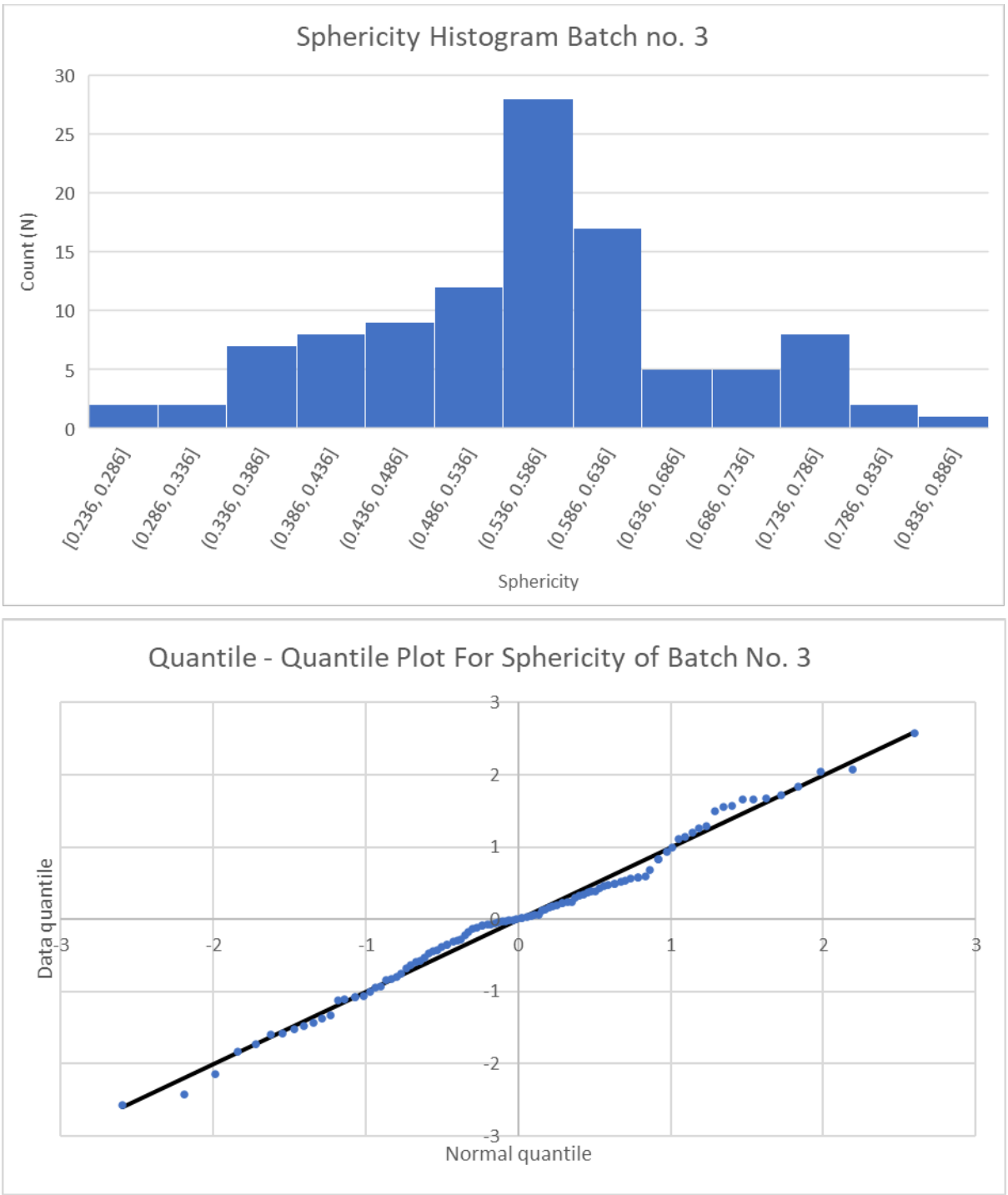

Figure A-3: Histogram and quantile plots for the sphericity of batch 3

The values of the quantile plot correspond well to the y = x line, thus indicating that the sphericity results of batch 3 has a normal distribution.

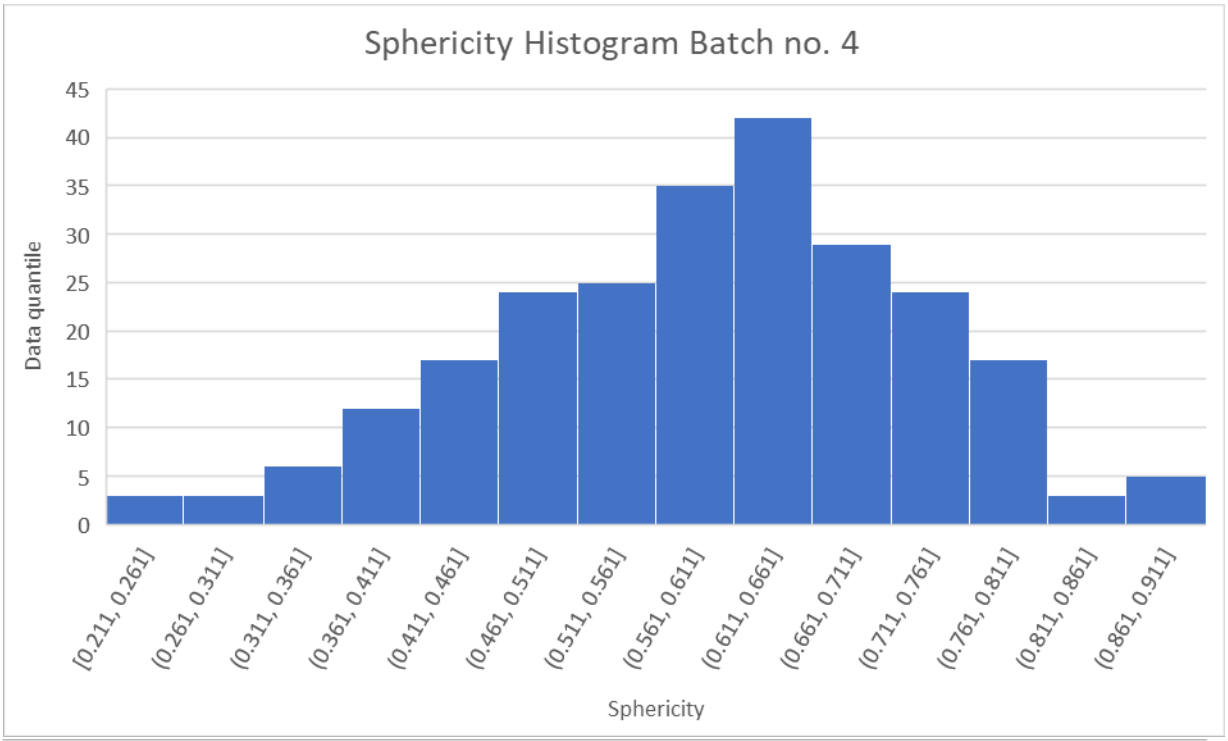

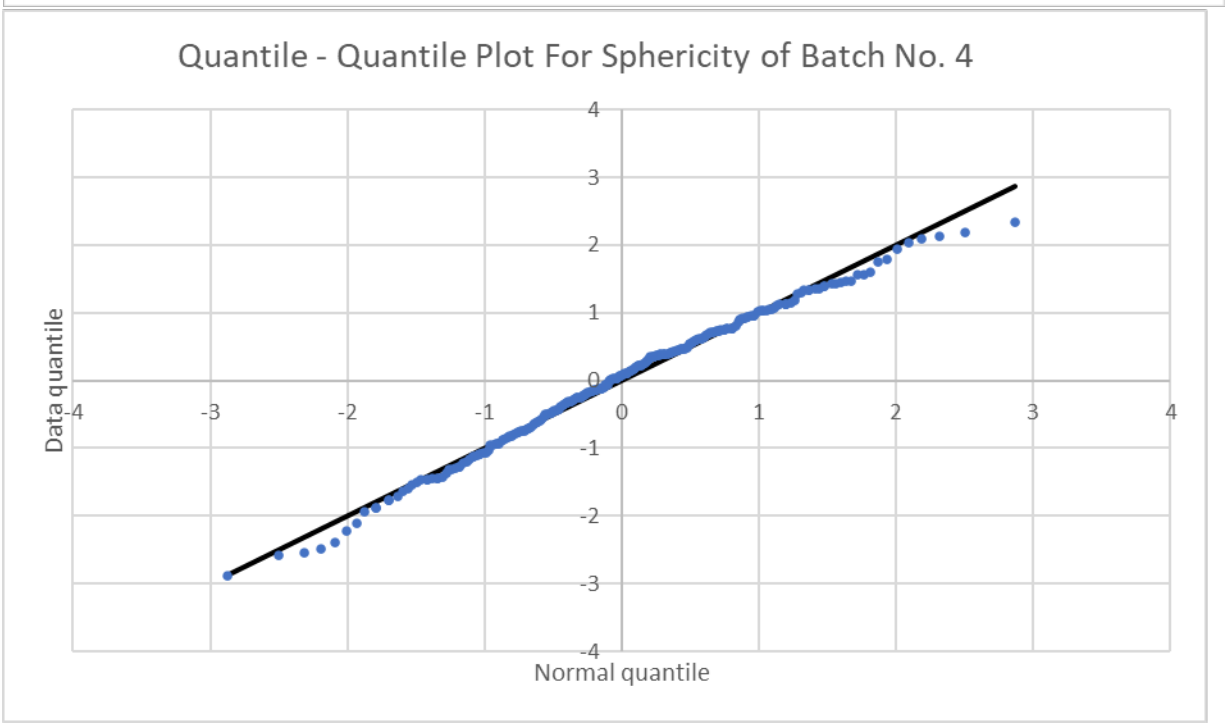

Figure A-4: Histogram and quantile plots for the sphericity of batch 4

The values of the quantile plot correspond well to the y = x line, thus indicating that the sphericity results of batch 4 has a normal distribution.

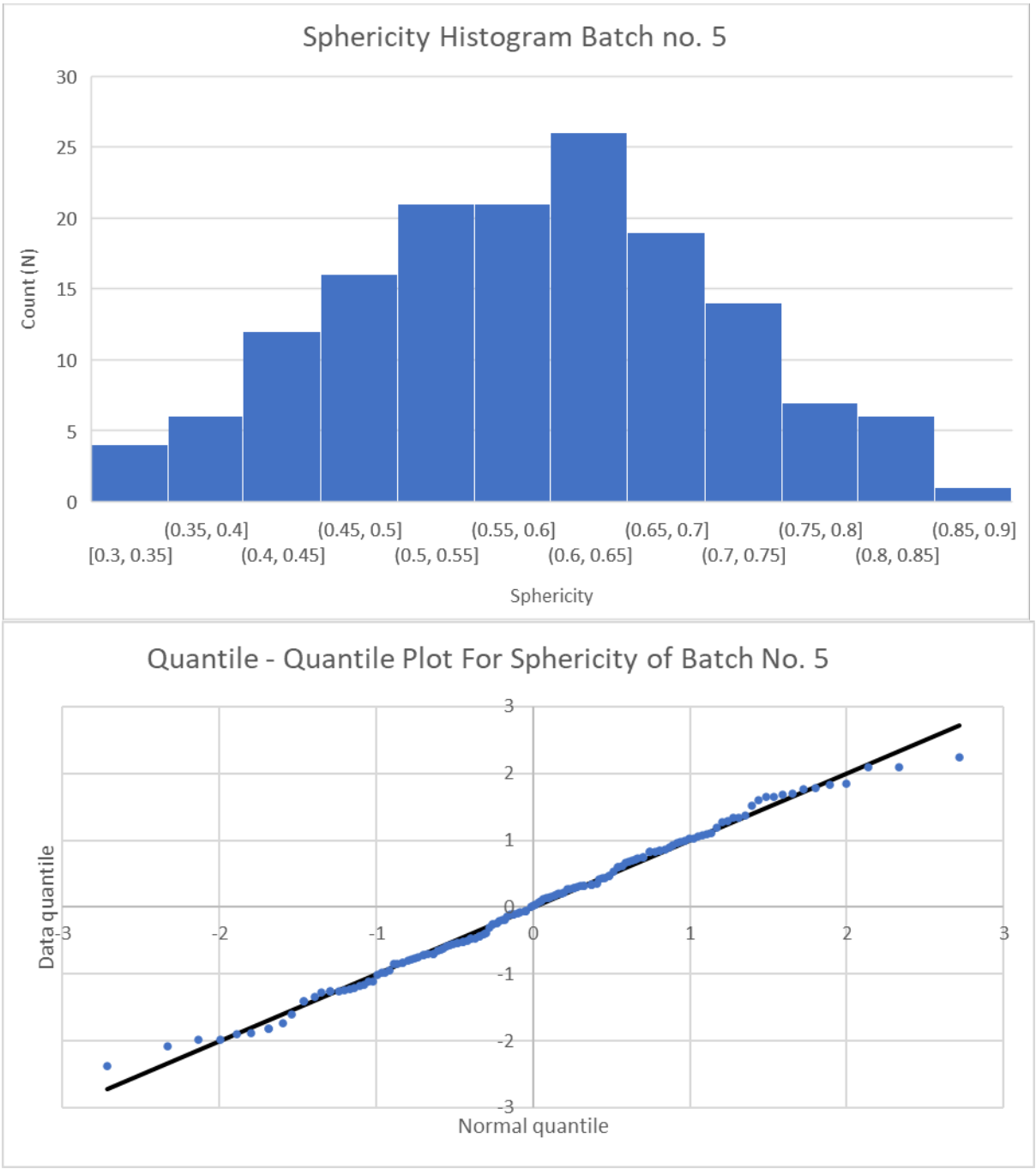

Figure A-5: Histogram and quantile plots for the sphericity of batch 5

The values of the quantile plot correspond well to the y = x line, thus indicating that the sphericity results of batch 5 has a normal distribution.

APPENDIX B: BINARY VOIDAGE MODELLING RESULTS

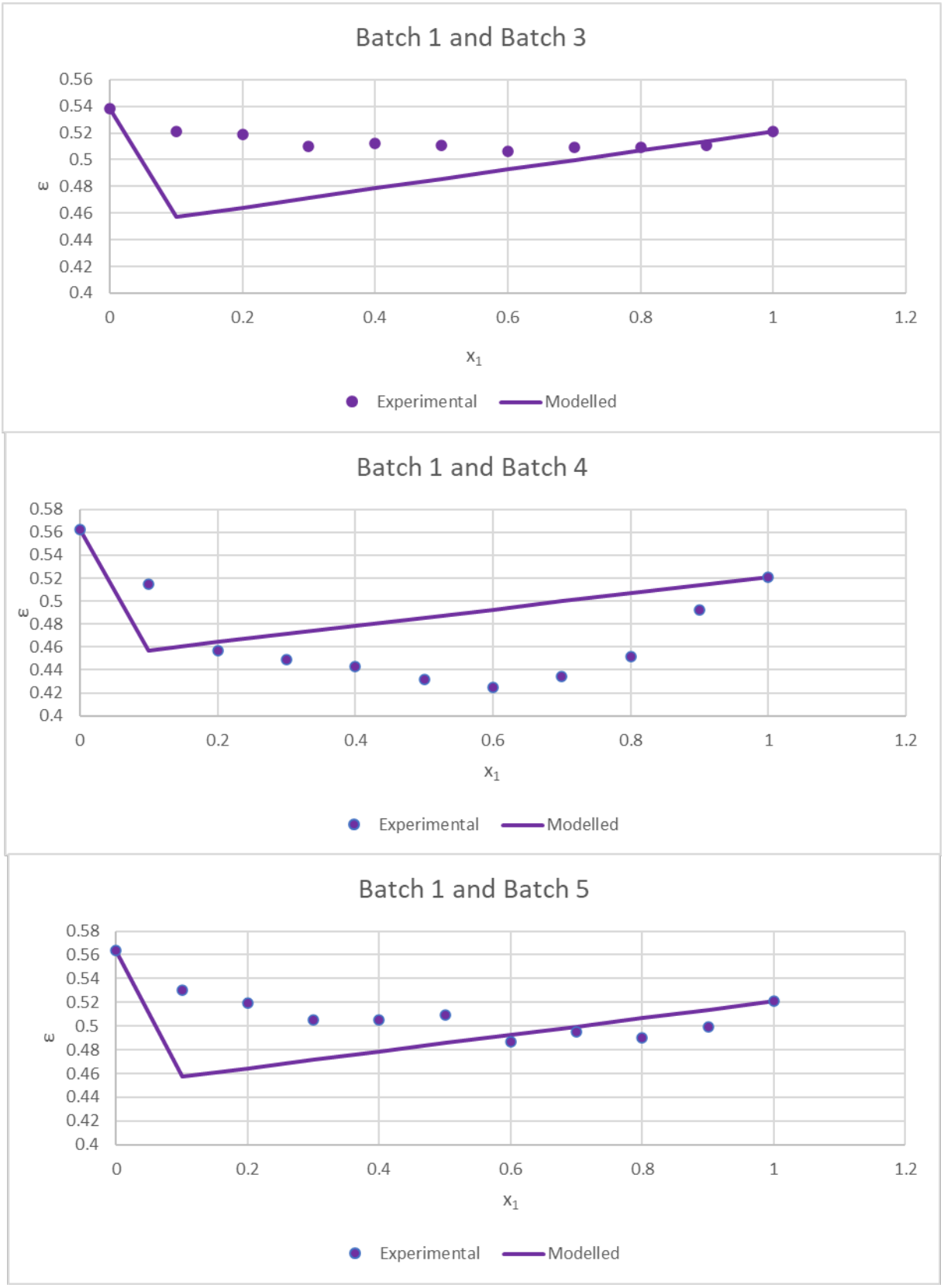

Figure B-1: Continuation of AG modelling results for char binary mixtures

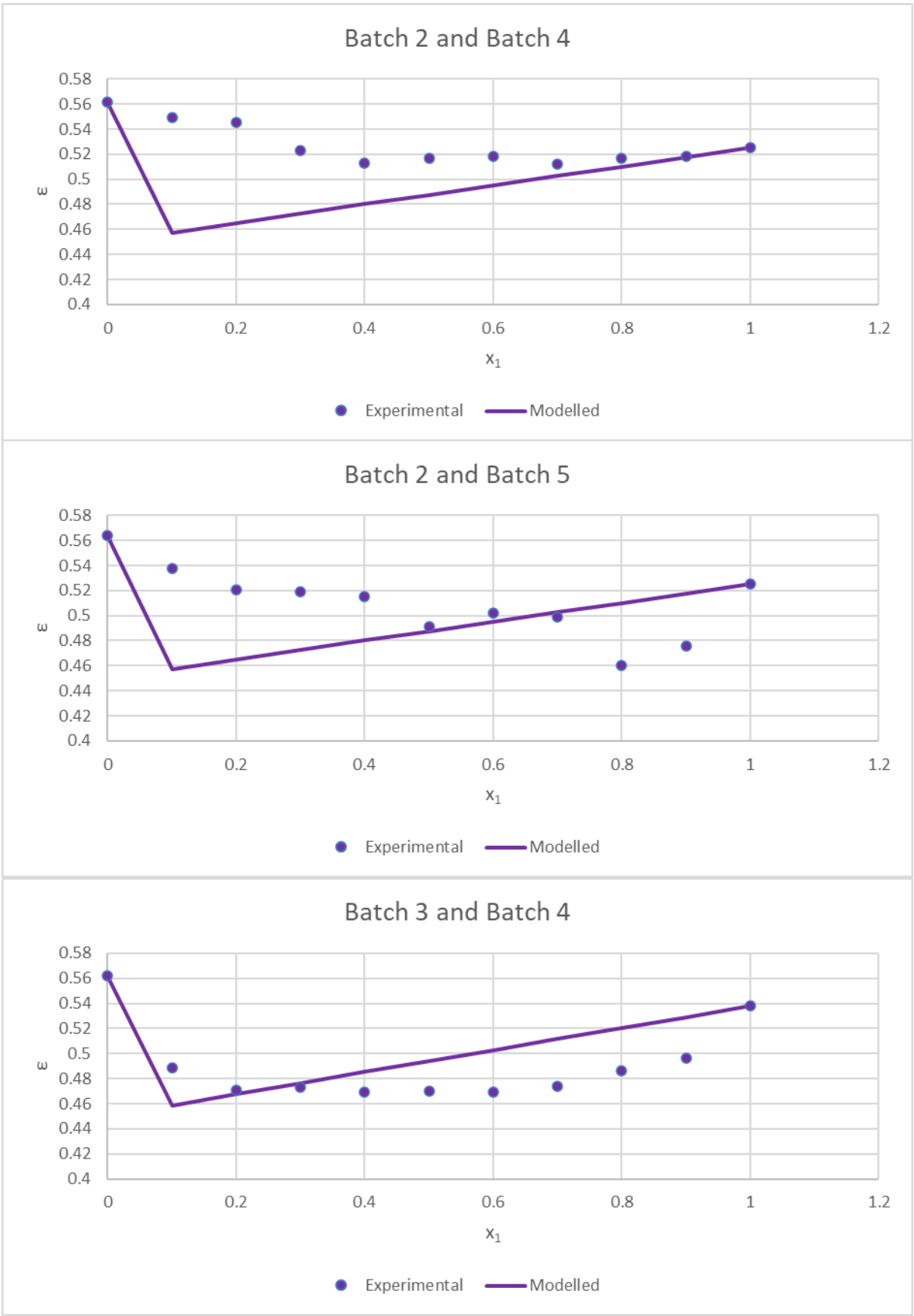

Figure B-2: Continuation of AG modelling results for char binary mixtures

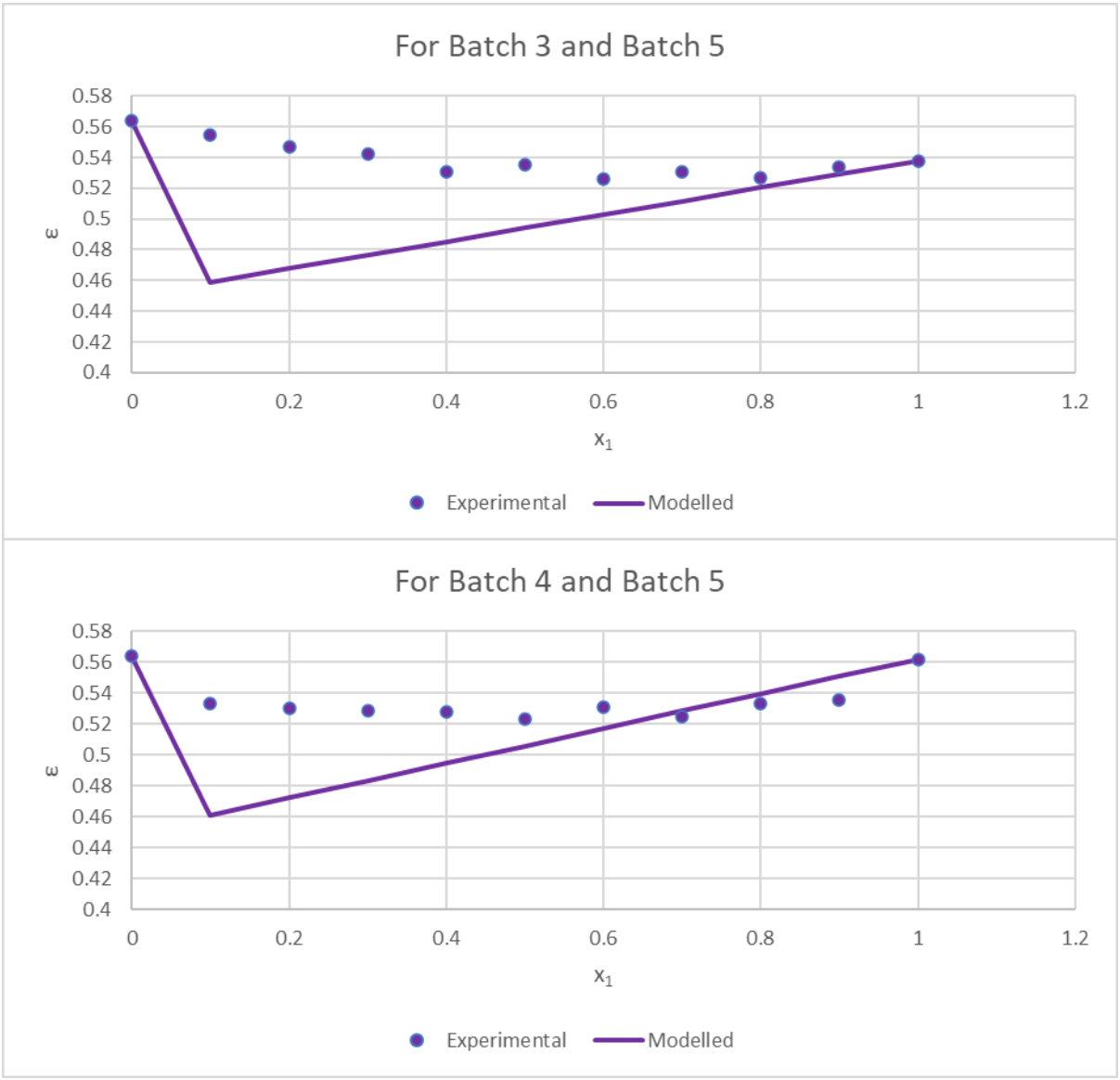

Figure B-3: Continuation of AG modelling results for char binary mixtures

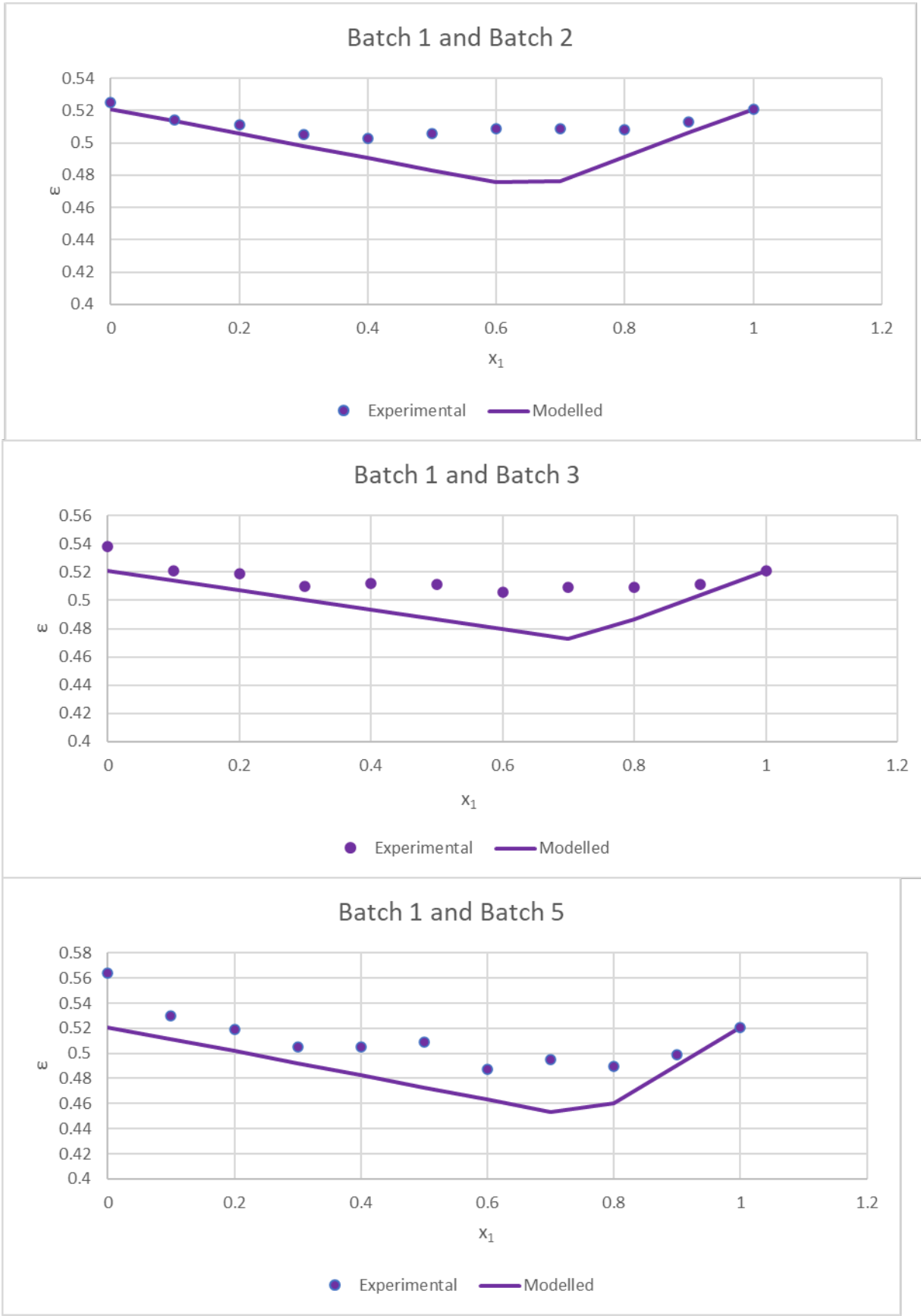

Figure B-4: Continuation of LPD modelling results for char binary mixtures

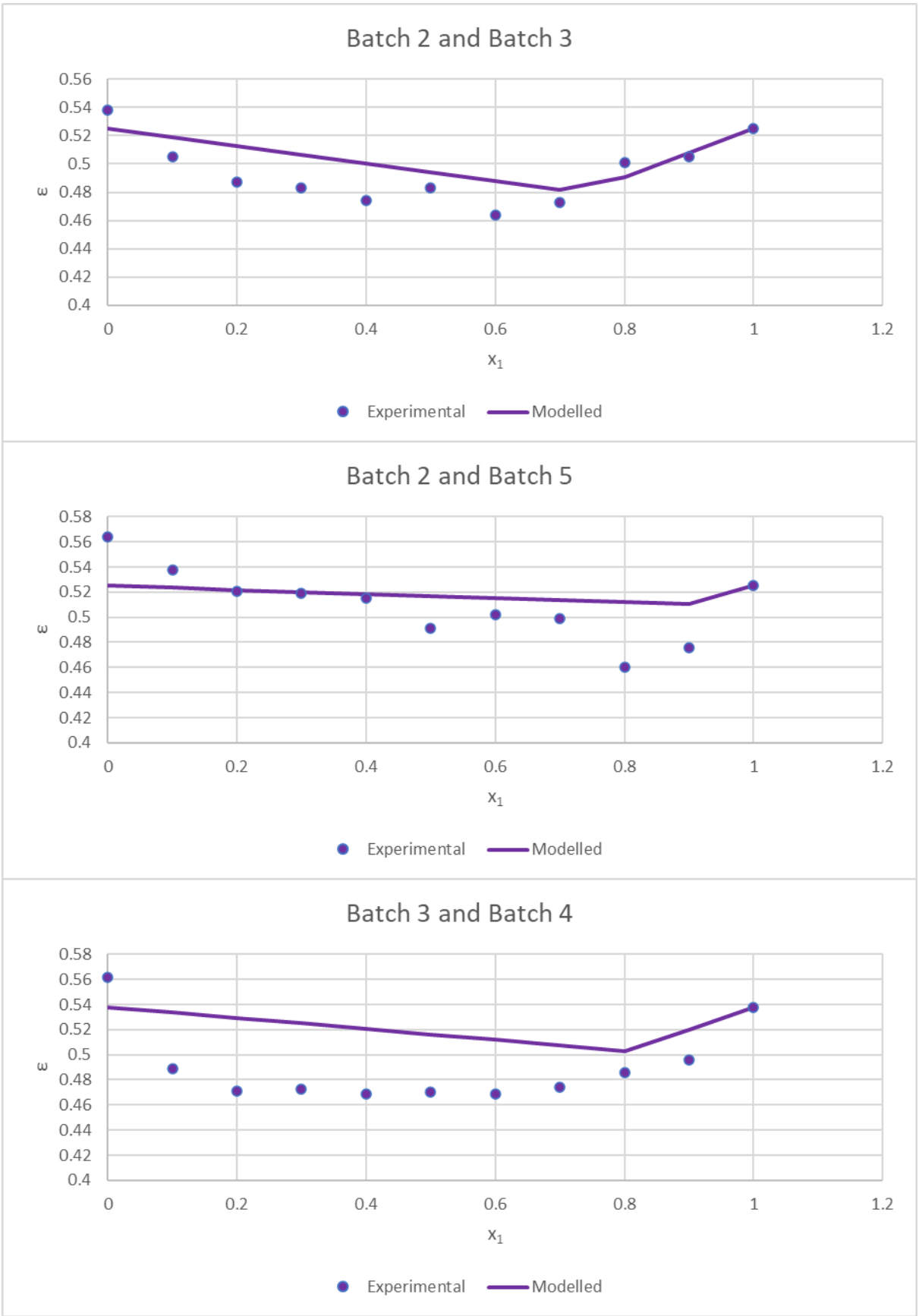

Figure B-5: Continuation LPD modelling results for char binary mixtures

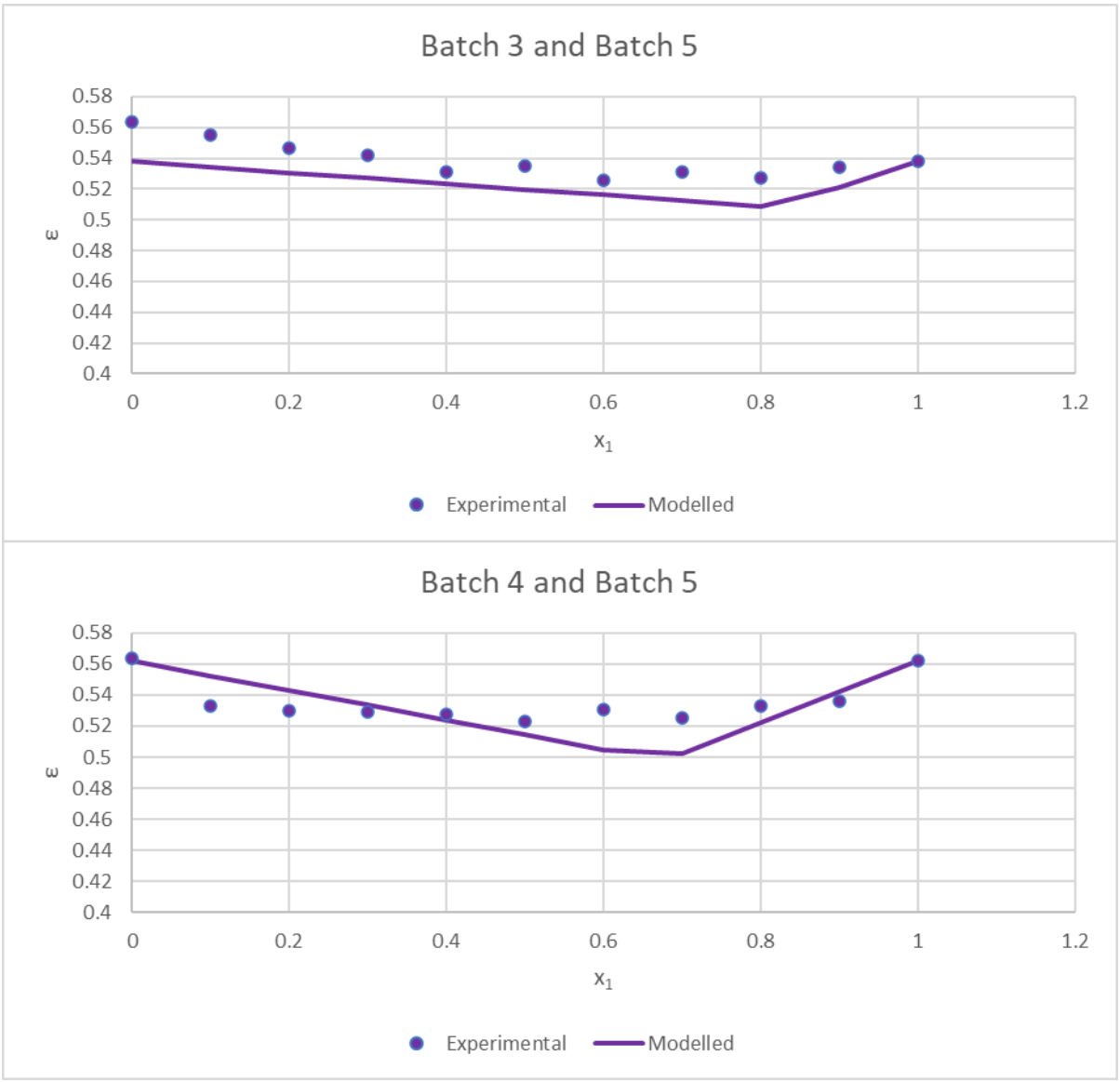

Figure B-6: Continuation LPD modelling results for char binary mixtures

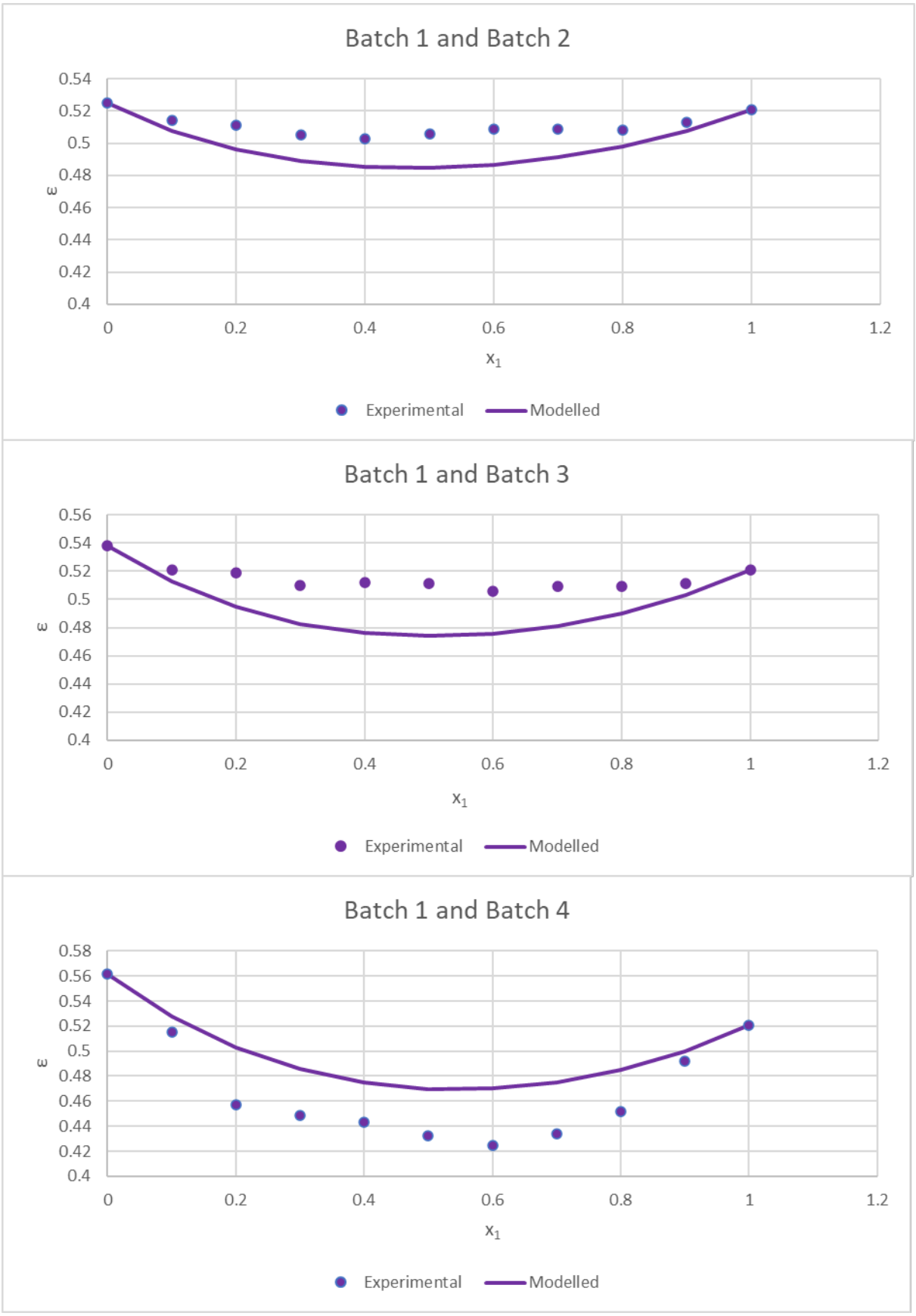

Figure B-7: Continuation of Toufar modelling results for char binary mixtures

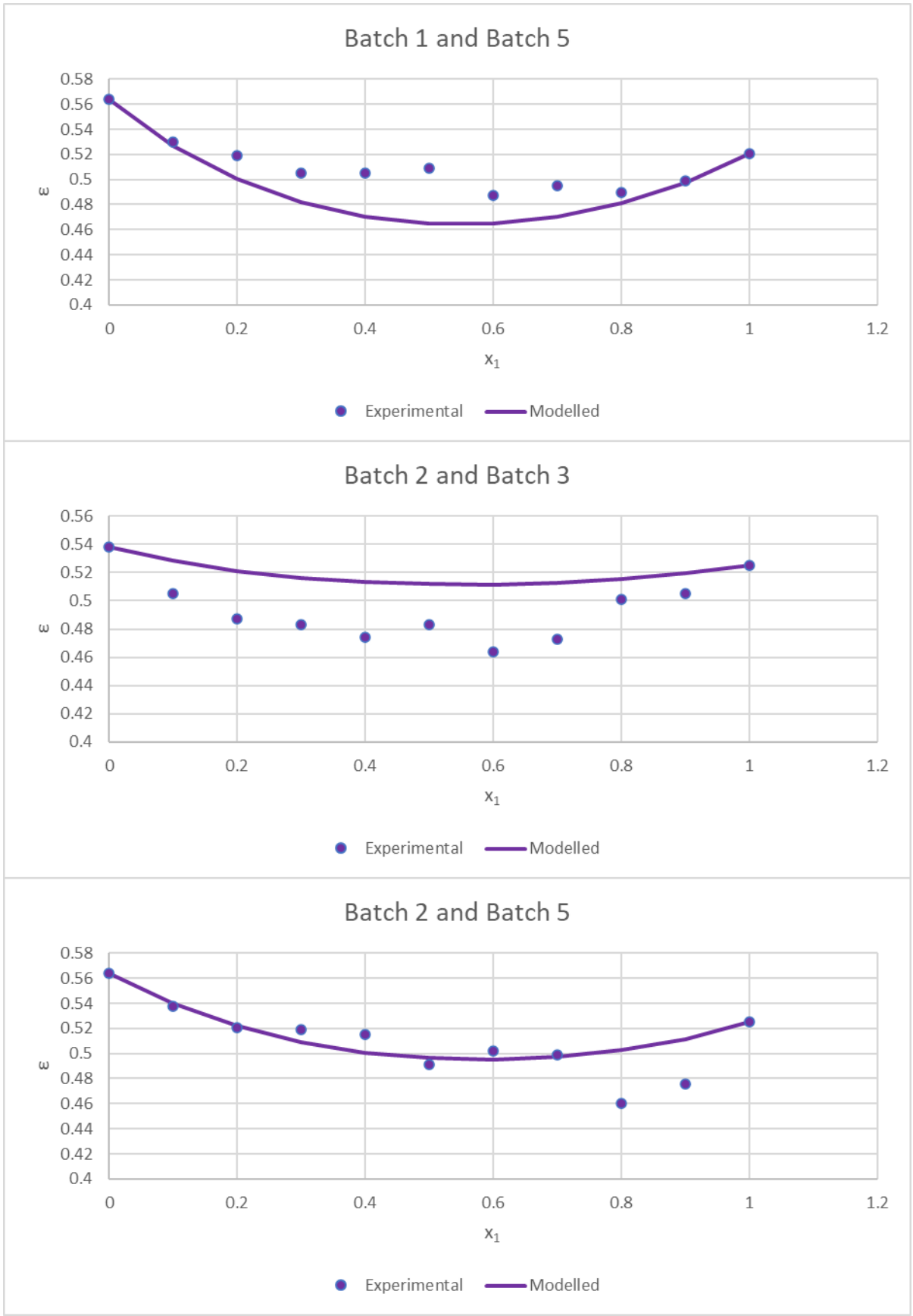

Figure B-8: Continuation of Toufar modelling results for char binary mixtures

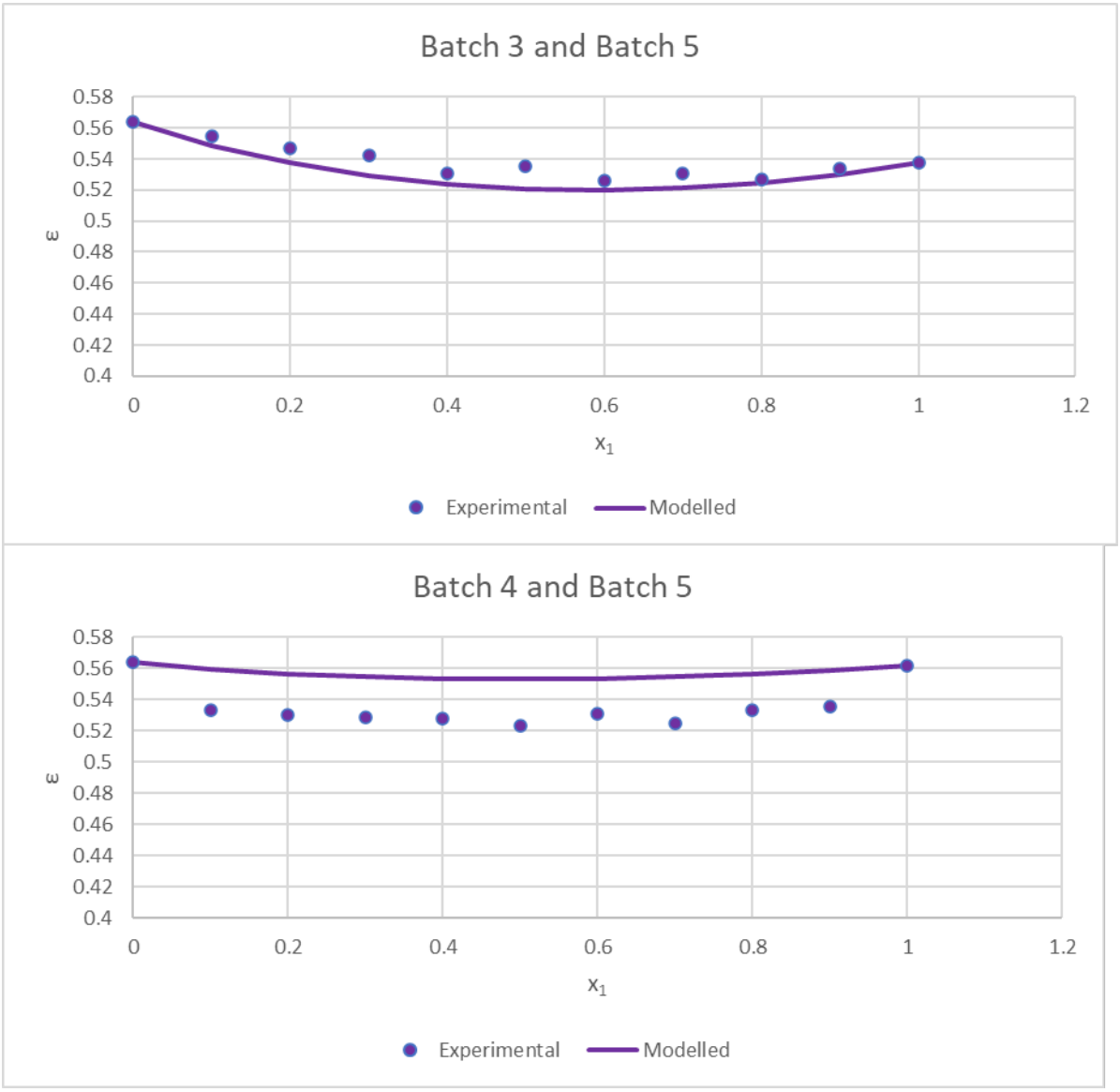

Figure B-9: Continuation Toufar modelling results for char binary mixtures

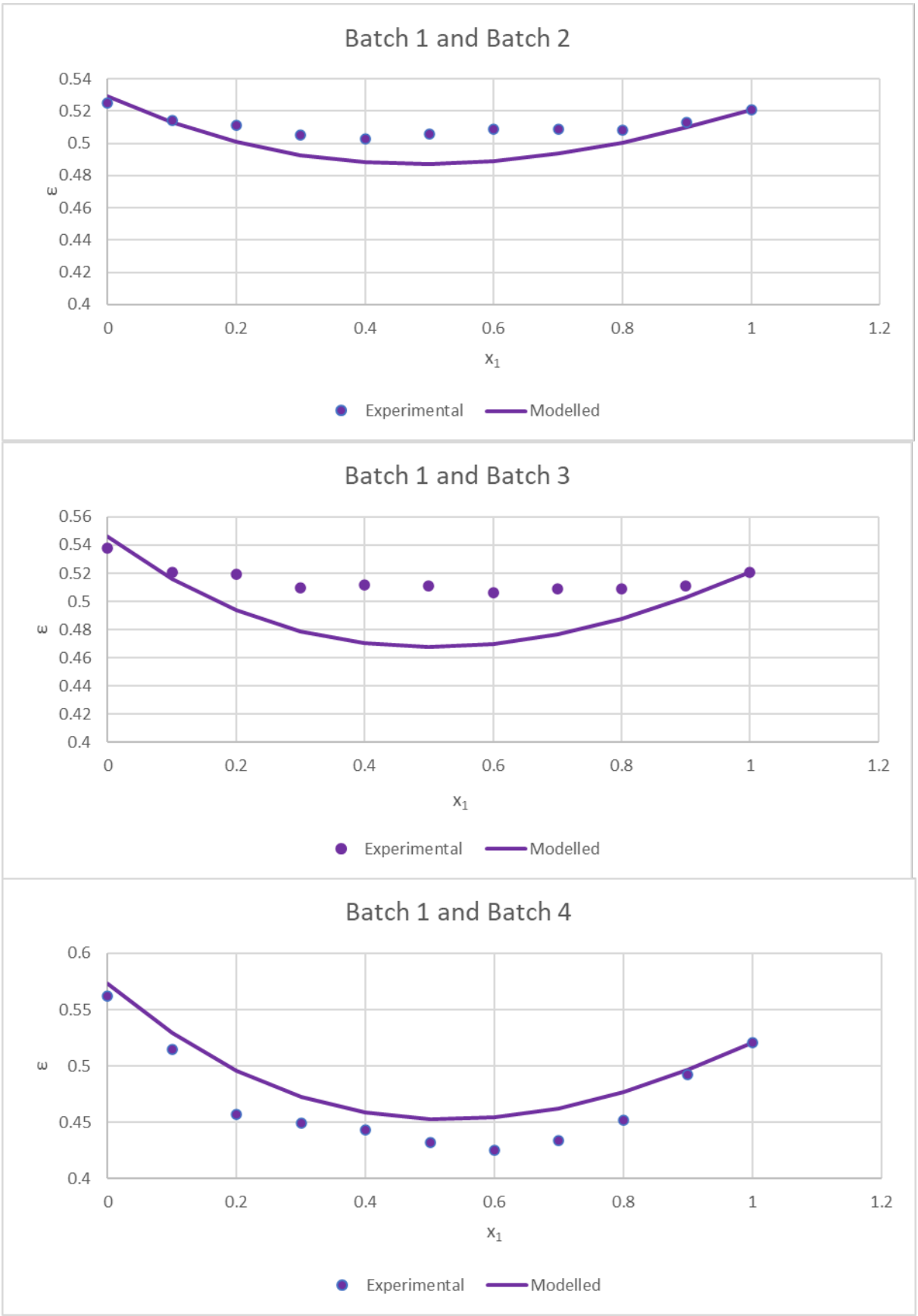

Figure B-10: Continuation of MK modelling results for char binary mixtures

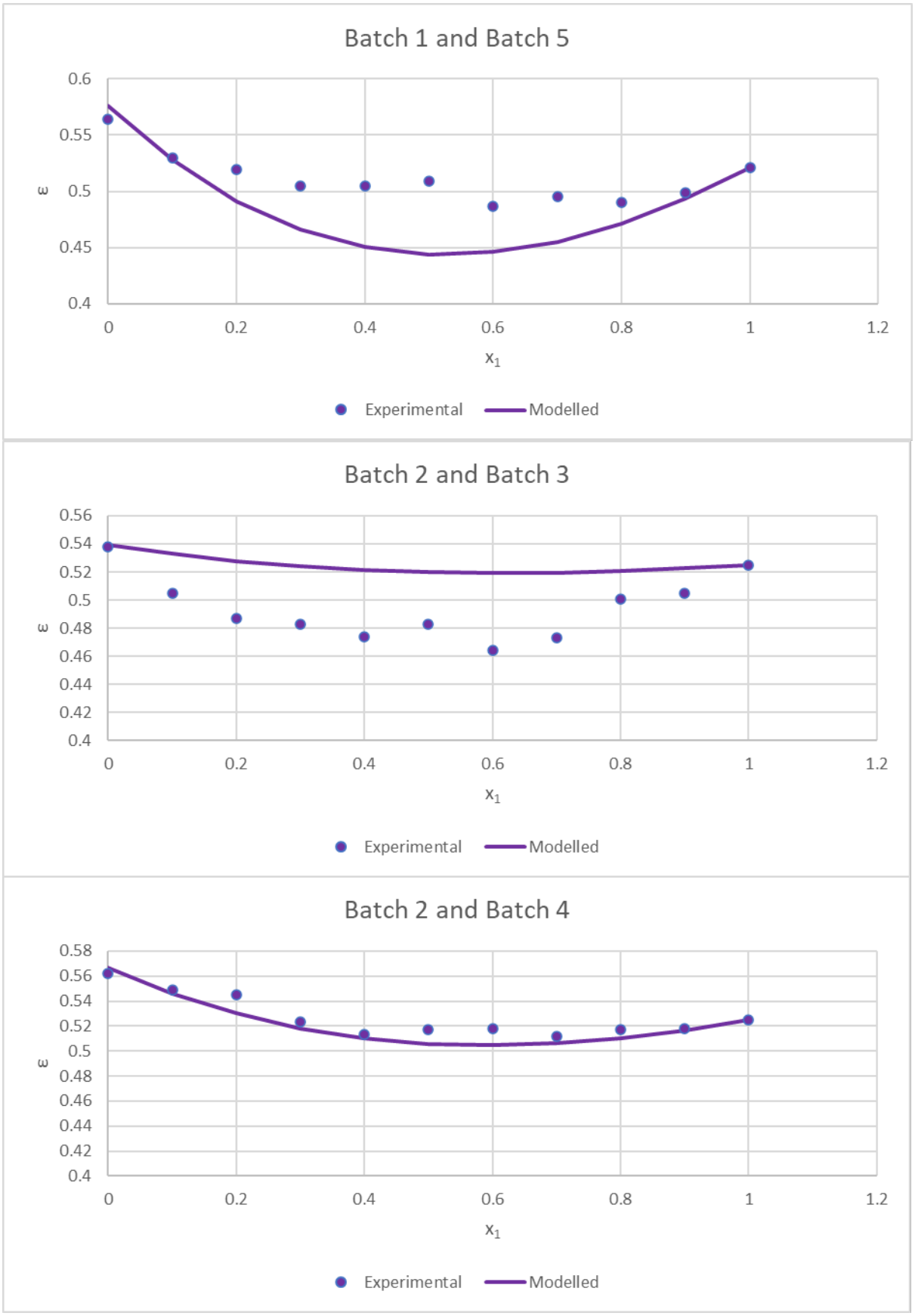

Figure B-11: Continuation of MK modelling results for char binary mixtures

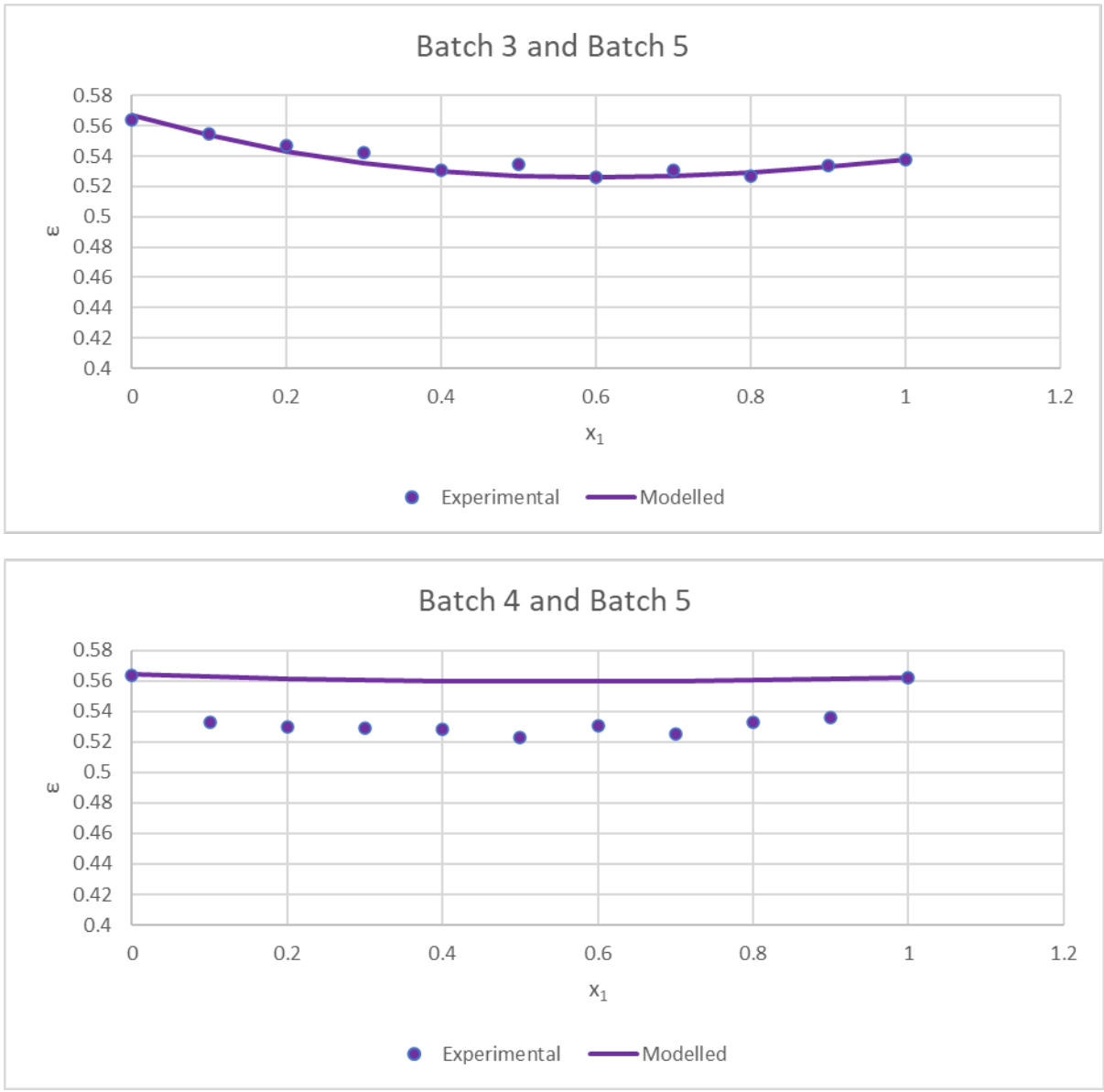

Figure B-12: Continuation of MK modelling results for char binary mixtures

APPENDIX C: MULTIPLE LINEAR REGRESSION RESULTS

Table C-1: Multiple linear regression analysis of A and B with Ergun parameters

Ergun Coefficient	Parameter	B_i	B_i*	t-value	p-value
A	intercept	-3502	-	-6.37	< 1.00E-4
A	dp	-13367	-0.355	-3.30	1.74E-4
A	φ	5101	0.534	-5.27	< 1.00E-4
A	ε	1902	0.736	-8.47	< 1.00E-4
B	intercept	-22.5	-	-5.50	< 1.00E-5
B	dp	-187	-0.653	-6.17	< 1.00E-5
B	φ	32.8	0.452	4.54	3.50E-5
B	ε	16.1	0.821	9.60	< 1.00E-5

For each parameter the p value is smaller than 0.05, thus indicating a linear proportionality between the A and B values of the Ergun equation to the intercept, dp, sphericity and voidage.